The Pennsylvania State University

The Graduate School

Department of Mechanical and Nuclear Engineering

DESIGN OPTIMIZATION OF HONEYCOMB SANDWICH PANELS FOR BLAST LOAD MITIGATION

A Dissertation in

Mechanical Engineering

by

Sumanta Kumar Nayak

Submitted in Partial Fulfillment
of the Requirements
for the Degree of

Doctor of Philosophy

August 2012

The dissertation of Sumanta Kumar Nayak was reviewed and approved* by the following:

Ashok D. Belegundu
Professor of Mechanical Engineering
Dissertation Adviser
Chair of Committee

Panagiotis Michaleris
Associate Professor of Mechanical Engineering

Christopher D. Rahn
Professor of Mechanical Engineering

Ali M. Memari
Professor of Architectural Engineering

Karen A. Thole
Professor of Mechanical Engineering
Head of the Department of Mechanical and Nuclear Engineering

*Signatures are on file in the Graduate School

ABSTRACT

A general process for optimization of a honeycomb core sandwich panel to minimize the effects of air blast loading is presented in this dissertation. This process can also be readily applied to other types of cellular core. The panel geometry consists of two metal face plates with a crushable honeycomb core. Metallic sandwich panel with a cellular core such as honeycomb has a great potential to absorb the impact energy of the blast by undergoing cyclic plastic buckling deformation at a nearly constant stress. The core also provides higher bending stiffness to weight ratio of the sandwich by maintaining larger gap between the face plates. The ability of the core to absorb the impact energy and provide stiffness is not only influenced by its cell size and height, but also by the thickness and shape of the face plates. Optimization is necessary as there is strong coupling between the several variables and the physics, which makes parametric studies relatively ineffective. The optimization study investigates the size and shape of the face plates, and depth and cell size of the core, to minimize dynamic deflection or acceleration of the backface plate. Constraints on total mass and on plastic strain in the face plates are imposed. A design of experiments (DOE) based response surface optimization method is used. Response equations are determined using the central composite face centered method, which are then interfaced to a gradient based optimizer in the MATLAB optimization toolbox. Function evaluations are done using LS-DYNA finite element (FE) software.

Considering the high computation time involved in the FE simulation of detailed honeycomb cells, an alternative technique is used to simplify the honeycomb core modeling and to reduce computation time. Specifically, virtual testing is used to develop a homogenized model for the stress-strain curve of the honeycomb core. The homogenized model is validated by comparison to existing results in the literature as well as to detailed FE models of test specimens. The homogenization approach can be readily applied to other types of cellular core.

For deflection minimization, results produce a stiffer front face plate which effectively distributes the blast load to a larger area of the core and also produce a stiff core by increasing both core density and core depth. For acceleration minimization, results again produce a stiffer front face plate, but accompanied by a sufficiently soft core. The mechanism of lowering the backface acceleration is by absorbing energy with low transmitted stress. Strain rate effects on the results are discussed. Further, a clear cut comparison between monolithic metal plates and sandwich plates, for the same loading and failure criteria, is presented here.

TABLE OF CONTENTS

LIST OF FIGURES ..... **viii**

LIST OF TABLES ..... **xii**

LIST OF NOMENCLATURES ..... **xiv**

ACKNOWLEDGEMENTS ..... **xvi**

Chapter 1 Introduction **1**

1.1 Introduction 1

1.2 Dissertation organization 4

Chapter 2 Literature Review **6**

2.1 Introduction 6

2.2 Past work on sandwich panels 6

2.3 Past work on crush stress of honeycomb cells 10

Chapter 3 Homogenization of Honeycomb Structure via Virtual Testing **13**

3.1 Finite element modeling of the unit cell 14

3.2 Virtual testing results 16

3.2.1 Mesh convergence study 18

3.2.2 Effect of cell dimensions on the folding length 19

3.2.3 Effect of honeycomb cell geometry on the load curve 21

3.3 Parameterization of the load curve in terms of *t* and *D* 23

3.3.1 Parameterization using response surface method 23

3.3.2 Parameterization using *t/D* as a single variable 26

3.4 Sensitivity study 29

3.4.1 Effect of non-rigid hammer, honeycomb without face plates, and geometric imperfections on load curve 29

3.4.2 Effect of strain rate 31
3.5 Validation of homogenization model 33
3.5.1 Validation of crush strength with commercially available data 33
3.5.2 Large scale uniaxial crush test of a detailed and homogenized FEM 34
3.5.3 Validation of honeycomb model through flexure tests 37
3.6 Summary 38

Chapter 4 Optimization Problem Description 39
4.1 Overview of the problem 39
4.2 Blast injury 40
4.3 Problem definition 40
4.3.1 Objective functions 40
4.3.2 Constraints 41
4.4 Finite element modeling of the problem 42
4.4.1 Sandwich model 42
4.4.2 Material properties 43
4.4.3 Blast load 45
4.5 Velocity field for creating the sandwich model 47

Chapter 5 Optimization by Response Surface Method 51
5.1 Overview of response surface methodology 51
5.1.1 Central composite design (CCD) 54
5.1.2 D-Optimal design 55
5.2 Optimization by response surface method 55
5.2.1 Responses for size optimization 57
5.2.2 Responses for size and shape optimization 58

Chapter 6 Optimization Results **59**

6.1 Introduction 59

6.2 Parametric study 60

6.3 Optimization results for minimizing displacement, δ_b 62

6.3.1 Optimization results for different mass limits of sandwich and monolithic plate 62

6.3.2 Comparison of results for 150 *kg* sandwich and monolithic plate 64

6.3.3 Mechanism causing the improvement in backface deflection 68

6.4 Optimization results for minimum acceleration, a_b 69

6.4.1 Optimization results for different mass limits of sandwich and monolithic plate 69

6.4.2 Comparison of results for 150 *kg* sandwich and monolithic plate 70

6.4.3 Mechanism causing the improvement in backface deflection 73

6.5 Analysis of energy absorption in 150 *kg* size optimized sandwich 76

6.6 Sensitivity analysis 79

6.6.1 Sensitivity analysis with respect to stiffener mass 79

6.6.2 Sensitivity analysis with respect to blast location 79

Chapter 7 Miscellaneous Studies **81**

7.1 Strain rate effect on the 150 *kg* optimized sandwich panel 81

7.2 Preliminary study on delamination in sandwich 82

7.3 Effect of off-center hammer load 86

7.4 Effect of hammer travel at an angle to transverse direction 87

Chapter 8 Conclusions and Future Work **90**

8.1 Conclusions 90

8.2 Contributions of the research 92

8.3 Future work 92

Bibliography **94**

LIST OF FIGURES

Figure **1-1**: Typical configuration of a honeycomb sandwich panel 2

Figure **1-2**: Shaped honeycomb core sandwich panel 3

Figure **3-1**: Honeycomb cell geometry 15

Figure **3-2**: Unit cell 15

Figure **3-3**: Boundary conditions on the unit cell 15

Figure **3-4**: Finite element model of the honeycomb unit cell 16

Figure **3-5**: Different stages of honeycomb unit cell crushing 17

Figure **3-6**: Load curve and its associated parameters of the honeycomb core 18

Figure **3-7**: Effect of mesh size on the load curve 19

Figure **3-8**: (a) Typical folding panel and (b) deformation of the folding panel 20

Figure **3-9**: Comparison of the folding wavelength at different cell size 20

Figure **3-10**: Comparison of the folding wavelength at different foil thickness 21

Figure **3-11**: Effect of the cell size *(D)* on the load curve 22

Figure **3-12**: Effect of the foil thickness *(t)* on the load curve 22

Figure **3-13**: Effect of core depth *(h)* on the load curve 23

Figure **3-14**: The design candidates for creating response equation using CCD 24

Figure **3-15**: Variation of crush strength with *t/D* 26

Figure **3-16**: Variation of the densification stress with *t/D* 27

Figure **3-17**: Variation of the peak strain with t/D 27

Figure **3-18**: Validation of the crush strength obtained from virtual test 28

Figure **3-19**: Unit cell crush test model: non-rigid hammer and base, no face plate attached to the core 30

Figure **3-20**: Geometric imperfections in unit cell test model 30

Figure **3-21**: Effect of edge conditions and geometric imperfections on load curve 31

Figure **3-22**: Effect of strain rate + inertia on load curve 32

Figure **3-23**: Effect of strain rate on crush strength 32

Figure **3-24**: Load curve for *t/D* = 0.00754, at different strain rate, used for *MAT_MODIFIED_CRUSHABLE_FOAM material model in section 7.1 33

Figure **3-25**: Large scale detailed model of honeycomb 35

Figure **3-26**: Homogenized unit cell and large scale FEM 35

Figure **3-27**: Energy absorption in unit cell and large scale model 36

Figure **3-28**: Energy absorption in unit cell and large scale model at hammer speed = 25 *m/s* 36

Figure **3-29**: Honeycomb ribbon orientation parallel to span of sandwich beam 37

Figure **3-30**: Load vs. midspan deflection 38

Figure **4-1**: Schematic model of the honeycomb sandwich panel used for optimization 39

Figure **4-2**: Honeycomb core sandwich model used for optimization study 43

Figure **4-3**: Load curve used in *MAT_CRUSHABLE _FOAM model 45

Figure **4-4**: Blast pressure verses time plot 46

Figure **4-5**: Sandwich panel with permissible bulges at the face plates 48

Figure **4-6**: Schematic sketch of rectangular plate 49

Figure **4-7**: Velocity field, $\mathbf{q}^1$ for a point load at the center of the square plate 50

Figure **5-1**: Three types of CCD designs (a) CCC (b) CCF and (c) CCI 54

Figure **5-2**: Flow chart of the steps followed for optimization using RSM 56

Figure **5-3**: Schematic model used for size optimization 56

Figure **5-4**: Schematic model used for size and shape optimization 56

Figure **5-5**: (a) Response surface and (b) Actual-predicted plot for δ_b minimization using size parameters 57

Figure **5-6**: (a) Response surface and (b) Actual-predicted plot for a_b minimization using size parameters 58

Figure **5-7**: (a) Response surface and (b) Actual-predicted plot for δ_b minimization using size and shape parameters 58

Figure **6-1**: Reflection of blast wave from (a) concave bulge and (b) convex bulge at front face plate 59

Figure **6-2**: Deflection of face plates with variation of core density 61

Figure **6-3**: Deflection of face plates with variation of core height 61

Figure **6-4**: Optimized sandwich panel and shape optimized monolithic plate of 150 *kg* mass for minimizing δ_b 65

Figure **6-5**: Comparison for minimum δ_b of 150 *kg* mass limit: (a) δ_b, (b) ε_{pmax} and (c) total Z-momentum 67

Figure **6-6**: Optimized sandwich panel and shape optimized monolithic plate of 150 *kg* mass for minimizing a_b 71

Figure **6-7**: Comparison for minimum a_b of 150 *kg* mass limit: (a) a_b, (b) ε_{pmax} and (c) total Z-momentum 72

Figure **6-8**: Stress (at the backface) for different density foams corresponding to same energy absorption 74

Figure **6-9**: Distribution of the *z*-strain in the *x*-*y* plane of core at the layer facing the front face, and at the layer facing the back face, respectively, for (a) δ_b -minimization, and (b) a_b-minimization 75

Figure **6-10**: Energy gained by different layers of sandwich of 150 *kg* size optimized sandwich for minimizing a_b, (a) KE, and (b) IE 77

Figure **6-11**: Energy gained by different layers of sandwich of 150 *kg* size optimized sandwich for minimizing δ_b, (a) KE, and (b) IE 78

Figure **7-1**: Strain rate in the core of 150 *kg* optimized panel for the element having maximum strain 81

Figure **7-2**: Model for delamination study 83

Figure **7-3**: Delaminations in sandwich 85

Figure **7-4**: Comparison of δ_b at different delamination case 85

Figure **7-5**: Model details for off-center hammer travel to crush the honeycomb 86

Figure **7-6**: Effect of off-center crushing on load curve 87

Figure **7-7**: Model details for crushing the core when hammer travel at an angle to transverse direction 88

Figure **7-8**: Effect of crushing at an angle on load curve 89

LIST OF TABLES

Table **3-1**: Material properties of the honeycomb unit cell model 16

Table **3-2**: Candidates for creating response equation 24

Table **3-3**: Load curve parameters at different design points 25

Table **3-4**: Validation of crush strength 34

Table **4-1**: Material properties of Aluminum 5052 used in *MAT_PLASTIC_Kinematic input card for the face plates 44

Table **4-2**: Material properties of the honeycomb core (for t/D = 0.02677) made from Aluminum 5052-foil and used in *MAT_CRUSHABLE_FOAM model 44

Table **4-3**: Blast load parameters 47

Table **6-1(a)**: Design limits for {t_b, t_f, h, t/D}-optimization, min δ_b 62

Table **6-1(b)**: Optimization results for {t_b, t_f, h, t/D}-optimization with varying mass limits, min δ_b 63

Table **6-2(a)**: Design limits for {t_b, t_f, h, t/D, s_b, s_f}-optimization, min δ_b 63

Table **6-2(b)**: Optimization results for {t_b, t_f, h, t/D, s_b, s_f }-optimization with varying mass limits, minδ_b 63

Table **6-3(a)**: Design limits for {t_p, s_b, s_f}-optimization, min δ_b 64

Table **6-3(b)**: Optimization results for {t_p, s_b, s_f}-optimization with varying mass limits, minδ_b 64

Table **6-4(a)**: Design limits for {t_b, t_f, h, t/D}-optimization, min a_b 69

Table **6-4(b)**: Optimization results for {t_b, t_f, h, t/D}-optimization with varying mass limits, min a_b 69

Table **6-5**: Optimization results for {t_p, s_b, s_f}-optimization with varying mass limits, min a_b 70

Table **6-6**: Comparison of honeycomb core energy absorption efficiency 74

Table **6-7**: Energy absorption in the sandwich 76

Table **6-8**: Stiffener mass sensitivity for 150 *kg* size optimized sandwich for δ_b minimum 79

Table **7-1**: Strain rate effect on the performance of 150 *kg* optimized sandwich and monolithic plate 82

Table **7-2**: Material properties of the bonding material for 150 *kg* size optimized sandwich δ_b minimum 84

LIST OF NOMENCLATURE

D	=	distance between opposite wall of honeycomb cell
t	=	thickness of honeycomb cell wall
h	=	honeycomb core depth
α	=	angle between honeycomb cell wall
$2H$	=	folding wavelength
σ_0	=	flow stress
σ_y	=	yield stress
σ_{sc}	=	static crush stress
$\sigma_{dc\text{-}wsr}$	=	dynamic crush stress with strain rate effect
$\sigma_{dc\text{-}wosr}$	=	dynamic crush stress without strain rate effect
$\sigma_{dc\text{-}wsr\text{-}woi}$	=	dynamic crush stress with strain rate effect but without inertia effect
$\boldsymbol{x}^L$	=	lower limit on design variables
$\boldsymbol{x}^U$	=	upper limit on design variables
$\boldsymbol{G}$	=	vector of x-, y-, z- coordinates of nodes in FE model
$\boldsymbol{q}^i$	=	i th velocity field or trial shape change vector
N_{dv}	=	Number of design variables
δ_b	=	Peak displacement of the backface plate relative to stiffener
a_b	=	Peak rigid body acceleration of the backface plate
ε_{pmax}	=	Maximum effective plastic strain
t_{f}	=	thickness of the front face plate
t_{b}	=	thickness of the backface plate
s_{f}	=	bulge height in the front face plate
s_{b}	=	bulge height in the backface plate
t_{p}	=	thickness of the monolithic plate

M	=	total mass of the sandwich
M_f	=	mass of the front face plate
M_c	=	mass of the honeycomb core
M_b	=	mass of the backface plate
M_{st}	=	mass of the stiffener
l	=	half side length of the square sandwich panel
η	=	core efficiency
ρ_f	=	mass density of face plates
ρ_c	=	mass density of core
p_z	=	total z-momentum of the sandwich
IE	=	internal energy
TIE	=	total internal energy of the sandwich
CIE	=	core internal energy
TE	=	total energy
KE	=	kinematic energy

ACKNOWLEDGEMENTS

I am highly indebted to my advisor Professor Ashok D. Belegundu for his invaluable support and guidance throughout this research. I would like to express my sincere thanks to him for allowing me to continue my PhD study even after I took up a job at Brookhaven National Laboratory, NY. I can't forget his immense help to hold meetings in the weekends, odd hours to suit my convenience. I am also thankful to my doctoral committee members; Prof Panagiotis Michaleris, Prof. Christopher D. Rahn and Prof. Ali M. Memari for their valuable comments and suggestions.

I specially thank Anand Kumar Singh for his technical support, cooperation and participation in numerous technical discussions in this research work. Thanks to computational support from the High Performance Computing group at Penn State under Mr. Vijay Agarwala. I also thank Jenny Houser for her special effort to my admission in to PhD study.

I would like to acknowledge partial financial assistance from USA Army Research Office and partial tuition assistance from Brookhaven National Laboratory.

I am deeply thankful to my wife and son for their support and patience during my PhD study. I also thank my parents, brother and sister for their support and encouragement.

Finally, I thank Michael Mapes, my supervisor at Brookhaven National Laboratory for allowing me to continue my PhD study. Encouragements from my colleagues and many friends are greatly appreciated.

Chapter 1

INTRODUCTION

1.1 Introduction

Design and development of blast resisting structures for civilian and military applications has always been of great interest to engineering communities and government agencies. Blast protection applications include protection of land vehicles, ships, helmets, explosive storages, packaging etc. Blast overpressure can directly crush the protective structure and cause injury to the occupants or it can transmit high inertial loads which can cause traumatic injury and/or loosen structural attachments which then become high speed flying debris. Irrespective of the type of application, one key aspect that makes the structure blast resistant is its ability to absorb energy inelastically without failure. Sandwich composites are formed by spacing multiple layers of various alloys such as steel, metallic cellular structure, ceramic, kevlar etc. This composite can afford blast protection by dissipating the energy of the impact and/or blast while subsequently preventing penetration of fragments from the blast. A sandwich-structured composite with a cellular core (mostly honeycomb or aluminum foam) is considered herein. The cellular core has the ability to absorb the impact energy of the blast or crash by undergoing large plastic deformation at almost constant nominal stress. This characteristic of the cellular core results in significant reduction in transmitted stress and thereby mitigates the damage causing potential of the blast impulse. Though metal sandwich panels have been used for a long time in aircraft and other light weight structures to maximize the bending stiffness per unit density, only recently have researchers begun investigating the possible use of sandwich panels for blast protection. While the design optimization of monolithic structures for blast protection use have been studied well [1], metal sandwich panels are relatively less understood for blast mitigation. Maximum crash protection can be obtained by optimizing various parameters associated with the sandwich.

The sandwich panel consists of three layers in which a low to moderate stiffness cellular core such as honeycomb or foam, is embedded between two stiff face plates. Depending upon the application, different material combination of face plate and core can be used. Metal face plates with high failure plastic strain are preferable. Face plates are attached to the core by an adhesive layer (Figure 1-1). Sometimes in case of metallic sandwich panel, face plates are brazed to the core for high strength application. Shaped honeycomb core sandwich panels are also manufactured, shown in Figure 1-2 [28].

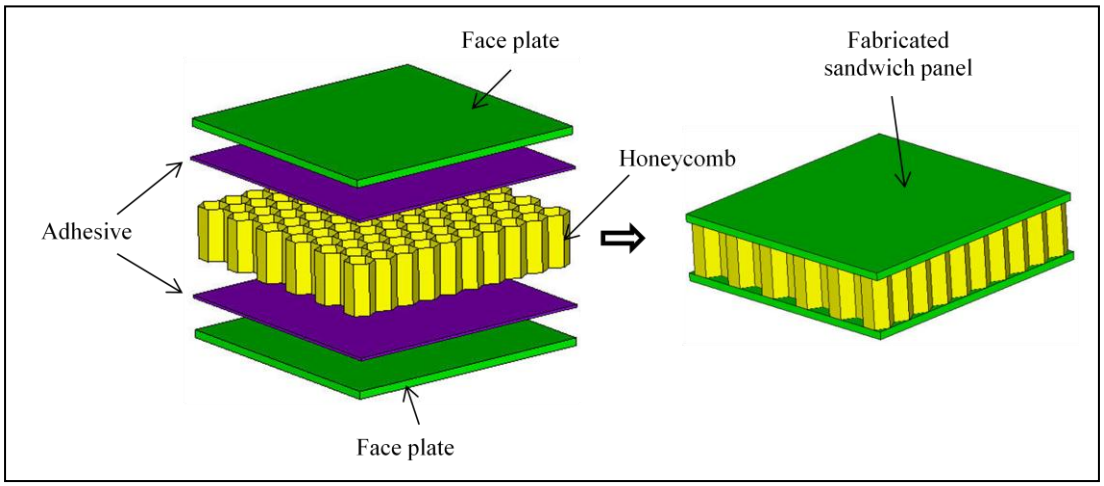

Figure **1-1**: Typical configuration of a honeycomb sandwich panel

Higher core depth in combination with two stiffer face plates provides high bending stiffness to weight ratio. For blast and crash application the core which acts as a sacrificing layer absorbs large amount of impact energy by undergoing cyclic plastic buckling deformation. The adhesive or brazing joint must rigidly attach the face plates to the core.

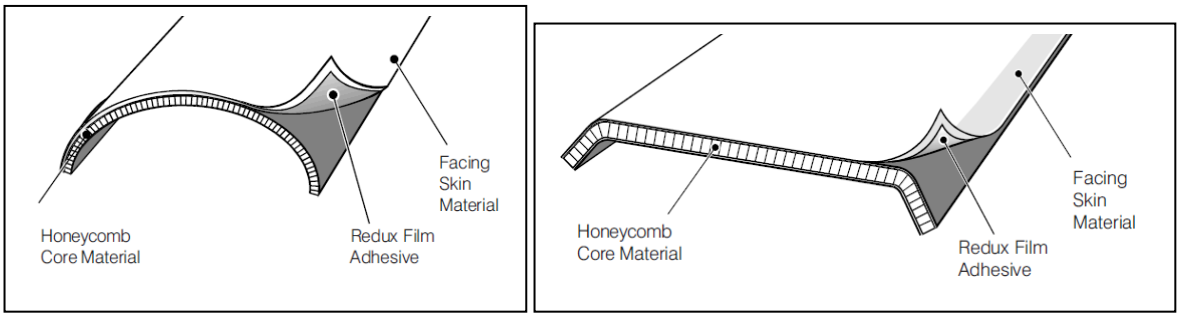

Figure **1-2**: Shaped honeycomb core sandwich panel [28]

This dissertation investigates the optimization of the honeycomb core sandwich panel for minimizing the backface plate deformation and backface plate acceleration subjected to air blast loading. Simultaneous optimization with several variables is necessary to capture interacting physics which include: (1) too thin a front face plate will result in a concave deformation under load that will increase the momentum on the structure which is detrimental, (2) front face plate facing the blast must transfer the blast impact to a larger area of the core, and also deflect the blast wave. The former can be achieved by providing sufficient thickness to the face plate and the latter by giving a suitable shape to the face plate., (3) backface plate must have sufficient stiffness to provide proper back support to the core and enable crushing, (4) the core must have the correct density so as to stiff enough to minimize peak backface displacement or to absorb energy, without densification, to minimize acceleration, (5) total mass and space or envelope constraints must be satisfied, and (6) face plates must be thick enough to maintain structural integrity. The challenge is to optimize the honeycomb core and face plate parameters simultaneously for maximizing protection.

This optimization work presented in this dissertation involves both size and shape of the face plates, size of the honeycomb core and core cell size. A design of experiments (DOE) based response surface optimization method in combination with LS-DYNA is used to minimize either dynamic deflection or acceleration of the backface plate. Constraints on mass and on plastic strain in the face plates are imposed. Design Expert software is used to create response equations from the function values

determined from sampled points based on central composite face centered design method. The response equations are used in FMINCON, a gradient based optimizer in MATLAB optimization toolbox, for optimization. A clear cut comparison between monolithic metal plates and sandwich plates for the same loading and failure criteria is also presented here.

Finite element modeling of each hexagonal cell of a large honeycomb core panel in LS-DYNA will generate a prohibitive large number of nodes and degrees of freedom. Here, the core is modeled as a homogenized solid plate of equivalent mechanical properties, determined by virtual testing. Virtual testing is carried out in LS-DYNA to study the crush behavior (or load curve) of a unit honeycomb cell under quasi-static impact load. The effect of different geometric parameters describing the honeycomb core on its crush behavior is analyzed, and relevant mechanical properties including the crush behavior is parameterized in terms of the most important honeycomb parameters. The mechanical property of the honeycomb core is modeled in LS-DYNA using the crushable foam model. The homogenization model has been corroborated with available formulas in the literature and commercially available data, and with detailed FE models of test specimens.

1.2 Dissertation organization

Chapter 2 presents literature reviews about the work done on sandwich structures for blast and crash protection, and on honeycomb structure crush strength. This covers the results obtained from experimental investigation, numerical simulation and analytical modeling.

In Chapter 3 homogenization of honeycomb structure via virtual testing is presented, including validation. Sensitivity study on honeycomb crushing characteristic covering different parameters are also done in this chapter. Optimization problem description and finite element modeling are covered in chapter 4, followed by the optimization procedure in Chapter 5. In Chapter 6, optimization results are discussed and interpreted. Preliminary studies involving strain rate effect, delamination and unit

cell crushing at an angle and by off-center load are given in Chapter 7. Conclusions and future work are given in Chapter 8.

Chapter 2

Literature Review

2.1 Introduction

Earlier, a study carried out in our group by Argod et al showed that the shape of a monolithic aluminum plate can be optimized to reduce dynamic displacement under blast [1]. They developed a robust methodology based on coupling Differential Evolution (DE) to LS-DYNA to minimize the plate's root mean square (RMS) displacement subjected to mass and maximum plastic strain constraint. The optimum shape had convex bulges on the front and back (front refers to charge side). This bulge deflects the blast and stiffens the plate, thereby mitigating the blast effect. The optimum shape also resulted in smearing of the plastic strain indicating better utilization of material. Although the shaped plate performed very well compared to the flat plate, greater blast resistance can be offered by using sandwich structures especially with respect to transmitted forces.

2.2 Past work on sandwich panels

Xue and Hutchinson [3] compared the performance of sandwich panels (such as pyramidal truss core, square honeycomb and folded plate) to a solid plate (monolithic plate) of equal weight for blast resistance. Square honeycomb and folded plate outperformed the pyramidal truss core, but all three sandwich panels were capable of offering higher blast resistance compared to the solid plate. Further, the sandwich panels were found to be more effective in water than in air, due to fluid structure interaction. A limited optimization study was carried out, which did not consider material failure, shape and certain core parameters. Their study showed that sandwich panels are promising structures for blast resistance and more research should be carried out for their effective use. Fleck and Deshpande [4] developed an analytical methodology to analyze the dynamic response of metallic sandwich beams subject to both air and water blasts. Their finding on the basis of simple analytical

formulas matched well with the result from Xue and Hutchinson's [3] three-dimensional FE calculations.

Yen, Skaggs and Cheeseman [5] carried out both experimental and computational analyses to study the effect of honeycomb crush strength on the dynamic response of a honeycomb core sandwich pendulum system. The result indicated that total impulse of the system increased due to concave deformation of the front face plate. Numerical results indicated that significant reduction in maximum stress amplitude propagating within the core can be achieved by suitable selection of honeycomb material with proper crush strength. It is understood that suitable shape of the front face plate can reduce the concave deformation and hence the total blast impulse. Numerical analyses carried out in LS-DYNA using ConWep air blast function validated the experimental result. Hanssen et al [6] performed similar tests on aluminum foam core sandwich panels with results similar.

Main and Gazonas [7] investigated the uniaxial crushing of a cellular sandwich plate subjected to air blast. This study was aimed to mitigate the shock transmission by suitably distributing the mass among the face plates and the core for a given mass of the sandwich. Fluid structure interaction (FSI) has also been considered. It is stated that the capacity of sandwich plate to mitigate shock transmission is limited by the critical impulse requited to produce complete crushing (or densification mentioned in the paper) of the core. After complete crushing of the core, the stress (or shock) transmitted to the backface plate gets amplified. The shock mitigation can be improved by increasing the mass fraction of front face and the core. At the same time too much reduction in mass fraction of the backface plate leads to increased backface acceleration. So, an optimization study was carried out to find the optimal mass distribution to maximize the impulse absorption while limiting the backface acceleration. While this study considered the effect of face plate thicknesses and core depth in designing a sandwich plate for blast shock mitigation, it did not consider parameter related to the core.

Chi et al [8] experimented to study the effect of core height and face plate thicknesses on the response of honeycomb sandwich panels under blast loading. Experiments showed that prior to densification, the core provided structural support to the front plate and regulated the stress transferred to the backface plate. Once the onset of core densification starts, higher stresses are transferred to the backface plate which exhibited steeply increasing deflection. The impulse required for onset of core densification increases with increase in core thickness. Deformation of face plate increases with decrease in its thickness and too much thinning results in tearing of the plates.

Zhu et al [9] used a ballistic pendulum test to investigate the structural response of honeycomb core sandwich panel under blast loading and validated the result with FE analysis. They found that thick face plates with relative high density honeycomb core sandwich structure significantly reduces the back plate deformation subjected to blast and, for a given panel configuration, the backface deflection increases with impulse, approximately linearly. Indenting or pitting failures at the center of front face plate, and large inelastic deformation at the center of backface plate are observed.

Zhu et al [24] also did the same study for aluminum foam core sandwich panel. Delamination crack occurred at the center of the panel in the foam core near to the front face plate. Deformation pattern of the panel before and after delamination is explained nicely. In both foam [24] and honeycomb core [9], no delamination is found near to the backface plate. A parametric study is also presented to explain the energy absorbing behavior of the sandwich panel. In addition Zhu et al [10] carried out a limited optimal design study of the honeycomb sandwich panel. For same mass and exposed area (to the blast) of the panel, square size panel results maximum deformation of the face plates. The panel shows similar response with independent variation of the core density and the core height for a given mass of the panel. To keep the total mass constant, mass of the face plates is adjusted. For each case, optimum core density and core height is found. The response of the sandwich panel to the blast impulse has been split in to three phases [10]. In stage I, the blast impulse is delivered to front face

plate of the sandwich, and the front face plate attains initial velocity, v_0 (Equation 2.1) while the core and backface plate remains stationary. So, for a particular impulse, lower is the front face plate thickness, higher is the KE, W_I (Equation 2.2) of the front face plate which is subsequently transferred to the sandwich. In stage II, the core is compressed and backface plate deforms. Then the whole sandwich attains an identical velocity. The KE, W_{II} at the end of this stage is given in Equation 2.3. Hence the energy absorption in core is given in Equation 2.4. In stage III, finally the structure is brought to rest by plastic bending and stretching. Using Equation 2.4 various parameters can be determined for maximum energy absorption in core; however paper has not discussed anything about the force transmitted through the core which is very important for blast protection.

$$v_0 = \frac{I}{A\rho_f t_f} \tag{2.1}$$

$$W_I = \frac{I^2}{2A\rho_f t_f} \tag{2.2}$$

$$W_{II} = \frac{I^2}{2A(\rho_f t_f + \rho_f t_b + \rho_c h)} \tag{2.3}$$

$$IE_c = W_I - W_{II} \tag{2.4}$$

Karagiozova et al [11] carried out numerical analyses to prove the sandwich structure's potential application as a blast resisting structure. It states that the optimum sandwich configuration depends upon the applied blast load and, an optimum structure compromises between energy absorption of the core and the load transfer to the backface plate of sandwich. For same load, the acceleration of the backface plate depends upon its mass. Paulius et al [27] investigated the structural response of polypropylene honeycomb core sandwich panel by both experimental testing and numerical analysis. Parametric study on energy absorption using different mass fraction of face plates and core showed

that honeycomb core absorbs 50% - 95% energy of all sandwich structure, the front face plate facing the blast absorbs between 7% - 35% and backface plate the least.

Avalle et al [23] examined the energy absorption characteristics of polymeric foams through energy absorption diagram method and efficiency diagram method. Foam efficiency is defined in Equation 2.5. Maximum efficiency indicates maximum energy absorption per unit volume while transmitting a specified stress, defined as per design requirement. Alternatively we can say, foam which can absorb higher energy while transmitting less stress is efficient. The efficiency diagram method is very useful to characterize the material and to design energy-absorbing components.

$$E = \frac{\int_0^{\varepsilon} \sigma d\varepsilon}{\sigma} \tag{2.5}$$

2.3 Past work on crush stress of honeycomb cells

Yamashita and Gotoh [12] studied the impact behavior of honeycomb cells through numerical simulations and experiments. Numerical simulation using a single 'Y' cross-sectional model predicted the crush behavior, quite well, using appropriate boundary conditions at the edges. Crush strength increased with foil thickness and the branch angle. However highest crush strength per unit mass was obtained when cell shape is of regular hexagon. Changing the branch angle from 180^0 to 30^0 can result 1.5 times increase in crush strength, which implies that functionally gradient honeycomb material in crush strength can be fabricated by suitably changing the branch angle. Experiment shows that crush strength increased with hammer travel which can be attributed to the air pressure enclosed in the honeycomb. Results from experiments with drop hammer velocity 10 *m/s* and its corresponding quasi-static experiment are very similar. T. Wierzbicki [13] developed a method for determining the crushing strength of regular hexagonal cell structures subjected to axial loading in terms of the cell diameter, foil thickness and the flow stress. The method is based on energy considerations in conjunction with a minimum principle in plasticity. In order to analyze the

crushing behavior, one representative element positioned at the junction of three neighboring cells is considered here. The mathematical model is based on the fact that, a part of the adhesive bond adjacent to the vertical edge is broken, and the two plates are partially torn off (peeling off). The problem is shown to be equivalent to the analysis of a system of collapsing angle elements (without sharp edges) undergoing bending and extensional deformations. Total plastic energy calculated for the above deformation is minimized with respect to the half wave length (of the cyclic folding of cells) and rolling radius. The crush strength is expressed in terms of an average flow stress of the material which is higher than yield stress and smaller than ultimate stress. The result from this analytical solution is well matched to the experimental results. The accuracy of crush strength determined by using Wierzbicki's relation depends upon the precise prediction of the flow stress (expressed in terms of the ultimate stress) of the material. Flow stress is greater than yield stress but less than ultimate stress.

Zhang and Ashby [14] analyzed the collapse behavior of the honeycomb under both axial compression and in plane shear load. Buckling, debonding and fracture are identified as possible collapse mechanisms. For flexible honeycombs such as those made from Nomex, buckling and fracture are dominant mode of failure in simple axial compression test, but for rigid-plastic honeycombs (made from aluminum), buckling and plastic yielding dominates. Depth of the honeycomb has no effect and cell angle has little effect on out-of-plane strengths (compressive and shear). These strengths are highly sensitive to the density of the honeycomb. With increase in density, failure switches from buckling to debonding in shear and buckling to fracture in compression. It is also found that out-of-plane loading has little effect on in-plane failure and vice versa. For a given density, honeycomb shows greater axial strength than foams, but foams shows better heat insulation than honeycomb. Metal foam is a cellular structure consisting of a solid metal, and a large volume fraction of gas-filled pores. Wu and Jiang [15] performed both quasi-static and high speed impact (up to 28.14 *m*/s) crush test on six types honeycomb cellular structure. They mentioned that smaller cell

size, short height honeycomb made from high strength material has high energy absorbing capacity. The test shows that crush strength is proportional to the initial striking velocity.

Crush stress of different sizes of commercially available honeycomb panels is given in *Hexweb honeycomb attributes and properties* data sheet [16].

Past research indicate that sandwich structures have potential to serve as blast resisting structures. Further, the papers clearly indicate that (1) densification in the core should be avoided to reduce the transmitted force, (2) shock mitigation and reduction in backface plate deflection can be achieved by using thicker front face plate and (3) thinner backface plate would increase its acceleration. Most of the published results are based upon parametric studies taking one or two parameters at a time. As a result, a methodology for detailed design, giving specific mass distribution in the sandwich, has not been published. In this dissertation, optimization study is carried out within a more general framework, where several design variables are considered simultaneously. A key step is use of a validated virtual testing based approach to homogenize the nonlinear stress-strain curve of the honeycomb, which also can be applied to other types of cellular core. Finally, one-on-one comparison between a sandwich and a monolithic plate presented here is new.

Chapter 3

Homogenization of Honeycomb Structure via Virtual Testing

The honeycomb cells could be regular hexagon or any modified version of it such as OX type, reinforced hexagonal type, flex type, double-flex type and tube type [16]. A cell with four equal side faces is referred as a square honeycomb. Each type has its special use in specific applications. The honeycomb core of different materials is commercially available. Some common materials are aluminum, fiberglass and Aramid fiber (Nomex, Kevlar and KOREX). Special honeycomb made from carbon and polyurethane is also available. In our study, Al5052 regular hexagon honeycomb cell is considered.

Finite element modeling of the honeycomb cellular core requires a high density mesh to capture the cyclic plastic buckling deformation accurately under axial compressive loading. Element size along the depth of the honeycomb should be sufficiently small enough to allow the cyclic folding of the cells to take place as it would do in the experiment. However high element density leads to high computation time and iterative finite element analysis of honeycomb sandwich structure with hundreds of cells would be computationally impossible. Thus, it is the best to substitute the discrete honeycomb cellular core by a homogenized solid plate of equivalent mechanical properties. Here, homogenized properties are determined using virtual testing method. As the name implies, virtual testing (VT) is a computer based finite element analysis technique to replace expensive mechanical tests. VT is used in the past to predict the material properties accurately [33] and subsequently used to homogenize the material [32]. Here, a unit cell of the honeycomb is modeled in LS-DYNA for VT.

3.1 Finite element modeling of the unit cell

Figures 3-1 and 3-2 show the hexagonal cell structure and its unit cell. The simplest repeating unit in this structure is a 'Y' shape, which is known as the unit cell. Unit cell has one side double wall and two side single walls. In double wall, two layers of foil are glued by adhesive. Finite element model of the unit cell is shown in Figure 3-4. The foil is modeled by quadrilateral Belytschko-Tsay shell elements, and the 0.01 *mm* thick layer of adhesive at the double wall is modeled by solid elements. Symmetric boundary conditions (B.Cs) are applied along all the edges of the foil (Figure 3-3), bottom areas are fixed and displacement load (crushing) is applied to an external rigid surface (like a drop hammer) which hits the top areas and moves with them. The main role of the top and bottom face plate is to contain the crushed honeycomb foil. In the actual mechanical test, a heavy steel hammer is used to crush the honeycomb. To replicate the actual test, the rigid surface is modeled using the rigid shell element and the mechanical properties are defined as that of steel but with a high fictitious density (Table 3-1). Al5052 aluminum alloy with bilinear isotropic-hardening inelastic material model is used for the foil (Table 3-1). Since the yield and ultimate strength of the Al5052 foil are very close, bilinear inelastic material model with very low tangent modulus is a reasonable approximation. For the adhesive, perfectly plastic material model is adopted (Table 3-1). *AUTOMATIC_SINGLE_SURFACE contact is applied to the model with sliding and sticking frictional coefficients equal to 0.2 and 0.3, respectively. These mechanical properties of the foil and the adhesive, and friction coefficient values are obtained from the literature [12]. All the tests are carried out at a hammer speed of 80 *mm/s* along the depth of the honeycomb, which can be considered as quasi-static tests since impact test involves very high hammer speeds in the order of *m/s*.

Mass scaling

In explicit method, the time step usually is kept small to maintain numerical stability. However, small step size increases the CPU cost. Here, to reduce the CPU cost and improve the performance, mass scaling is used to increase the time step size in each cycle. Unit cell is modeled in the unit of *mm*, material stress and stiffness parameters are defined in N/mm^2 (*MPa*), and density is defined in kg/mm^3. For consistent units, density should be defined in the unit of $tonne/mm^3$. So, here mass is scaled up by 1000 times. Since the loading rate is very small (80 *mm/s*), which is being treated as quasi-static test, it is expected that mass scaling would not affect the result.

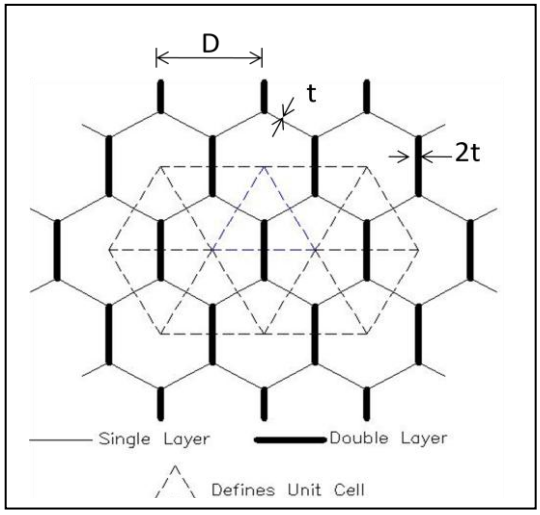

(a)

Figure **3-1**: Honeycomb cell geometry

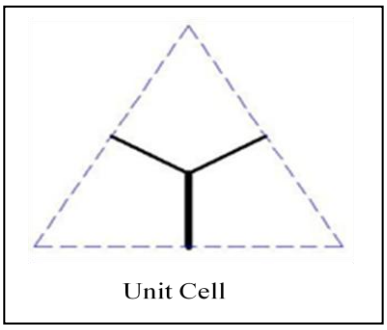

(b)

Figure **3-2**: Unit cell

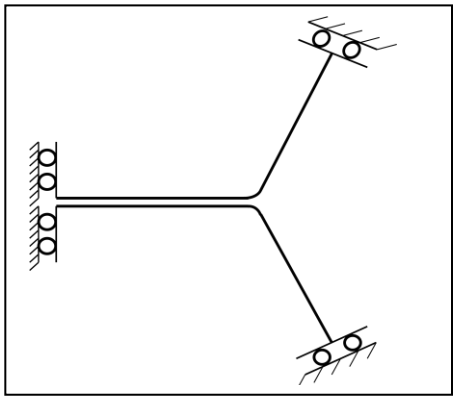

Figure **3-3**: Boundary conditions on the unit cell

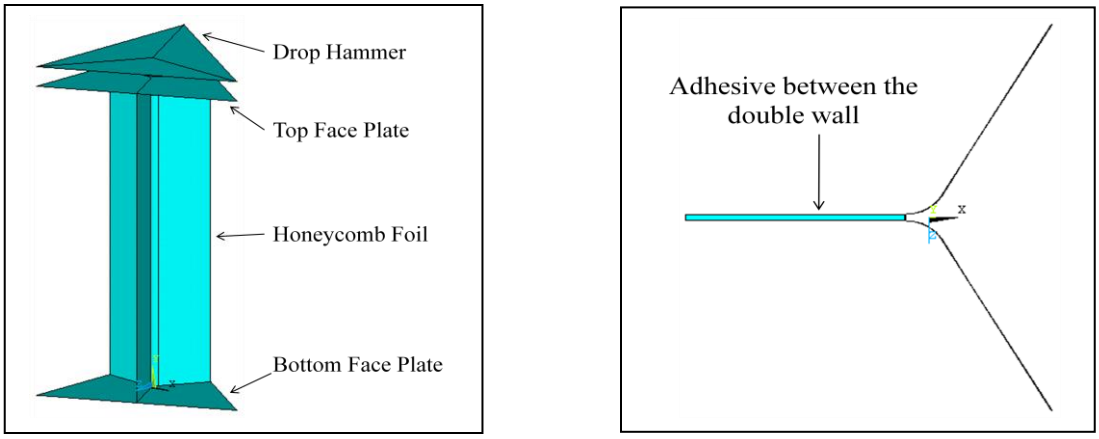

Figure **3-4**: Finite element model of the honeycomb unit cell

Table **3-1**: Material properties of the honeycomb unit cell model

Material	Density *(kg/ m^3)*	Young's Modulus *(GPa)*	Yield Stress *(MPa)*	Tangent Modulus *(MPa)*	Poison's Ratio
Foil-Al5052	2680	72	300	50	0.34
Adhesive	2000	5	30	0	0.3
Drop Hammer-Steel	288E5	200	-	-	0.24

3.2 Virtual testing results

Figure 3-5 and 3-6 shows a typical crushing phenomenon and its load curve obtained from the test. As the hammer travels, buckling of the foil starts from near the impact edge and propagates downward. Figure 3-6 shows the variation of nominal compressive stress with the volumetric strain. Compressive stress is defined as the reaction force experienced by the hammer divided by the unit cell area and the volumetric strain is calculated by the change in core depth divided by its original value. The core resists buckling until the peak stress point and then the first onset of buckling (Figure 3-5 (a)) starts which causes a sudden drop in the compressive stress. Compressive stress drops until the first folding of the cell wall is complete (Figure 3-5 (b)) and then stress increases. The similar

process goes on (though the peaks are very small in comparison to the first peak) until the whole depth of the honeycomb is folded. The crush stress is the average of the oscillatory stress during the cyclic collapse of the foil. Once the entire core is folded, then densification starts resulting very high compressive stress. The crush stress is a vital property which reduces the blast shock transmission by absorbing the energy. Large amount of energy gets dissipated through the plastic deformation of the cell wall at each folding. Higher depth of the honeycomb would produce more folds, thus increase energy absorbing capacity. Although sufficient care has been taken in approximating the load curve, it is not possible to define the crush start and end strain very accurately.

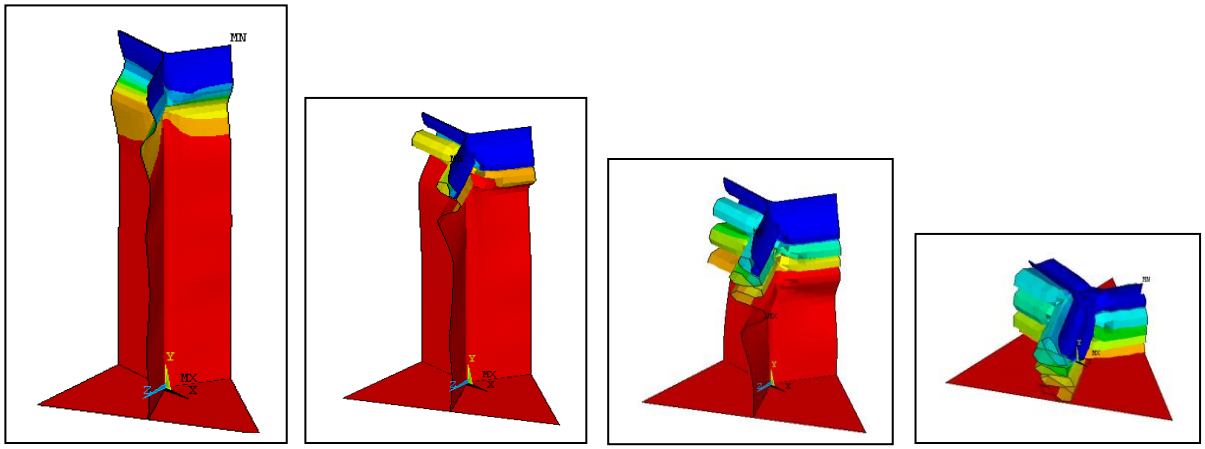

(a) (b) (c) (d)

Figure **3-5**: Different stages of honeycomb unit cell crushing

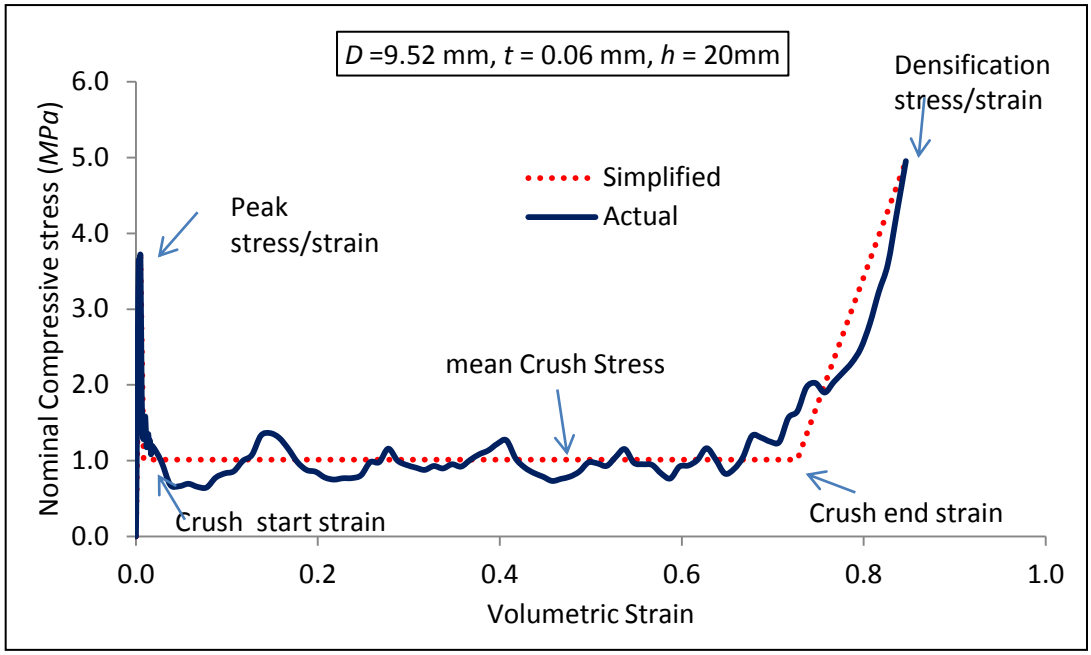

Figure **3-6**: Load curve and its associated parameters of the honeycomb core

3.2.1 Mesh convergence study

Three different element sizes (Figure 3-7) are used to study their effect on the load curve. Element size along its depth should be sufficiently small enough to allow the cell wall to fold in a natural way. No noticeable change in load curve is observed when element size is decreased from 0.5 *mm* to 0.25 *mm*.

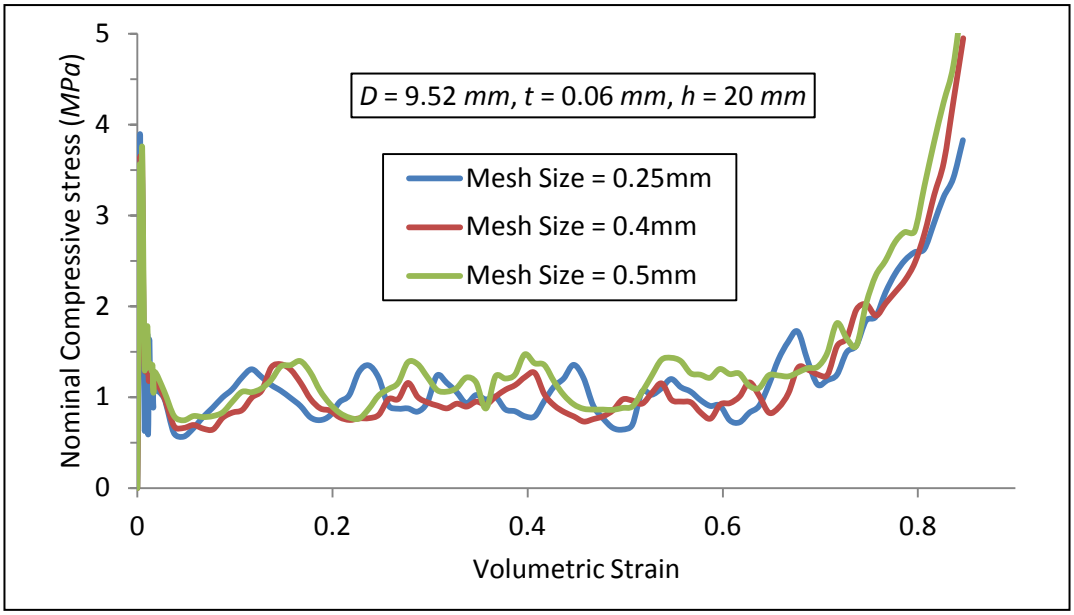

Figure **3-7**: Effect of mesh size on the load curve

3.2.2 Effect of cell dimensions on the folding wavelength

Folding length (2H) refers to the length of the honeycomb along its depth to create a single fold. Folding wavelength (Figure 3-8) which is a function of the cell size and the foil thickness is given in Equation 3.1 [13]. Here, it is calculated as per Equation 3.2. It is more sensitive to the cell size than the foil thickness. Precise evaluation of the folding length is vital as it controls the crush strength. Wierzbicki [13] considered that the main constituent of the collapsing cell is the angle element which deforms by developing stationary and moving plastic hinges. Since the strength of the adhesive is smaller than the foil, folding takes place when the two plates adjacent to the bond are partially torn off. For accurate prediction of the crush behavior, the smallest size of the element along the depth of the honeycomb should be smaller than the half of the wavelength (2H). In all the tests, element length of 0.4 *mm* is taken along the honeycomb depth. Figure 3-9 and 3-10 shows the comparison between the wavelengths obtained from the FEA and the analytical equation [13]. The small deviation can be

attributed to the end effect and the role of the adhesive strength which aren't considered in the analytical formulation.

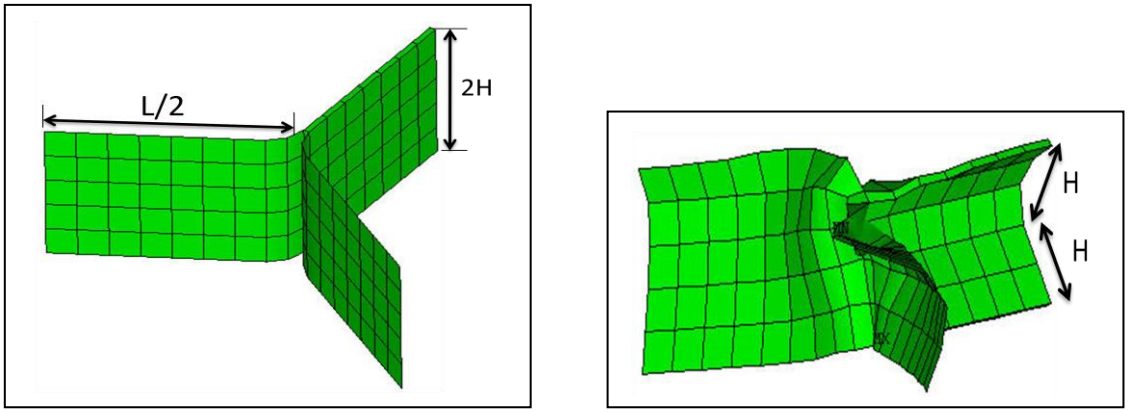

(a) (b)

Figure **3-8**: (a) Typical folding panel and (b) deformation of the folding panel

$$2H = 2 \times 0.821 \times \left[\frac{t \times D^2}{3}\right]^{1/3} \quad (3.1)$$

$$2H = \frac{Core\ depth}{Number\ of\ foldings} \quad (3.2)$$

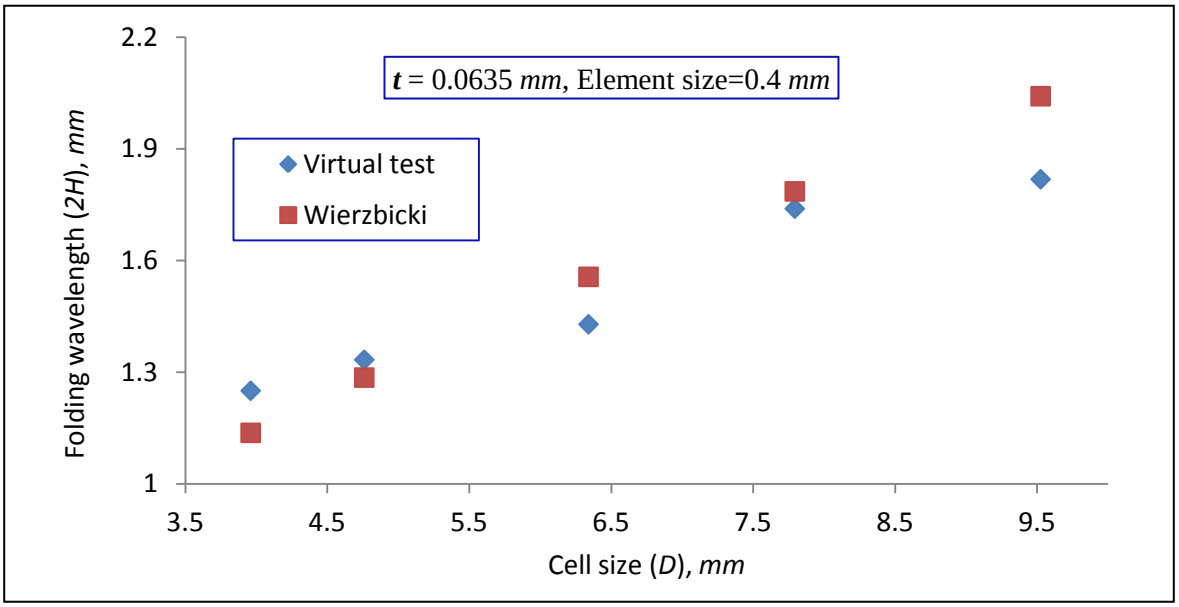

Figure **3-9**: Comparison of the folding wavelength at different cell size

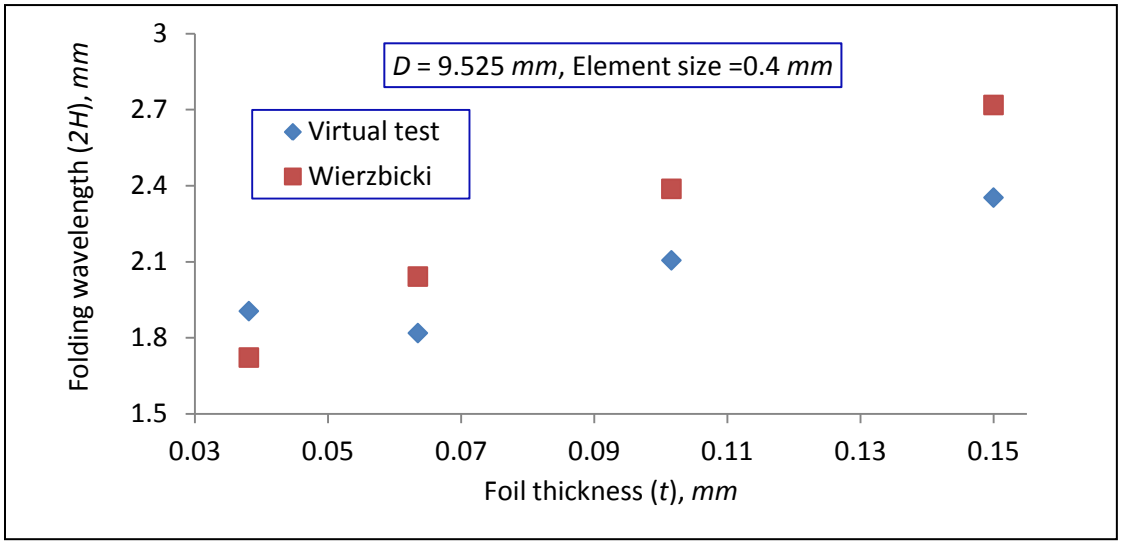

Figure **3-10**: Comparison of the folding wavelength at different foil thickness

3.2.3 Effect of honeycomb cell geometry on the load curve

Following parameters of the honeycomb cell geometry affect its loading curve.

1. Foil thickness, *t*
2. Cell size, *D*
3. Branch angle, *α*
4. Core depth, *h*

Since the regular hexagon cell ($\alpha = 120^0$) gives highest crush strength per unit mass [12], subsequent studies are carried out for the regular cell only. The magnitude of the load curve changes significantly with *D* (Figure 3-11) and *t* (Figure 3-12), but the nature of the curve remain the same. Any change in *D* and *t* alter the mass density of the honeycomb, so load curve is a function of the mass density. Load curve doesn't show any visible change (Figure 3-13) with the core depth. Load curve for *h=5 mm* doesn't show any noticeable ripples during crushing. Such a low core depth doesn't allow sufficient number of folds to occur and hence attains densification very fast.

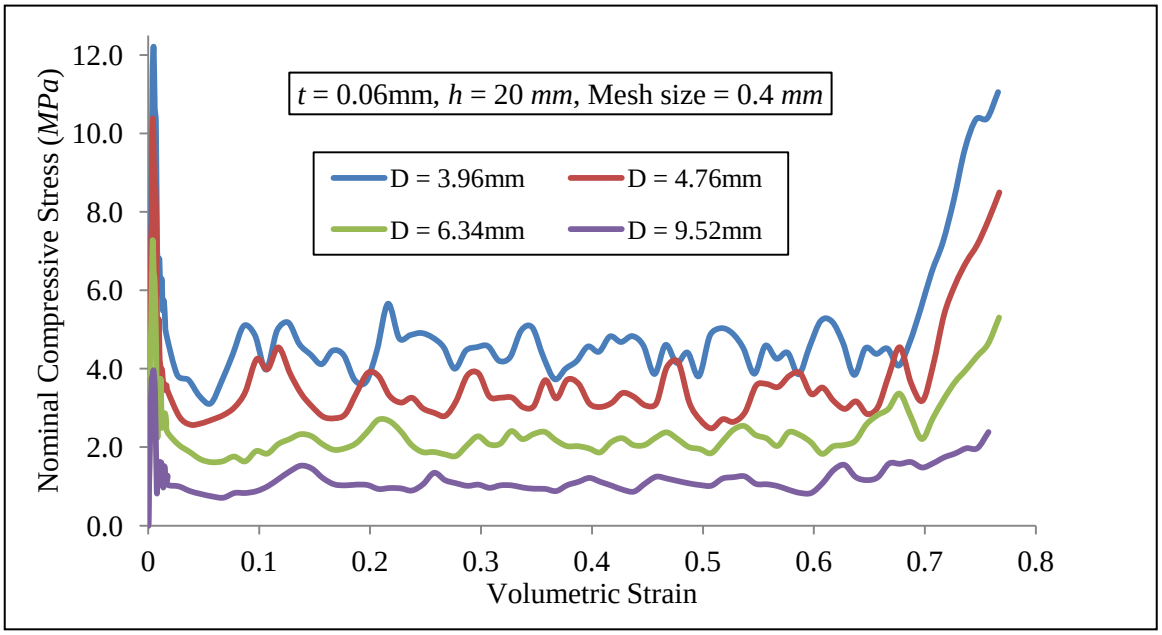

Figure **3-11**: Effect of the cell size *(D)* on the load curve

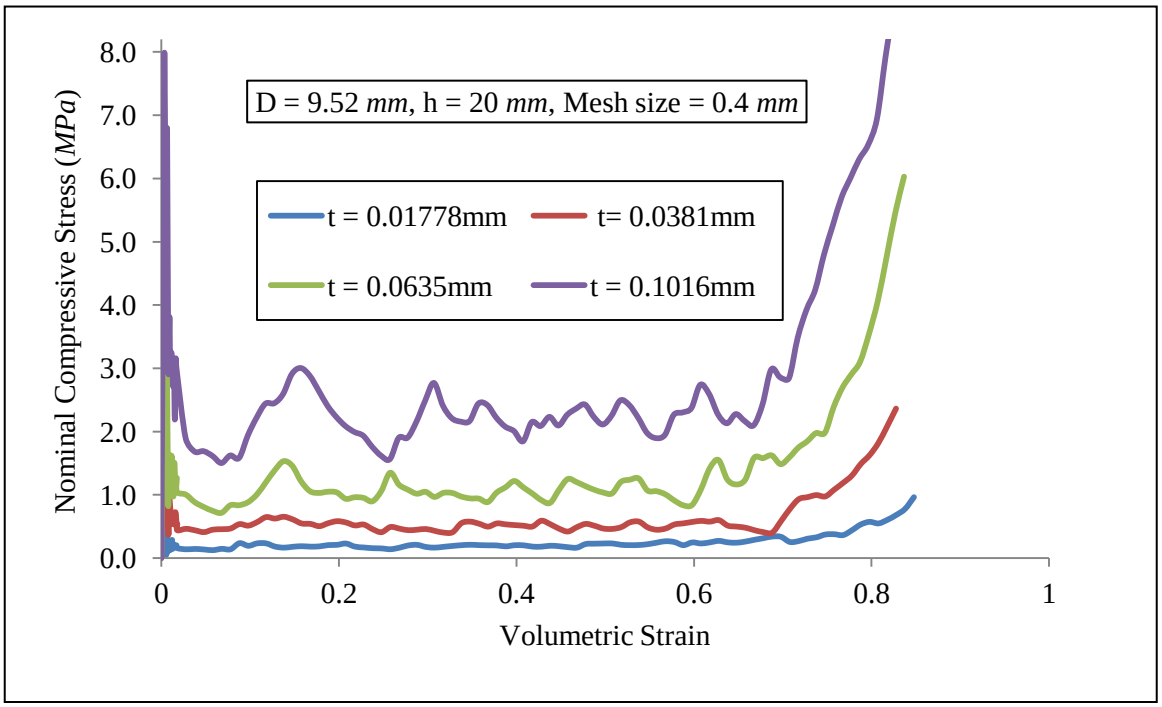

Figure **3-12**: Effect of the foil thickness (*t*) on the load curve

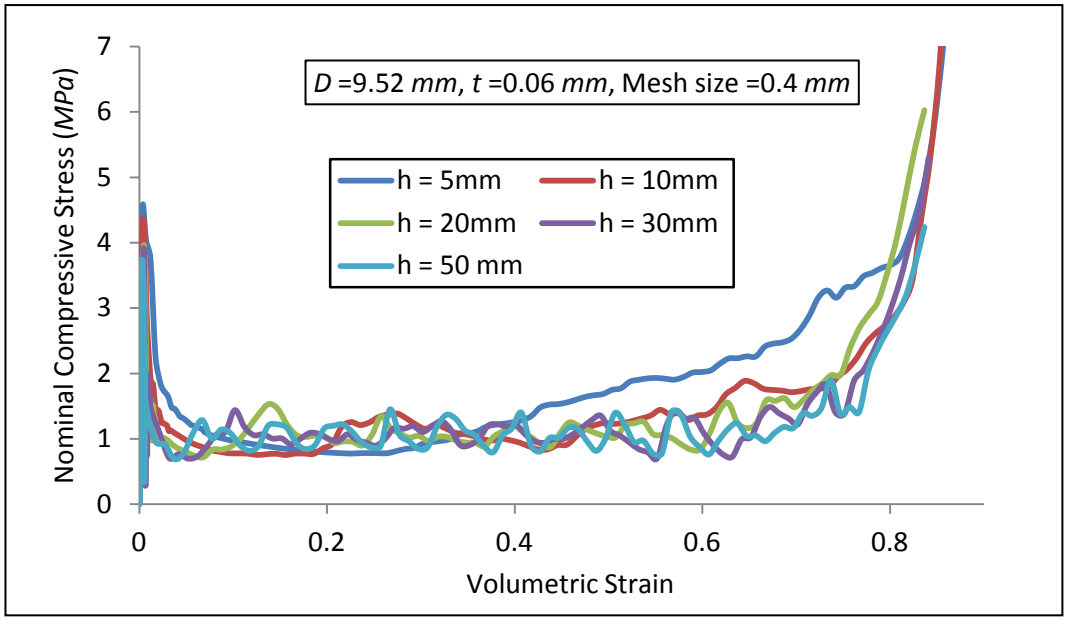

Figure **3-13**: Effect of core depth (*h*) on the load curve

3.3 Parameterization of the load curve in terms of *t* and *D*

From above, foil thickness (*t*) and cell size (*D*) govern the load curve. The upper and lower limits of *t* and *D* are defined as per commercially available honeycomb cell sizes [16] for AL5052 material. The depth of honeycomb for all the tests presented hereafter is taken from standard specimen size used for testing [16] i.e. 0.625 *inches* (15.875 *mm*). Peak stress, crush stress and the densification stress varies considerably with *t* and *D*. Crush start and end strain doesn't show much change with *t* and *D*, hence they can be assumed to be independent. Densification stress is evaluated at strain = 0.85 for all the cases. Parameterization is carried out in terms of *t* and *D* using RSM and only *t/D*.

3.3.1 Parameterization using response surface method

Central composite design (CCD) method is used to create response equation for the load curve in terms of *t* and *D* using Design-Expert software. Design candidates taken for creating the response

equation is shown in Figure 3-14 and Table 3-2. Load curve control points at different design points are mentioned in Table 3-3.

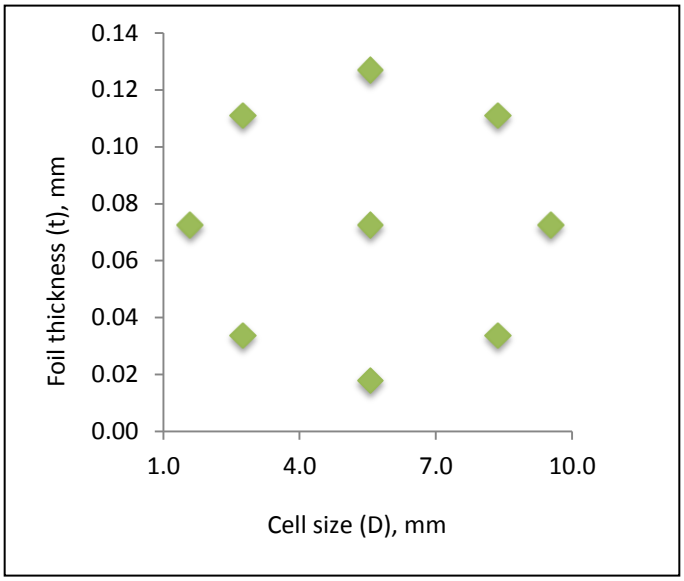

Figure **3-14**: The design candidates for creating response equation using CCD

Table **3-2**: Candidates for creating response equation

Run	Actual factors		Coded factors		Points type
	Cell size (D), *mm*	Foil thickness (t), *mm*	Cell size (D)	Foil thickness (t)	
1	5.55629	0.017781	0	-1.414	Axial
2	8.36258	0.111	+1	+1	Factorial
3	5.55629	0.072388	0	0	Center
4	8.36258	0.033775	+1	-1	Factorial
5	2.75	0.033775	-1	-1	Factorial
6	5.55629	0.126994	0	+1.414	Axial
7	1.587597	0.072388	-1.414	0	Axial
8	2.75	0.111	-1	+1	Factorial
9	9.524983	0.072388	+1.414	0	Axial

Table **3-3**: Load curve parameters at different design points

Cell Size *(D), mm*	Foil Thickness *(t), mm*	*t/D*	Peak Stress *(MPa)*	Peak Strain	Crush Stress *(MPa)*	Crush Start Strain	Crush End Strain	Densifi-cation Stress *(MPa)*	Final Strain
9.52	0.072	0.00760	4.97	0.0038	1.46	0.01	0.753	8.13	0.85
5.55	0.127	0.02286	18.6	0.0051	8.2	0.0078	0.752	76.1	0.85
1.58	0.072	0.04560	37.6	0.0074	24.3	0.012	0.745	178	0.85
5.55	0.018	0.00320	1.77	0.0043	0.5	0.0081	0.753	2.76	0.85
5.55	0.072	0.01303	9.63	0.0046	3.5	0.0114	0.723	22.6	0.85
8.36	0.111	0.01327	9.91	0.0039	3.29	0.0086	0.752	23.1	0.85
2.75	0.111	0.04037	33.2	0.0047	19.9	0.011	0.741	182	0.85
2.75	0.034	0.01228	9.99	0.0043	3.48	0.008	0.732	15.9	0.85
8.36	0.034	0.00404	2.93	0.0034	0.6	0.0073	0.744	3.1	0.85

The responses for peak strength crush strength and densification strength determined at design candidate points are used in regression fitting in Design-Expert software. The best response equations in terms of the actual factors are shown below.

$$\log_{10} Crush\ stress = 0.60859 - 0.30062D + 22.16382t - 0.0467Dt + 0.014177D^2 - 79.67109,\ (R^2=0.9895) \quad (3.3)$$

$$\log_{10} Peak\ stress = 0.96878 - 0.22826D + 17.71809t + 0.017612Dt + 0.011204D^2 - 67.25904t^2,\ (R^2=0.9530) \quad (3.4)$$

$$\log_{10} Densification\ stress = 1.14551 - 0.2699D + 25.60747t - 0.42687Dt + 0.013026D^2 - 71.73044t^2,\ (R^2=0.9890) \quad (3.5)$$

3.3.2 Parameterization using *t/D* as a single variable

Wierzbicki [13] showed that the mean crush strength (Equation 3.6) of the metal honeycomb is a function of *t/D*. It is also obvious from the Table 3-3 that peak strength, crush strength and the finals strength are proportional to *t/D*. Figure 3-15, 16 and 17 shows the plot of peak strength, mean crush strength, final strength and peak strain. Their corresponding trend-line is also shown in the plot. Trend line for the peak strength and mean crush strength is well fitted around the virtual testing response data. Trend line for the peak strain is assumed to be linear. Crush start and end strain are assumed to be independent of *t/D* and corresponding strain values are taken as 0.009 and 0.744 respectively. Final strain is fixed at 0.85. Crush strength obtained from the virtual testing matched well (Figure 3-18) with analytical formula developed by Wierzbicki. Since difference between yield stress and ultimate stress is very small for AL5052, flow stress is assumed to be same as yield stress.

$$Crush\ strength = 16.56 \times \sigma_0 \times \left(t/D\right)^{5/3} \tag{3.6}$$

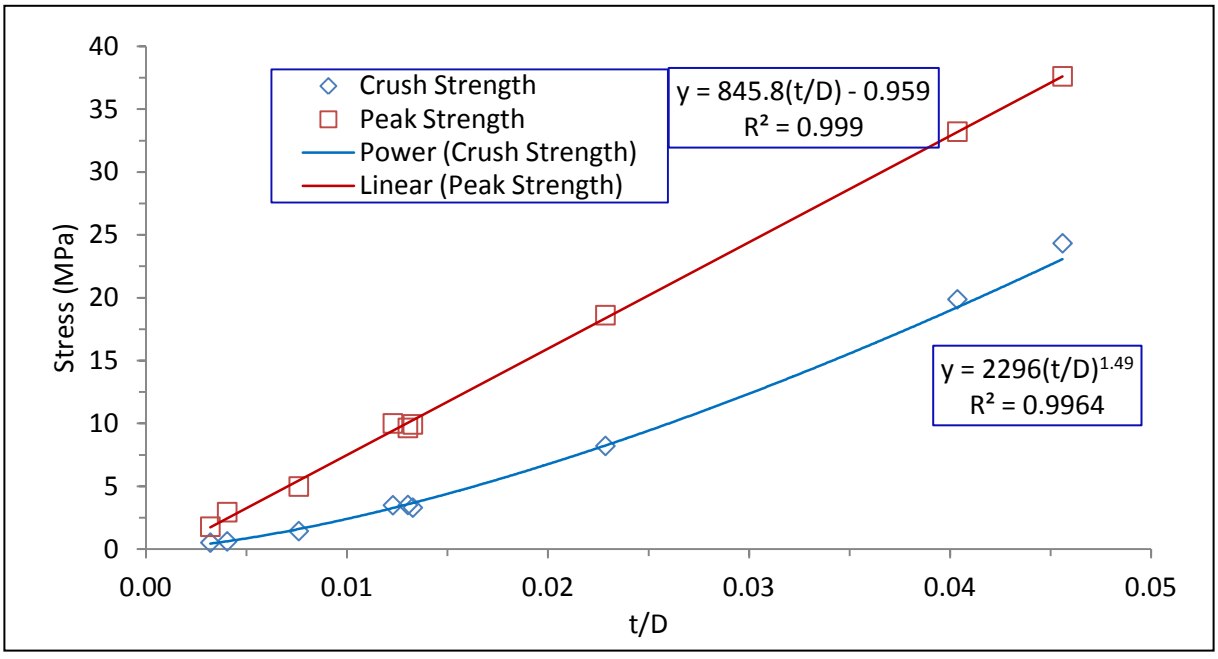

Figure **3-15**: Variation of crush strength and peak strength with *t/D* (Virtual test data and trend lines are shown)

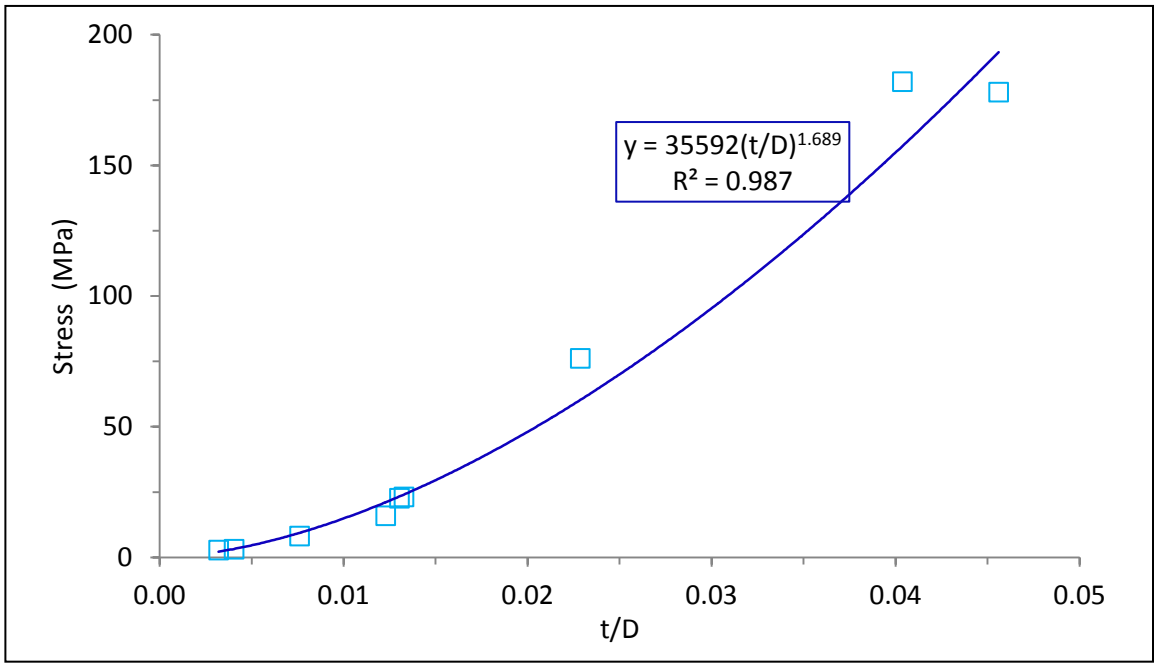

Figure **3-16**: Variation of the densification stress (at strain = 0.85) with *t/D*

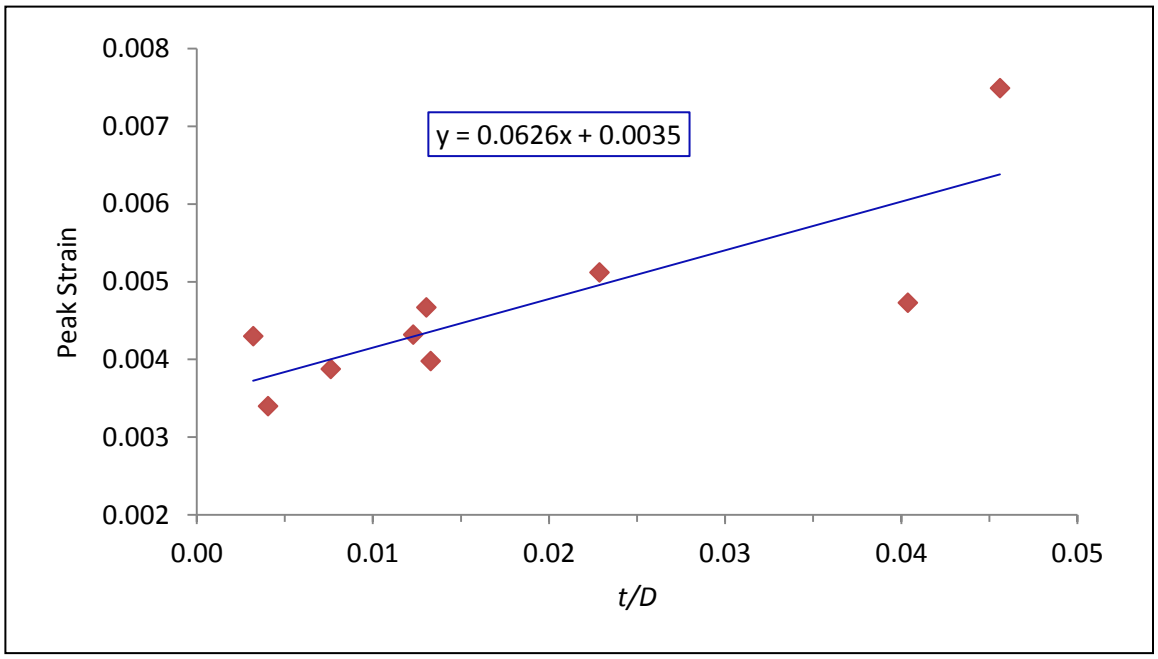

Figure **3-17**: Variation of the peak strain with *t/D*

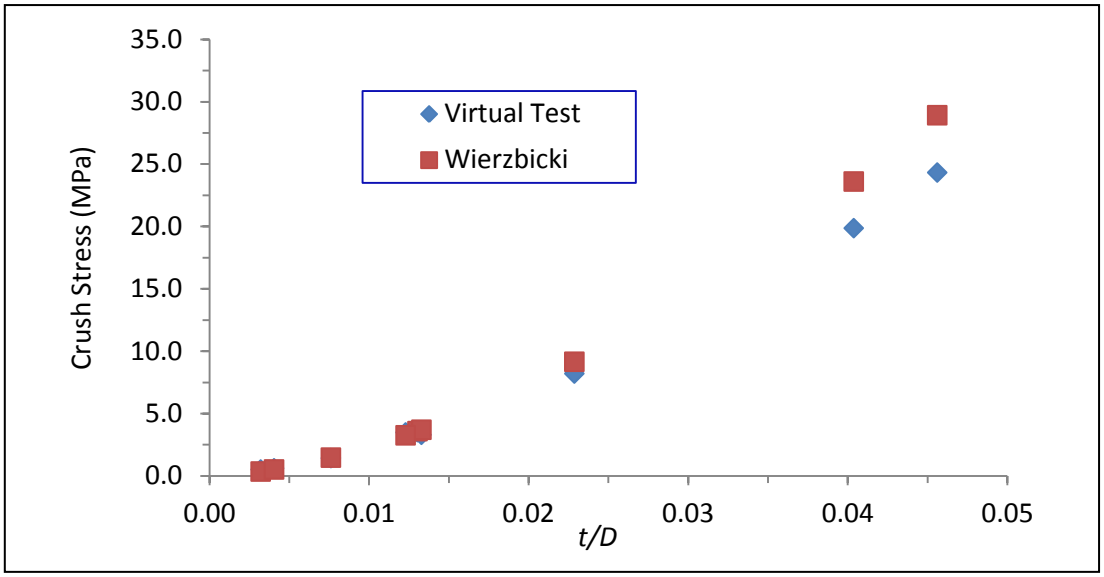

Figure **3-18**: Validation of the crush strength obtained from the virtual test with $Crush\ strength = 16.56 \times \sigma_0 \times \left({}^{t}/_{D}\right)^{5/3}$ [13]

Crush strength is the most important properties of the load curve. Since it is well represented in terms of *t/D* and handling a single variable in optimization code is easy, the load curve is parameterized in terms of *t/D*. All the relevant parameters used in defining the load curve are given below.

$$Peak\ strain = 0.0626\,(t/D) + 0.0035$$

$$Peak\ stress\ (MPa) = 845.8\,(t/D) - 0.959$$

$$Crushing\ start\ strain = 0.009$$

$$Crushing\ end\ strain = 0.744$$

$$Mean\ Crush\ strength\ (MPa) = 2296\ (t/D)^{1.49} \tag{3.7}$$

$$Densification\ strain = 0.85$$

$$Densification\ Stress\ (MPa) = 35592\,(t/D)^{1.69}$$

$$Tensile\ stress\ cut\ off\ (MPa) = (8/3)\,\sigma_y\,(t/D)$$

$$Mass\ Density\ (kg/m3) = (8/3)\,\rho_f\,(t/D)$$

Mass density refers to the mass per unit cell area and per unit depth. Yield stress and density refer to that of AL5052 material.

3.4 Sensitivity study

3.4.1 Effect of non-rigid hammer, honeycomb without face plates, and geometric imperfections on load curve

The model shown in Figure 3-4 uses rigid base and hammer, and the core is attached to the face plates. The solution is based on explicit dynamic analysis, and mass scaling is used for computational efficiency. A sensitivity study is carried out to see the effect of using non-rigid hammer without face plates attached to the core. The effect of geometric imperfections in the honeycomb is also studied. All the following results are based upon implicit static analysis and no mass scaling is used. Cell size = 9.52 *mm*, foil thickness = 0.0724 *mm* are chosen for the sensitivity study.

Since the core is attached to the face plates, top and bottom edges of core would not bend and it is expected, that would increase the peak crush strength. In Figure 3-19, core is freely placed between two steel blocks (non rigid hammer and base). *AUTOMATIC_NODES_TO_SURFACE contacts are defined between base and foil, and hammer and foil. Displacement load is applied to the top face of the hammer and bottom face of base is fixed. No Mass scaling is used, mass density is defined in *tonne/mm*^{3}. Implicit static analysis is carried out. In the absence of face plates, honeycomb bends at both top and bottom edges (Figure 3-19), peak and crush stress gets reduced and densification strain increases (Figure 3-21). Though these changes are obvious, there are no significant changes to the load curve.

In the FEM of honeycomb unit cell discussed in section 3.3 and 3.4, foil walls are assumed to be perfectly planar structure and edges are perfectly square. Though the effect of such imperfections will not be significant when crush test is done on a honeycomb panel consisting hundreds of unit cells, but it will be interesting to see its effect in a unit cell test. In a unit cell model, any geometric imperfection is expected to reduce the compressive strength of the honeycomb. Imperfections (Figure 3-20) are introduced in the honeycomb by moving the nodes of foil in FEM by a very small amount

(+/- 5 μm maximum) in a random manner. No significant changes to the load curve observed (Figure 3-21).

It is also observed that results obtained from explicit dynamic analysis (section 3.3) with mass scaling and hammer travel rate 80 *mm/s* match well with the result from implicit static analysis without any mass scaling (Figure 3-21). So hammer travel rate 80 *mm/s* can be used for quasi-static test.

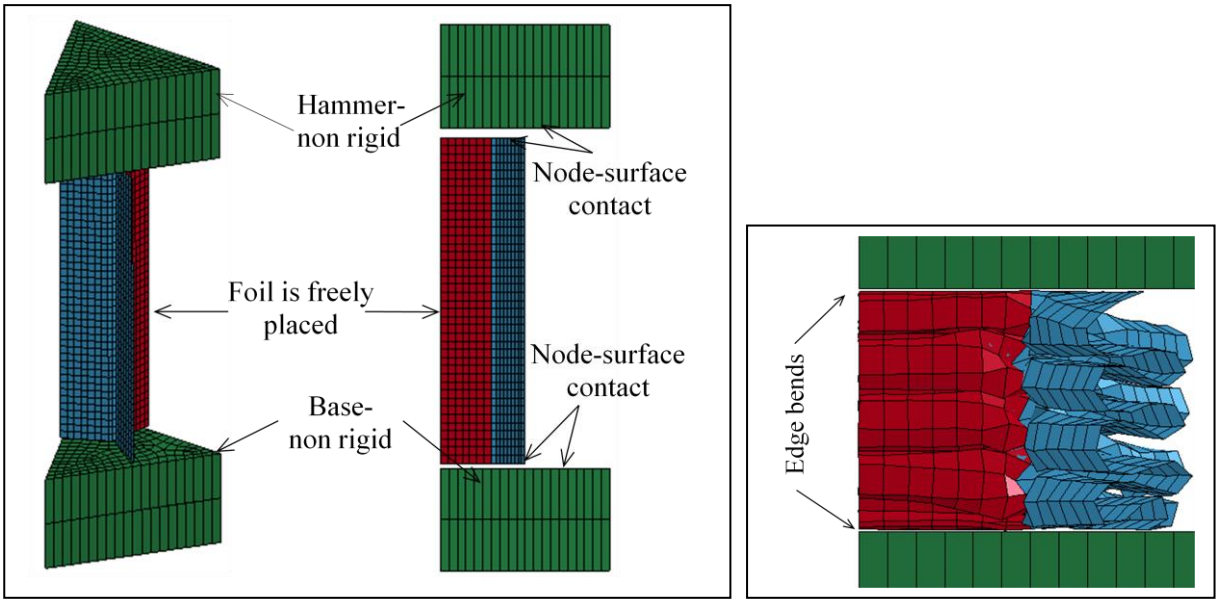

Figure **3-19**: Unit cell crush test model: non-rigid hammer and base, no face plate attached to core

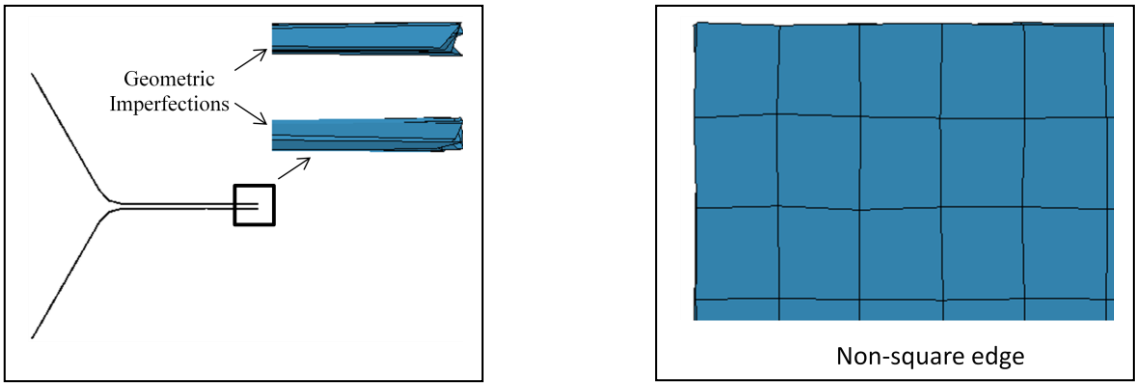

Figure **3-20**: Geometric imperfections in unit cell test model

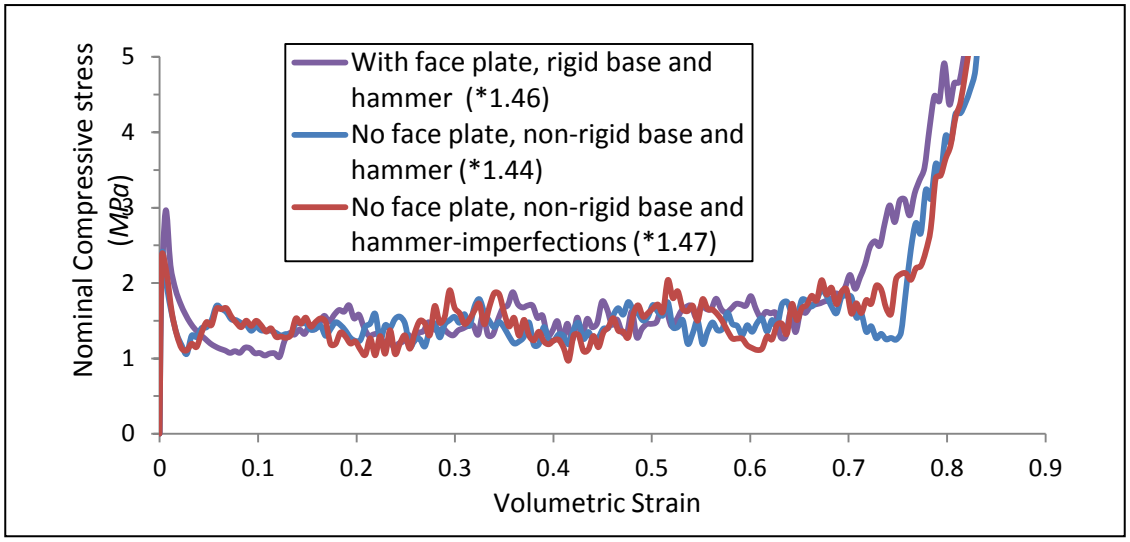

Figure **3-21**: Effect of edge conditions and imperfections on load curve (* refers to average crush strength)

3.4.2 Effect of strain rate

Both strain rate and inertia effects play an important role in the dynamic crushing of an energy absorbing material. However, both effects are absent in a static crush. The strain rate in the honeycomb for the problem discussed in Chapter 4 can go up to 2500 s^{-1}. So it is important to include the strain rate effect. It is incorporated by using the Cowper-Symonds (CS) constitutive model (Equation 3.8). The value of C and p for aluminum are taken to be 6500 s^{-1} and 4 respectively [29]. The load curve at different strain is plotted in Figure 3-22. This plot includes both strain rate and inertia effect. Strain rate effect is an intrinsic property of the material. Assuming that strain rate effect due to Cowper Symonds model and the inertia effect are independent of each other, Equation 3.9 is used to remove the inertia effect from a dynamic crush test; the corresponding crush strengths are shown in Figure 3-23. With strain rate the crush strength increases. The effect of inertia cannot be neglected at high strain rate. This analysis is carried out for D = 9.525 *mm* and t = 0.0724 *mm* (t/D = 0.00754), and the factors obtained here (Figure 3-23) are assumed to remain same for other t/D ratios. These factors without inertia effect are used in section 7.1 to create a material model with strain rate effect (Figure 3-24) to evaluate the sandwich performance.

$$\sigma = \sigma_y \left[1 + \left(\frac{\dot{\varepsilon}}{C}\right)^{1/p}\right] \tag{3.8}$$

$$\sigma_{dc\text{-}wsr\text{-}woi} = \sigma_{dc\text{-}wsr} - (\sigma_{dc\text{-}wosr} - \sigma_{sc}) \tag{3.9}$$

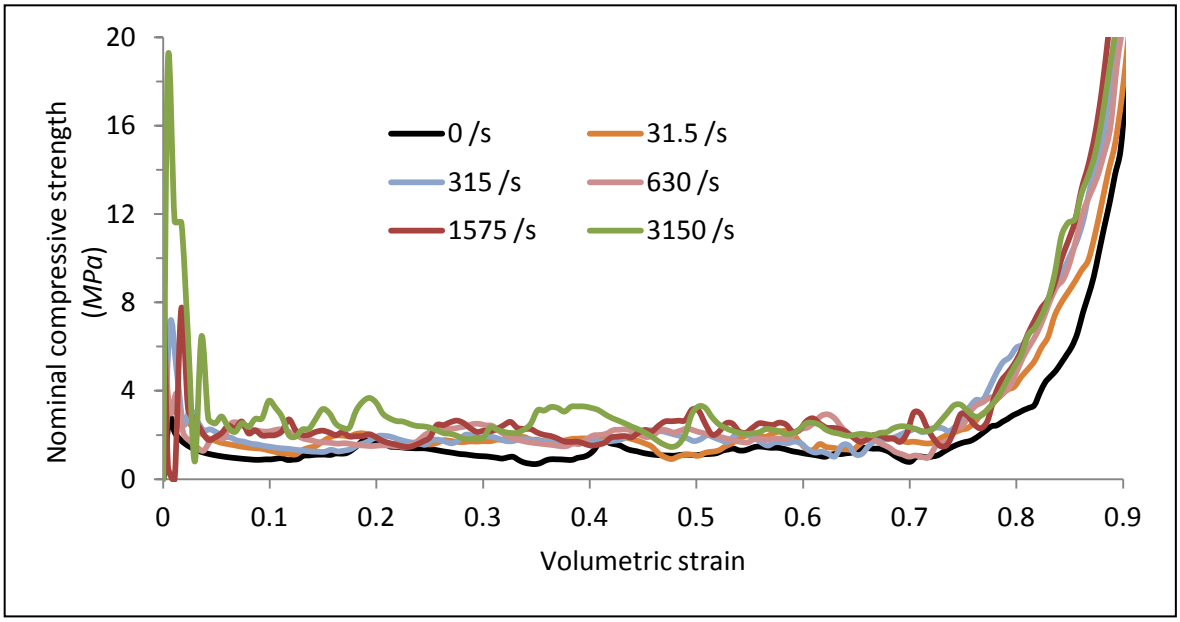

Figure **3-22**: Effect of strain rate + inertia on load curve

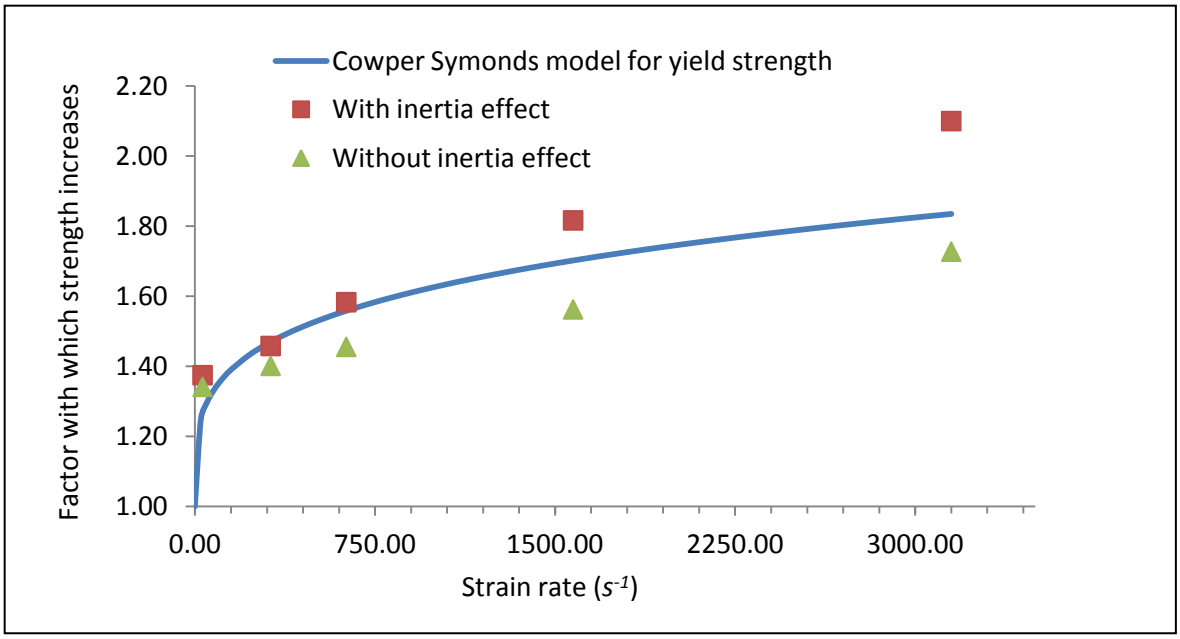

Figure **3-23**: Effect of strain rate on crush strength

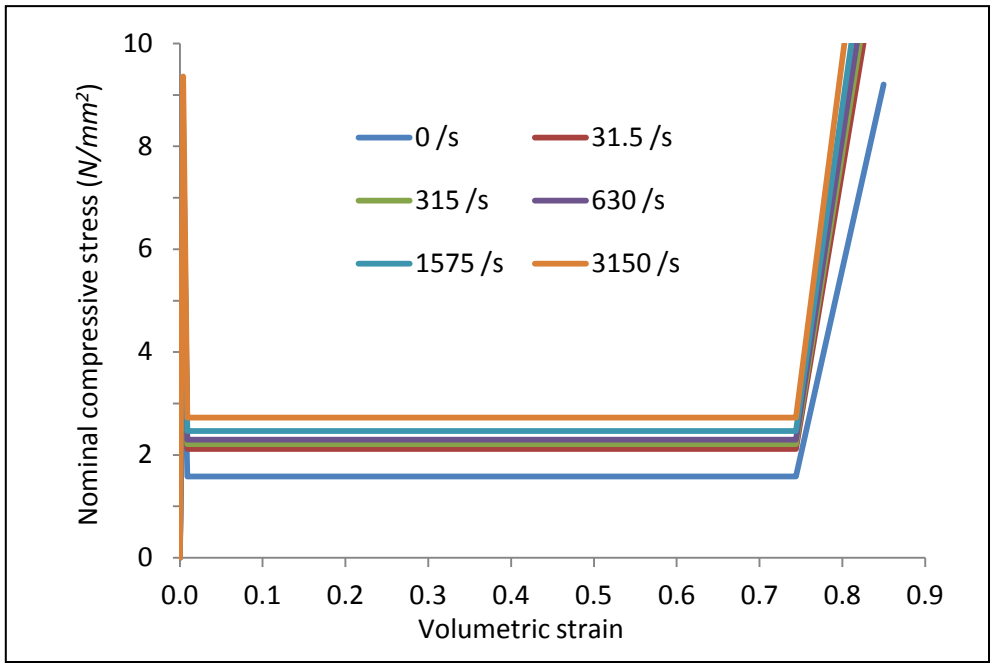

Figure **3-24**: Load curve (for *t/D* = 0.00754), at different strain rate, used for *MAT_MODIFIED _CRUSHABLE_FOAM material model in section 7.1

3.5 Validation of homogenization model

In this section, unit cell test results are compared with the data available in the literature. Also, these results are compared with large scale FEA of honeycomb structures [25]. The energy absorption characteristic of unit cell, large scale honeycomb are compared with their equivalent homogenized model. Since the homogenized model is based on crushing, and the blast panel is subject to both bending and crushing, validation via both bending and crushing are performed [25].

3.5.1 Validation of crush strength with commercially available data

The mean crush strength formula $(2296\ (t/D)^{1.49})$ obtained after parameterization is validated using the data available in Hexcel Corporation [16] for commercial use. Crush strength mentioned in [16] refers to the average value obtained from several tests for a particular specimen. For a particular *t/D*,

crush strength values indicated in [16] are very close which again indicates that it is only a function of *t/D*. Results from unit cell test match well (Table 3-4) to the data given in [16].

Table **3-4**: Validation of crush strength

Cell Size (D) *mm* (*in*)	Foil thickness (t) *mm* (*in*)	*t/D*	Crush strength from Hexcel [16] *MPa* (*psi*)	Crush strength from unit cell virtual test *MPa*	% Difference
4.76 (3/16)	0.0254 (0.001)	0.0053	0.90 (130)	0.94	5.13
3.18 (1/8)	0.01778 (0.0007)	0.0056	0.90 (130)	1.01	13.06
4.76 (3/16)	0.0381 (0.0015)	0.008	1.72 (250)	1.72	0
3.18 (1/8)	0.0254 (0.001)	0.008	1.79 (260)	1.72	3.82
3.97 (5/32)	0.0381 (0.0015)	0.0096	2.34 (340)	2.26	3.49
6.35 (1/4)	0.0635 (0.0025)	0.01	2.31 (335)	2.40	4.09
3.97 (5/32)	0.0508 (0.002)	0.0128	3.96 (575)	3.47	12.40
4.76 (3/16)	0.0635 (0.0025)	0.0133	3.96 (575)	3.69	6.90
6.35 (1/4)	0.1016 (0.004)	0.016	5 (725)	4.84	3.12
3.18 (1/8)	0.0508 (0.002)	0.0160	5.17 (750)	4.84	6.35
4.76 (3/16)	0.0762 (0.003)	0.0160	5.17 (750)	4.84	6.35

3.5.2 Large scale uniaxial crush test of a detailed and homogenized FEM

In the unit cell crush test suitable boundary conditions are applied so that result would represent to that of a panel consisting several number of honeycomb cells. To verify that, large scale detailed FEM is developed (Figure 3-25) and tested for its crush strength by Anand [25]. The stress-strain

characteristics match well. The homogenized stress strain plot obtained from unit cell crush test is used to simulate the homogenized unit cell and large scale model (Figure 3-26). The energy absorption is compared between unit cell, large scale detailed model, unit cell homogenized model and large scale homogenized model (Figure 3-27). Percentage of error in IE between detailed and homogenized model is 11%.

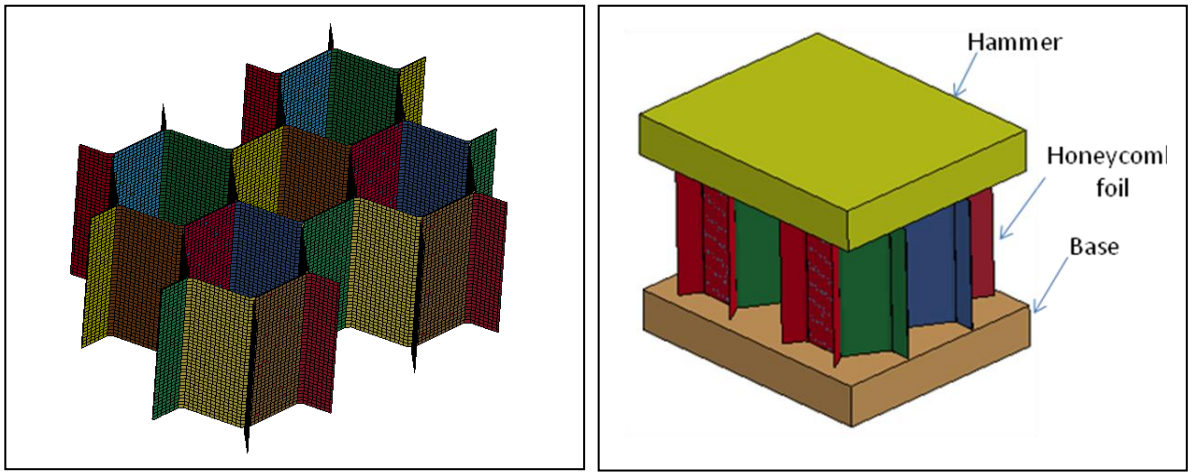

Figure **3-25**: Large scale detailed model of honeycomb [25]

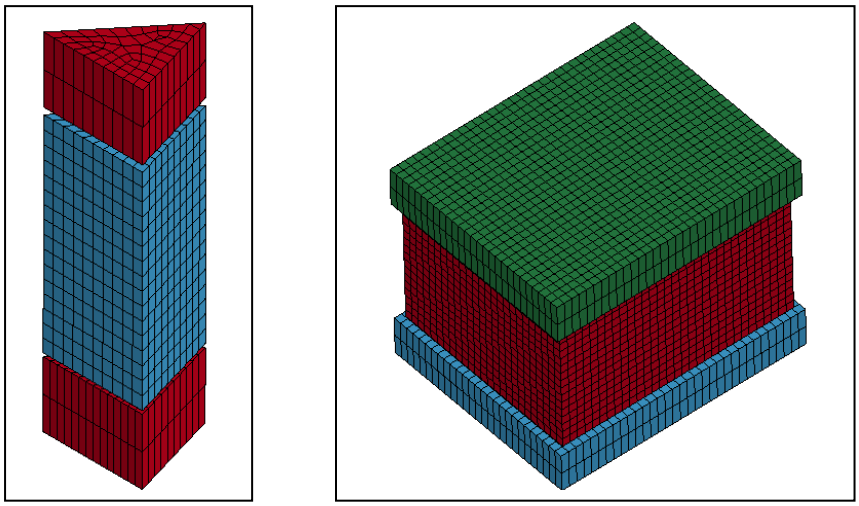

Figure **3-26**: Homogenized unit cell and large scale FEM

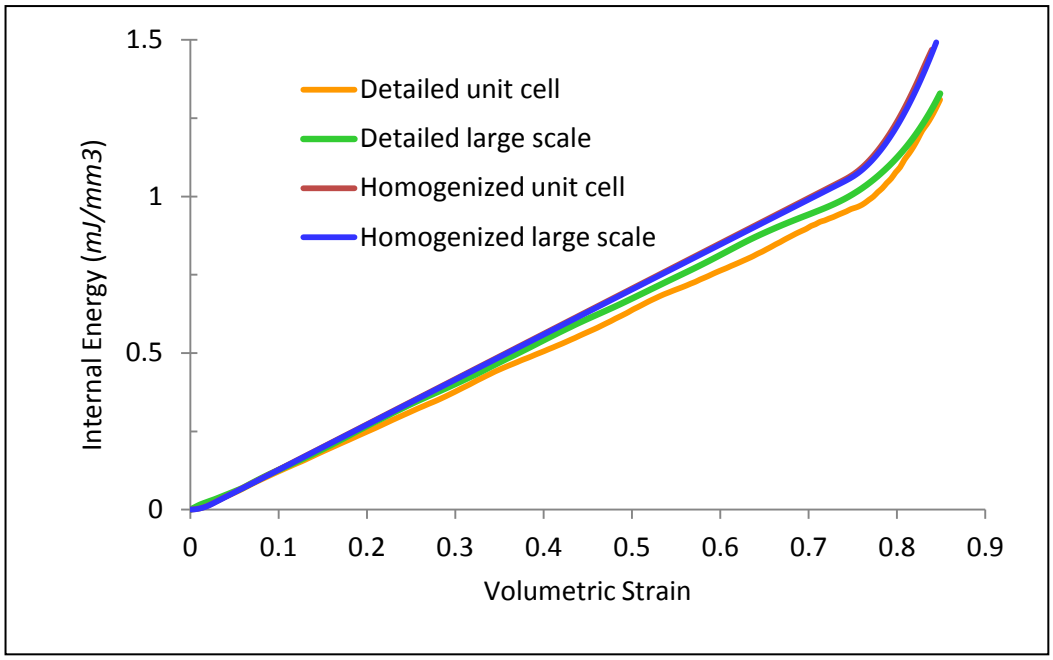

Figure **3-27**: Energy absorption in unit cell and large scale model

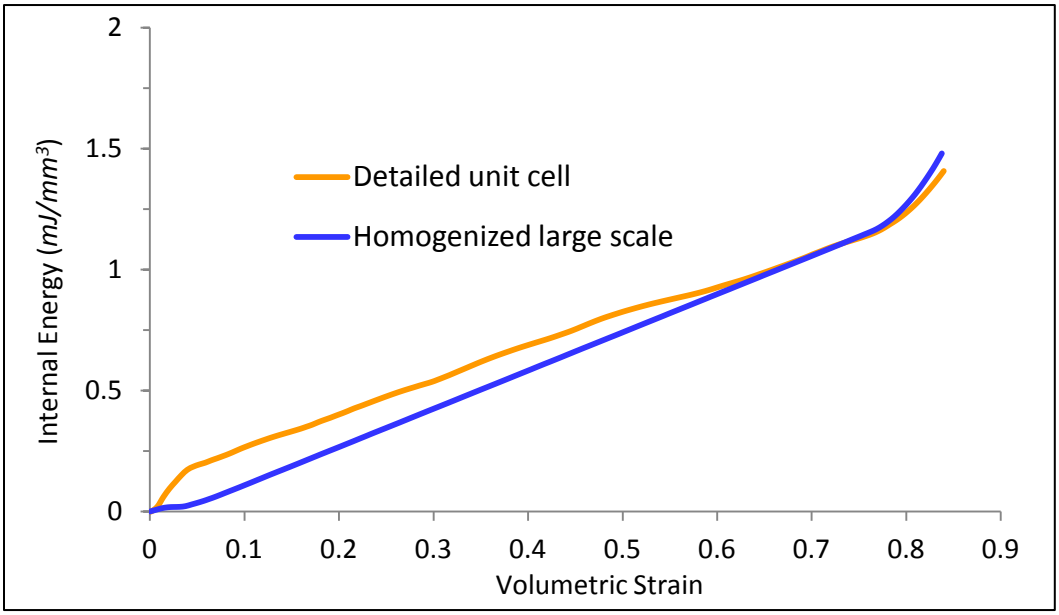

Figure **3-28**: Energy absorption in unit cell and large scale model at hammer speed = 25 *m/s*

Figure 3-28 compares the energy absorption in a dynamic test where the hammer moves at 25 *m/s*. Here, no Cowper-Symonds strain rate model is considered. The homogenized model here uses the load curve in crushable foam material model obtained from a quasi-static test. Since crushing is more uniform along the depth of the core in a homogenized model, energy absorption is linear until densification starts. The internal energy absorption between detailed unit cell and large scale homogenized model is in good agreement.

3.5.3 Validation of honeycomb model through flexure tests

Since the blast panel undergoes bending as well as crushing, a three-point bend test comparing the homogenized model with a detailed virtual test specimen is carried by Singh [25]. For this test, provisions of ASTM standards D 7250 and C 393 are used. The testing is done with the ribbon of the honeycomb core both parallel (Figure 3-29) and perpendicular to the span to exclude any interference from core orthotropy. Half symmetric models are used to reduce the computation time. Mid span deflection (Figure 3-30) and internal energy absorption are found to be in good agreement.

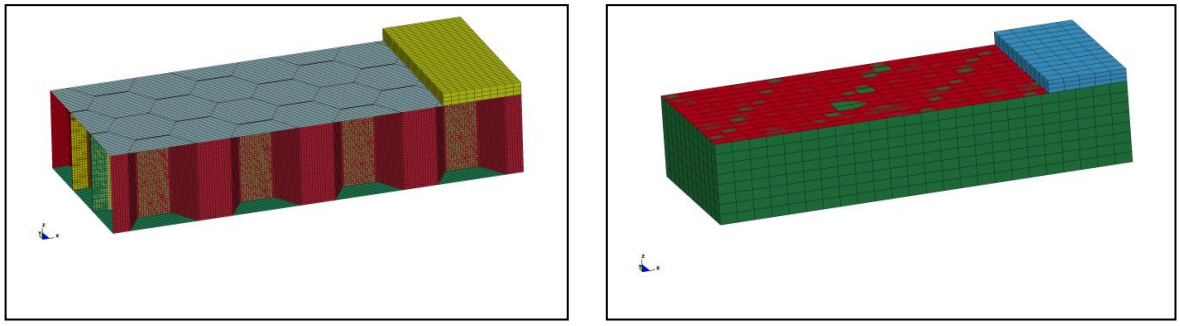

(a) Detailed Model (b) Homogenized Model

Figure **3-29**: Honeycomb ribbon orientation parallel to span of sandwich beam

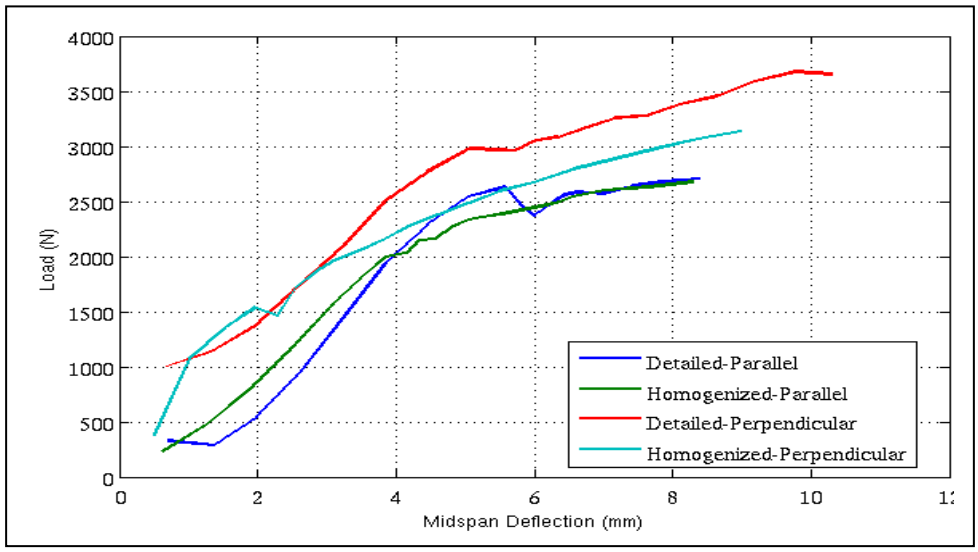

Figure **3-30**: Load vs. midspan deflection

It can be concluded that homogenized stress-strain curve obtained from uniaxial-unit cell crush test can be used to represent the material properties of the core modeled as a solid structure without introducing much error to its dynamic response.

3.6 Summary

First virtual quasistatic crush tests are carried out on unit cell honeycomb of different cell sizes attached to face plates using rigid hammer. Effect of different cell parameters on crush strength is studied. Then the load curve is parameterized in terms of key cell parameters (t and D). Effects of cells without face plates, non-rigid hammer and geometric imperfections on the load curve are analyzed. Results from implicit static analysis and quasistatic explicit dynamic analysis are compared. Results are validated with available data.

Unit cell crush test results are compared with results from large scale model of honeycomb structures followed by comparing the energy absorption between detailed and homogenized model. Lastly, three-point bend tests have also been conducted, thereby validating both compression and bending response of the homogenized models.

Chapter 4

Optimization Problem Description

4.1 Overview of the problem

Optimal design of a square honeycomb core sandwich panel subjected to air blast loading is considered. Design variables are thickness and shape of the face plates, core depth and core *t/D* ratio (or core density). The objective of the design is to minimize either the maximum backface deflection or the backface rigid body acceleration*t*, subject to mass and plastic strain limits. These objectives are considered in separate cases. A schematic diagram of the honeycomb sandwich used for optimization is shown in Figure 4-1**.** The standoff distance of the blast charge is taken as 0.4064 *m*. A stiffener is used to support the sandwich and to impart sufficient inertia. Though a different combination of materials can be used in a sandwich, here aluminum Al5052 is considered for the whole sandwich such that results can be easily compared with Al5052 monolithic plate.

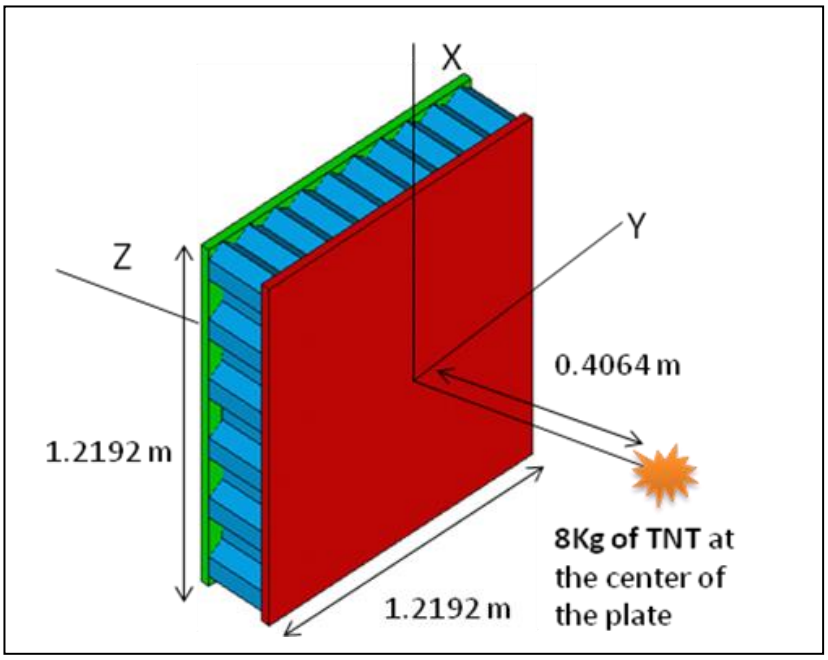

Figure **4-1**: Schematic model of the honeycomb sandwich panel used for optimization (stiffener is not shown)

4.2 Blast injury

Blast injuries are caused by (I) significant indentations in backface plate, (II) material failure leading to projectile or shrapnel penetration, and (III) high g-loads which can cause trauma or create secondary projectiles in the cabin. Thus, minimizing backface deflection and acceleration while maintaining the structural integrity, would mitigate the blast related injuries.

4.3 Problem definition

Mathematically, the design optimization problem can be stated as follows:

Minimize $max\ \delta_b$ (case-1) (4.1)

$max\ a_b$ (case-2) (4.2)

subject to

$\varepsilon_{pj} \leq \varepsilon_{pmax}$ for each element j of the face plates

$M \leq M_{max}$

$\mathbf{x}^{\mathrm{L}} \leq \mathbf{x} \leq \mathbf{x}^{\mathrm{U}}$

$det\ J_j(\mathbf{x}) \geq 0$ for each element j

Where, the notation is explained in the nomenclature section.

4.3.1 Objective functions

The sandwich core is meant as a sacrificing layer and absorbs most of the blast energy, whereas the front face plate provides sufficient stiffness for better utilization of the core. Backface plate acts as a protective layer for human occupants or cabin equipments. Maximum deflection of the backface plate is chosen as an objective function to be minimized.

Since the sandwich model is not constrained, the maximum *Z*-deflection of the backface plate is obtained by subtracting the rigid body displacement of the stiffener (Equation 4.3(a)). Displacements

along the *x*- and *y*- direction are not significant and are not considered. The displacement is a function of time, and the peak value is monitored.

$Objective - 1\text{: } \delta_b = \delta_{z-max} - \delta_{st}$ (4.3 (a))

$Objective - 2\text{: } a_b$ (4.3 (b))

A second objective function is also considered, viz. Z- rigid body acceleration of the backface plate. As this is a function of time, the absolute maximum acceleration is considered. Rigid body acceleration refers to net force divided by net mass. For a particular mass of backface plate, its acceleration is proportional to transmitted force through the core.

4.3.2 Constraints

Plastic strain

A plastic strain limit is imposed only on the face plates. No plastic strain limit is imposed on the core. To act as a protective structure, it is necessary that the face plates maintain their structural integrity. The plastic strain in each element increases with simulation time until it reaches a plateau. This saturated or maximum value is considered. The maximum value of the all elements in the face plates is monitored.

Mass constraint

Mass constraint (*M*) (Equation 4.4) considers the mass of the mass of the front and backface plates and of the core. Mass of the stiffener remains constant during optimization and is not included in *M*.

$M = M_f + M_c + M_b$ (4.4)

Design limits

Bounds are imposed on face plate thicknesses and their outward bulge, core depth and *t/D*. Lower limit on the face plate thickness is based on limiting the maximum aspect ratio of element to a value

of 15. Lower limits on the core depth and *t/D* are based on avoiding excessive element distortion. High element distortion causes the simulation to terminate. A lower limit of zero on the bulge design variable corresponds to a flat plate. Higher limits on *t/D*, face plate thicknesses, core depth and the bulge are taken such that design space is reasonably sufficient for design space exploration.

4.4 Finite element modeling using LS-DYNA

4.4.1 Sandwich model

The model used for this study is shown in Figure 4-2. The model is free to move in space. Backface plate is not restrained completely and can deform freely without creating high plastic strain. The role of the stiffener at the top is to impose high inertia to the backface plate and hence the sandwich. Mass of stiffener is 1850 *kg*. High fictitious density is defined for stiffener. In the absence of the stiffener, the sandwich will fly away without the core getting crushed. In a vehicle application, the sandwich panel will represent the underside and the stiffener will represent the rest of the vehicle. The contacts between the face plate and the core, and between the backface plate and the stiffener are defined using *CONTACT features and *TIED_SURFACE_TO_SURFACE_ID card. The tied contact eliminates the separation at the contact face and makes sure that the whole model behaves as a single unit.

Eight-noded solid elements are used to mesh all the parts. After a mesh convergence study (which is not presented here), element mesh of 38 x 38 x2 for face plates, 28 x 28 x 3 for the core and 20 x 20 x 2 for the stiffener, are taken.

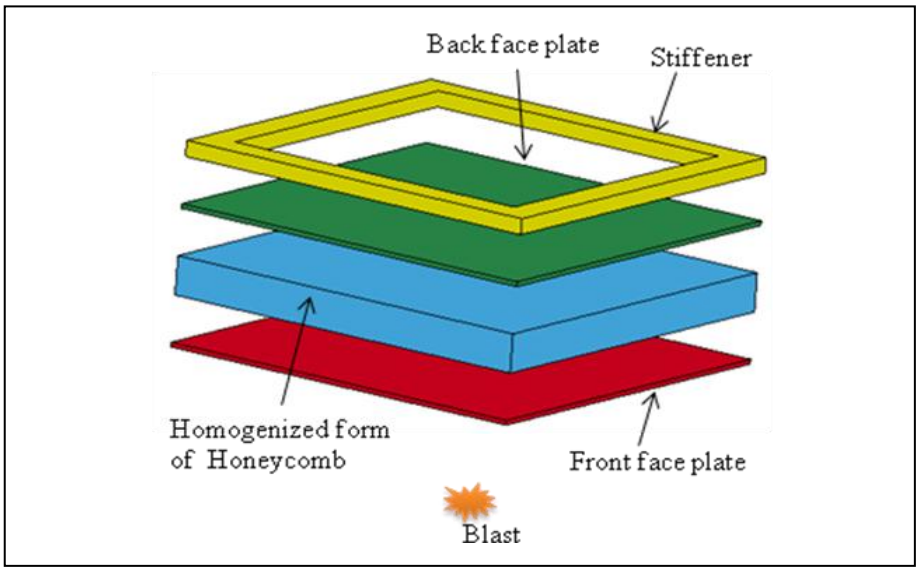

(a) Exploded view

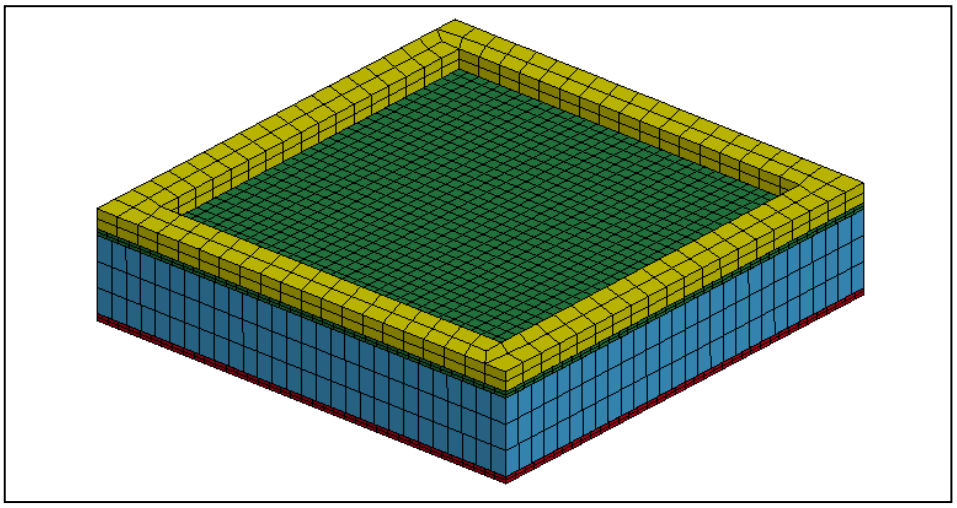

(b) Finite element model

Figure **4-2**: Honeycomb core sandwich model used for optimization study

4.4.2 Material properties

Aluminum 5052 is used for the face plates. The stiffener also uses the same material but with very high fictitious density i.e. 80180.32 kg/m^3. The *MAT_PLASTIC_KINEMATIC material model is used for them. The honeycomb cellular core is not directly used in the model; however a homogenized solid plate of equivalent mechanical properties to the honeycomb core is used (see

Chapter-3). The base material for the honeycomb core is also Aluminum 5052. The mechanical property of the core is a function of *t/D* and varies during the optimization process. *MAT_CRUSHABLE_FOAM material model is used for the core. Typical mechanical properties of the core used in this model are shown in Table 4-2 and Figure 4-3. The Poisson's ratio is taken as zero for the core and no damping is considered.

Table **4-1**: Material Properties of Aluminum 5052 used in *MAT_PLASTIC_KINEMATIC input card for the face plates

Property	*Value*
Mass Density	2680 *kg*/m^3
Young's Modulus	72.0 *GPa*
Poisson's Ratio	0.34
Yield Stress	300 *GPa*
Tangent Modulus	50 *MPa*
Hardening Parameter	1.0
Failure Strain	0.038

Table **4-2**: Material Properties of the honeycomb core (for *t/D*=0.02677) made from Aluminum 5052-foil and used in *MAT_CRUSHABLE_FOAM model

Property	*Value*
Mass Density	191.32 *kg*/m^3
Young's Modulus	4.19 *GPa*
Poisson's Ratio	0.0
Tensile stress cut off	21.41 *MPa*
Damping coefficient	0.0

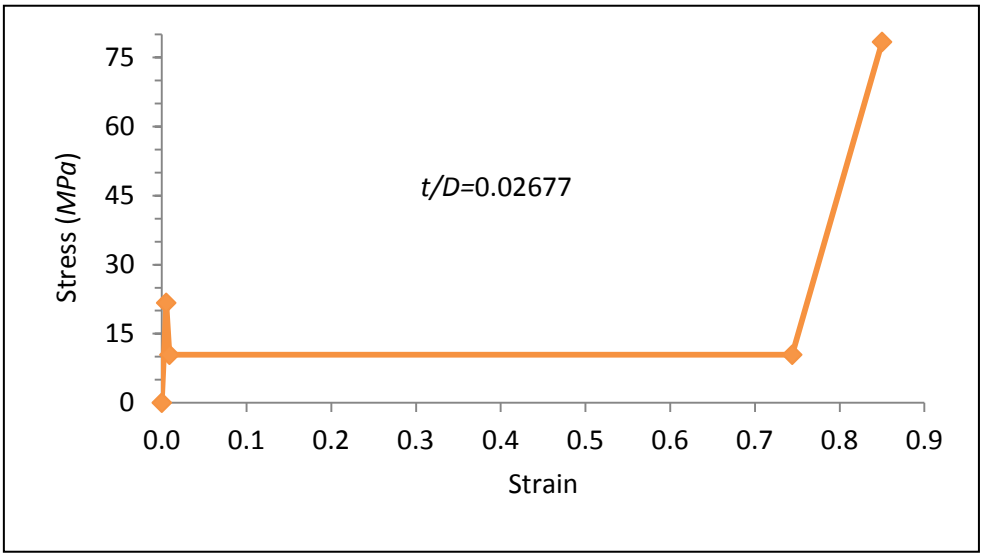

Figure **4-3**: Load curve used in *MAT_CRUSHABLE_FOAM model

4.4.3 Blast load

Blast refers to a release of energy in an extreme manner which subsequently increases the volume of the air (or any gas) and creates high pressure wave pulses. This pressure wave pulses propagate in a radially outward direction from the blast centre until it is stopped by object. The reflected blast wave from the object when meets the incident blast wave creates a single vertical wave front at a certain distance from the object. Any structure between the vertical wave front and the blast source experiences single shock, whereas structure lying above this point experiences a shock history which is resultant of the incident and reflected wave [19]. Blast pressure verses time for a typical blast is shown in Figure 4-4 and is described by Friedlander's Equation 4.5. With time the blast pressure decreases from its peak over pressure value P_0 and goes below the atmospheric pressure at time t_0, then regains to the atmospheric pressure. Since the positive region of the pressure creates damage to the structure, it is only considered for evaluating the blast load. The impulse per unit of the projected area is given in Equation 4.6.

$$P(t) = P_0\left(1 - \frac{t}{t_0}\right)\exp\left(-\propto \frac{t}{t_0}\right) \tag{4.5}$$

$$I_s = \int_0^{t_0} P(t)dt = P_0 t_0 \left[\frac{1}{\propto} - \frac{1}{\propto^2}(1 - \exp(-\propto))\right] \quad (4.6)$$

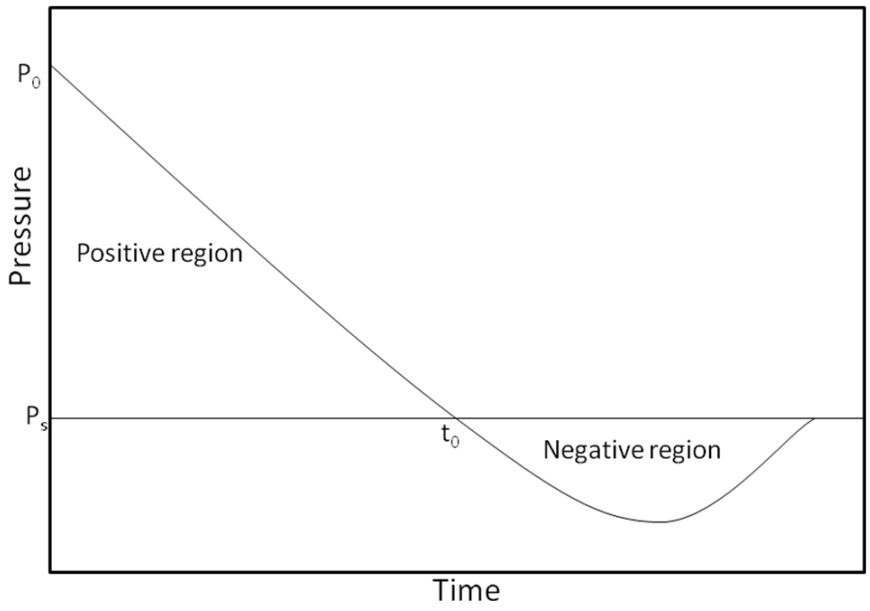

Figure **4-4**: Blast pressure verses time plot

Irrespective of the type of explosive material, the blast load is expressed in terms of equivalent mass of the Tri-Nitro-Toluene (TNT). The blast characteristic of any given mass of the TNT can be obtained from a known blast characteristic of a reference TNT mass using the blast scaling law (Equation 4.7) developed by Hopkinson. No scaling is used on the P_0 and the decay parameter α, but the values correspond to scaled distance and time are used.

$$Z = \frac{R_n}{W_n^{1/3}} = \frac{R}{W^{1/3}} \quad (4.7)$$

$$t_{sc} = \frac{t_n}{W_n^{1/3}} = \frac{t}{W^{1/3}} \quad (4.8)$$

Ballistic Research Laboratory (BRL) [18] carried out a number of tests using different explosive mass and developed a database in the form of pressure versus radial distance for specified time steps. From the database, BRL derived empirical fit to the data in the form of polynomial functions. It is

implemented in CONWEP algorithm which is used in *LOAD_BLAST function of LS-DYNA [20]. Load blast function uses Friendlander's equation (Equation 4.5) and Hoffman's scaling law (Equation 4.7) to calculate the pressure load for a given TNT amount and standoff distance. This blast function can be used in two cases: free air detonation of a spherical charge, and the ground surface detonation of a hemispherical charge.

Table **4-3**: Blast load parameters

Parameters	*Value*
Equivalent mass of TNT	8 *kg*
Blast Location	(0.0,0.0,-0.4064) *m*
Type of Burst	Air Blast (Spherical Charge)

The *LOAD_BLAST input parameters (Table 4-3) used are equivalent TNT mass, type of blast (surface or air), load curve, charge location, and surface identification on which blast wave strikes. It ignores the effect of soil type, soil moisture and burial depth of the charge. The blast pressure applied to surface varies from point to point depending upon the location from blast center and the incidence angle. Higher is the incidence angle, lower is the blast pressure. This is taken care by CONWEP algorithm. The face of the front face plate takes the blast load. Here, no thermal load due to blast is considered.

4.5 Velocity field for creating the sandwich model

The sandwich panel mesh is created using the concept of velocity field. For brevity, $\{t_b, t_f, h, t/D\}$-optimized panel is referred as, 'size-optimized panel', and $\{t_b, t_f, h, t/D, s_b, s_f\}$-optimized panel as, 'size+shape optimized panel'.The variable t/D is a parameter that defines the stress-strain curve

which is input into LS-DYNA. The remaining five variables $\{t_b, t_f, h, s_b, s_f\}$ require a change in the coordinates of the nodes in the 3D finite element model. That is, they affect the *shape* of the structure.

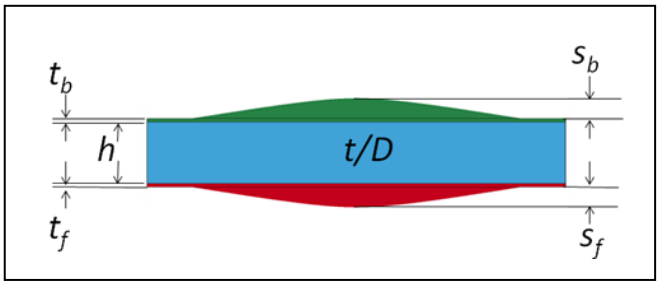

Figure **4-5**: Optimization parameters for the sandwich optimization

The key equation to implement shape optimization is [26]

$$\boldsymbol{G}(\boldsymbol{x}) = \boldsymbol{G}_{\boldsymbol{original}} + \sum_{\boldsymbol{i=1}}^{\boldsymbol{N_{dv}}} \boldsymbol{x_i q^i} \tag{4.9}$$

Where $\boldsymbol{G}$ is a grid point coordinates vector, representing x-, y-, z- coordinates of all nodes in the model. Each x_k represents the amplitude of a 'permissible shape change vector' or what is commonly called a 'velocity field' vector $\boldsymbol{q^k}$. Velocity fields have nothing to do with actual velocities of the model under loading. Vectors $\{\boldsymbol{q}^k\}$ are generated just once in the optimization procedure. $\boldsymbol{G_{original}}$ is the current (flat) shape. Visualization of a $\{\boldsymbol{q}^i\}$ is identical to visualization of a displacement field in finite elements: $\{\boldsymbol{q}^k\}$ is multiplied by a magnification scalar and added to the current grid to obtain a displaced grid, except that here the displaced grid represents a new shape and is called a *basis shape*.

Velocity fields associated with variables t_b, t_f, h are straightforward: nodes are moved in the +/- z-direction, maintaining equal spacing, to result in the desired thicknesses. For variables s_b and s_f, which are the amplitudes of basis shapes that correspond to *bulges* in the face plates as shown in Figure 4-5, a procedure is needed to generate $\boldsymbol{q}^i$. The velocity fields $\boldsymbol{q}^i$ are generated here by first applying a dummy load on each of the plate surfaces as shown in Figure 4-6 and using analytical expressions in Timoshenko [21], Equation 145, page 142 (Equation 4.10), to obtain the corresponding nodal

displacements on all nodes on the surface. Then, equal spacing in the z-direction is used to complete the definition of $\boldsymbol{q}^i$. A square portion (1.016 *m* x 1.016 *m*) at the center of the face plates is taken as the domain for applying velocity fields. Asymmetric shape variations are not necessary in this problem owing to centrally located charge. Lower bounds s_b and s_f are zero implying that only convex (outward) bulges are allowed for shape changes, as this has found to be beneficial in deflecting the waves in the monolithic plate [1].

As variables $\boldsymbol{x} = \{t_b, t_f, h, t/D, s_b, s_f\}$ are changed for each sampling point in RSM, the grid point coordinates $\boldsymbol{G}$, the load curve from Equation 3.7, and thickness values are updated, an LS-DYNA input file is then written, and an analysis is carried out to evaluate the various functions in the optimization problem.

The process is schematically given as:

Use current values of $\{t_b, t_f, h, s_b, s_f\}$ at sampling point $\boldsymbol{x}^k$, construct $\boldsymbol{G}$ using $\{\boldsymbol{q}^i\}$; from current value of $\{t/D\}$, construct the stress-strain curve data using Equation 3.7 → Write input file and perform LS-DYNA analysis → Evaluate objective and constraint functions → Create response equations → Run optimizer

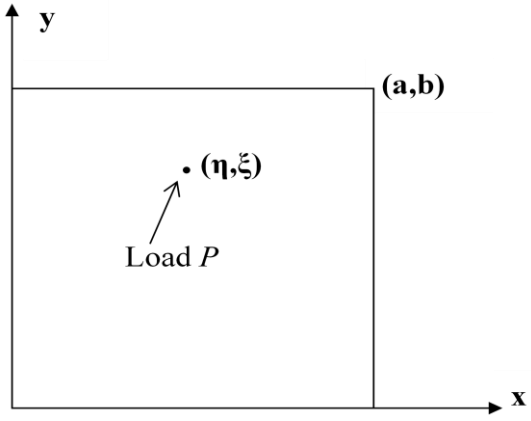

Figure **4-6**: Schematic sketch of rectangular plate

$$W(x,y) =$$

$$\frac{Pa^2}{\pi^3 D}\sum_{m=1}^{\infty}\left(1+\beta_m coth\beta_m - \frac{\beta_m y_1}{b}coth\frac{\beta_m y_1}{b} - \frac{\beta_m \eta}{b}coth\frac{\beta_m \eta}{b}\right)\frac{sinh\frac{\beta_m \eta}{b}sinh\frac{\beta_m y_1}{b}sin\frac{m\pi\xi}{a}sin\frac{m\pi x}{a}}{m^3 sinh\beta_m} \qquad (4.10)$$

Where, $\beta_m = \frac{mxb}{a}$, $y_1 = b - y$, $y \geq \eta$

If $y < \eta$, the quantity y_1 must be replaced by y, and the quantity η by $\eta_1 = b\text{-}\eta$ in the above expression.

It can be noted that, changing the location (η, ξ) of P, different basis shapes can be generated. Combination of such different basis shapes can also be used for shape optimization. Here, the basis shape (Figure 4-7) corresponding to P at center of the plate ((η, ξ)=(0.5,0.5)) is used.

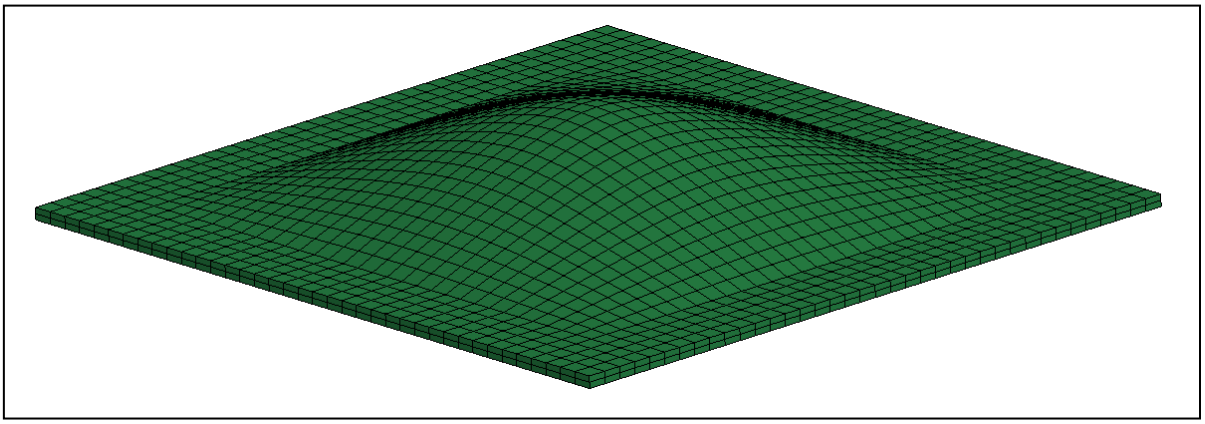

Figure **4-7**: Velocity field, $\mathbf{q}^1$ for a point load at the center of the square plate.

Chapter 5

Optimization by Response Surface Method

The optimization problem discussed in Chapter 4 is carried out in two steps, (I) size optimization, with thickness of the face plates, core depth and *t/D* of the honeycomb core as design variables, and (II) simultaneous size and shape optimization, which includes all the sizing variables as noted above and also the amplitudes of the convex bulges on the both face plates. Size and shape optimization of a monolithic plate is also carried out and its results are compared with that of the sandwich.

Response surface method (RSM) is used to create response equations which are then used in FMINCON, a gradient based optimizer in MATLAB optimization toolbox, for optimization. In the past, both RSM and differential evolution (DE) have been used to optimize the sandwich panel [31]. Results obtained from both methods are in good agreement.

5.1 Overview of response surface methodology

The main objectives of the Response surface methodology (RSM) are to map a response surface for objective and constraint functions over a particular region of interest and to then optimize. It was introduced by G. E. P. Box and K. B. Wilson in 1951. It uses statistical and mathematical techniques to analyze and optimize the responses influenced by several independent variables [22]. RSM develops response equations by regression fitting to the response data obtained from the designed experiments. Suppose the response *y* of a system depends upon the controllable input variables $\xi_1, \xi_2, \ldots, \xi_k$. The response is expressed as

$$y = f(\xi_1, \xi_2, \ldots, \xi_k) + \varepsilon \tag{5.1}$$

The true form of the response function *f* is unknown; the above equation represents the approximate form of the response and ε is a statistical error term. The ε is assumed to have normal distribution

with mean zero and variance σ^2. The magnitude and standard deviation of the error term can be reduced with suitable selection of the design points and the regression model. RSM uses the coded variables such as $x_1, x_{2,\ldots,}x_k$ which are obtained by transforming the natural variables $\xi_1, \xi_{2,\ldots,}\xi_k$. The coded variables are dimensionless with their mean zero and the same spread or standard deviation.

Different types of regression models such as linear, factorial, quadratic and cubic can be tried to map the response. Each model determines various coefficients of the response equation by minimizing the error. The model which results least minimum error can be accepted as the best model. In most of the cases, linear and quadratic model are proved to be the best. The true response equations in the form of linear and quadratic model in terms of the coded variables $x_1, x_{2,\ldots,}x_k$ are

$$y = \beta_0 + \sum_{i=1}^{k} \beta_i x_i + \varepsilon \tag{5.2}$$

$$y = \beta_0 + \sum_{i=1}^{k} \beta_i x_i + \sum_{i=1}^{k} \beta_{ii} {x_i}^2 + \sum \sum_{j<i=2}^{k} \beta_{ji} x_j x_i + \varepsilon \tag{5.3}$$

The coefficients of the Equation 5.2 and 5.3 can be determined by least square method i.e. to minimize the sum of square of the error term. The Equation 5.2 for *n* number of observations is written in Equation 5.4.

$$y_j = \beta_0 + \sum_{i=1}^{k} \beta_i x_{ij} + \varepsilon_j, \; j = 1,2,\ldots.,n \tag{5.4}$$

The least square function is

$$L = \sum_{j=1}^{n} {\varepsilon_j}^2 = \sum_{j=1}^{n} \left(y_j - \beta_0 + \sum_{i=1}^{k} \beta_i x_{ij} \right)^2 \tag{5.5}$$

The function *L* is minimized with respect to $\beta_0, \beta_1, \ldots., \beta_k$

$$\frac{\partial L}{\partial \beta_0} = 0 \; and \; \frac{\partial L}{\partial \beta_i} = 0 \,, \; i = 1, 2, \ldots., k \tag{5.6}$$

Equation 5.4 can be represented in matrix form as

$$y = X\beta + \varepsilon \tag{5.7}$$

Where,

$$y = \begin{bmatrix} y_1 \\ y_2 \\ . \\ . \\ . \\ y_n \end{bmatrix}, \qquad X = \begin{bmatrix} 1 & x_{11} & x_{12} & \dots\dots & x_{1k} \\ 1 & x_{21} & x_{22} & \dots\dots & x_{2k} \\ & & . & & \\ & & . & & \\ & & . & & \\ 1 & x_{n1} & x_{n2} & \dots\dots & x_{nk} \end{bmatrix}, \qquad \beta = \begin{bmatrix} \beta_0 \\ \beta_1 \\ . \\ . \\ . \\ \beta_n \end{bmatrix}, \qquad \varepsilon = \begin{bmatrix} \varepsilon_1 \\ \varepsilon_2 \\ . \\ . \\ . \\ \varepsilon_n \end{bmatrix}$$

The least square estimate of β which is defined as *b* is given below.

$$b = (X^T X)^{-1} X^T y$$

The covariance matrix of *b* is $Cov(b) = \sigma^2 (X^T X)^{-1}$

Where σ^2 is the variance on *y* and can be defined as

$$\sigma^2 = \frac{SS_E}{n-k-1} \; and \; SS_E = y^T y - b^T X^T y$$

SS_E is the sum of square of the residuals on *y*.

The value of the adjusted coefficient of multiple determinations R_{adj}^2 is used to judge the quality of the response surface. R_{adj}^2 is defined as

$$R_{adj}^2 = 1 - \frac{SS_E/(n-k-1)}{SS_T/(n-1)} \tag{5.8}$$

Where $SS_T = y^T y - \frac{\left(\sum_{j=1}^{n} y_j\right)^2}{n}$

The value of the R_{adj}^2 varies between 0 and 1. Closer its value to 1, better the response surface is.

5.1.1 Central composite design (CCD)

Central composite design method is one of the most commonly used response surface designs for fitting the second order models. This design was introduced by Box and Wilson in 1951. It contains 2^k factorial design points, $2k$ axial design points and $2k$ central design points, where k is number of variables. The factorial points are used to fit all linear interaction points. The axial points are meant for estimating the quadratic terms in the model. Multiple runs at the center of the design space consider the pure error coming from the experiment and also contribute to the estimation of quadratic terms. However in a computational experiment, multiple runs at the same point return same result. Figure 5-1 depicts three types of central composite design for two variable problems depending upon the location of the axial points. The central composite circumscribed (CCC) is the original form of the CCD. The star points define the extreme low and high of the variable and are at α distance from the center. The inner square region defines the design space. These design points have circular, spherical or hyper spherical symmetry. In the central composite face centered (CCF) case, α = ±1. Axial points are at the center of the each face. The central composite inscribed (CCI) is a scaled down CCC design with each factor divided by α. This method is used when the specified design limits are true limits.

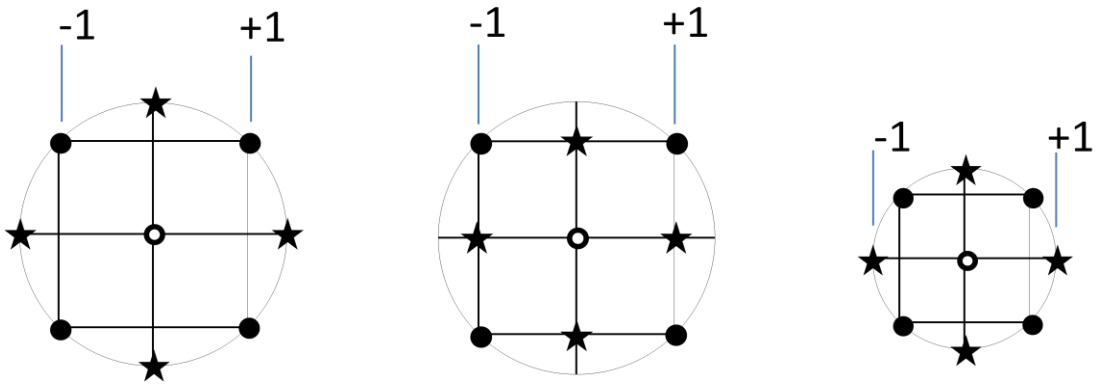

(a) (b) (c)

Figure **5-1**: Three types of CCD designs (a) CCC (b) CCF and (c) CCI

To maintain the rotatability,

$$\alpha = [2^k]^{1/4} \tag{5.9}$$

Sometimes, depending upon the number of design variables *k*, practical value of α which is less than from the equation [22] can be taken.

5.1.2 D-Optimal design

D-Optimal design is mostly used because of two reasons. First, when the standard factorial design such as CCD requires too many runs (or experiments) for the resources or time available. Second, when it is not feasible to run all the design points in the design space or design space is not rectangular. This design minimizes the covariance ($Cov(b)$) of the parameter estimates for a pre-defined model which is equivalent to maximizing the determinant $D = |X^T X|$. Unlike traditional designs, D-Optimal design does not need to have orthogonal matrices.

5.2 Optimization by response surface method

Design Expert, commercially available software is used for mapping the response surface in the design space. It implements the RSM to develop the response equation. Using the response equations, optimization is carried out by FMINCON, a gradient based optimizer in MATLAB optimization toolbox. Figure 5-2 shows the overview of the steps followed for optimization. Since the lower limit on the factor is the design limit, CCF method is adopted to create design points. It uses only 3 levels for each factor. Figure 5-3 and 5-4 shows the design parameters used.

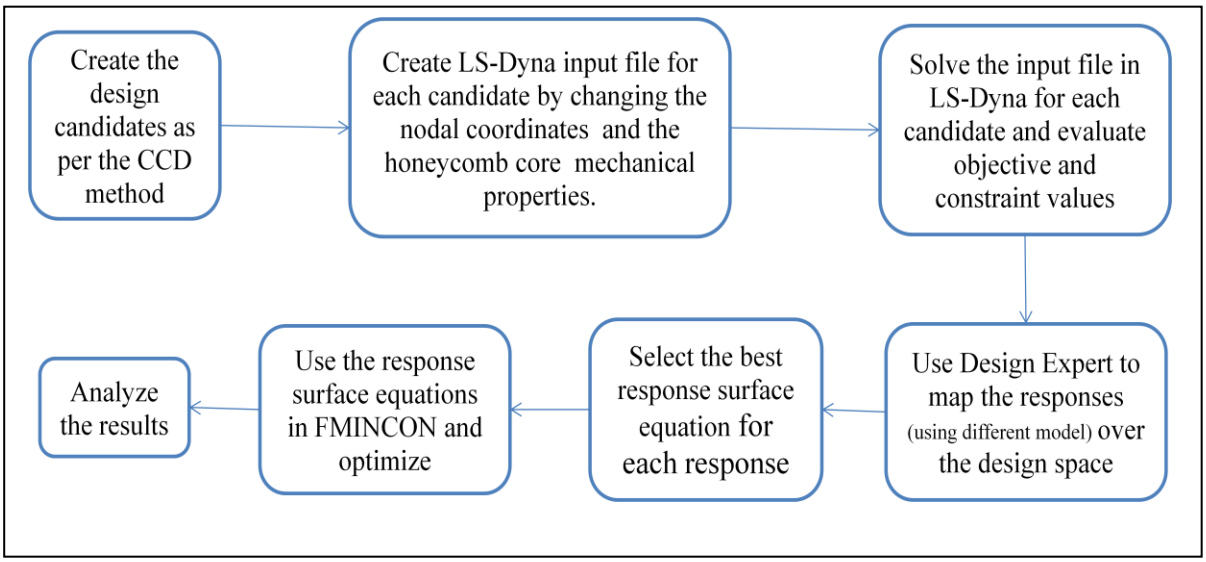

Figure **5-2**: Flow chart of the steps followed for optimization using RSM

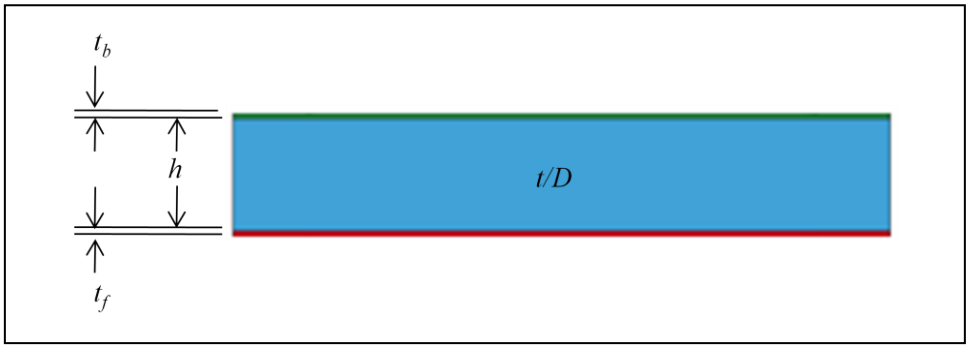

Figure **5-3**: Schematic model used for size optimization

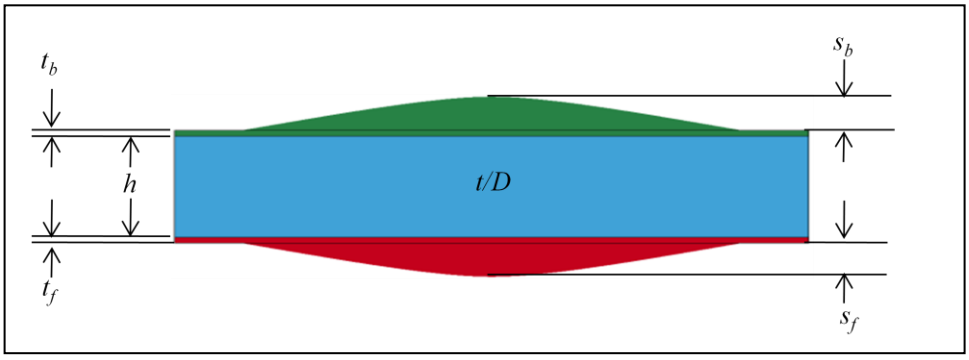

Figure **5-4**: Schematic model used for size and shape optimization

Sizing optimization has four design variables ($k=4$) and number of design candidates required for CCD is determined by following equation.

$$N = 2^k(factorial\ points) + 2k(axial\ points) + 2k(center\ points) =$$

$$16 + 8 + 1(no\ repetition) = 25 \quad (5.10)$$

2k at the center point refers to the *2k* experiments for a single design candidate. Since computational experiment produces same result, only one run is considered. Similarly for sizing and shape optimization (*k=6*), the number of design candidates required for CCD is 77.

5.2.1 Responses for size optimization

The responses are mapped in the design space by using different types of transformation functions. The best response equations are selected after evaluating its R_{adj}^2 value and standard deviation. The response surfaces of displacement (δ_b) and acceleration (a_b) for typical cases obtained for size optimization (k=4) are given in Figure 5-5 (a) and 5-5 (b) respectively. The actual and predicted values are very close in both cases (Figure 5-5 (b) and 5-6(b)). The response equations of plastic strains for both face plates are also developed. No response for the mass is fitted as an analytical formula exists.

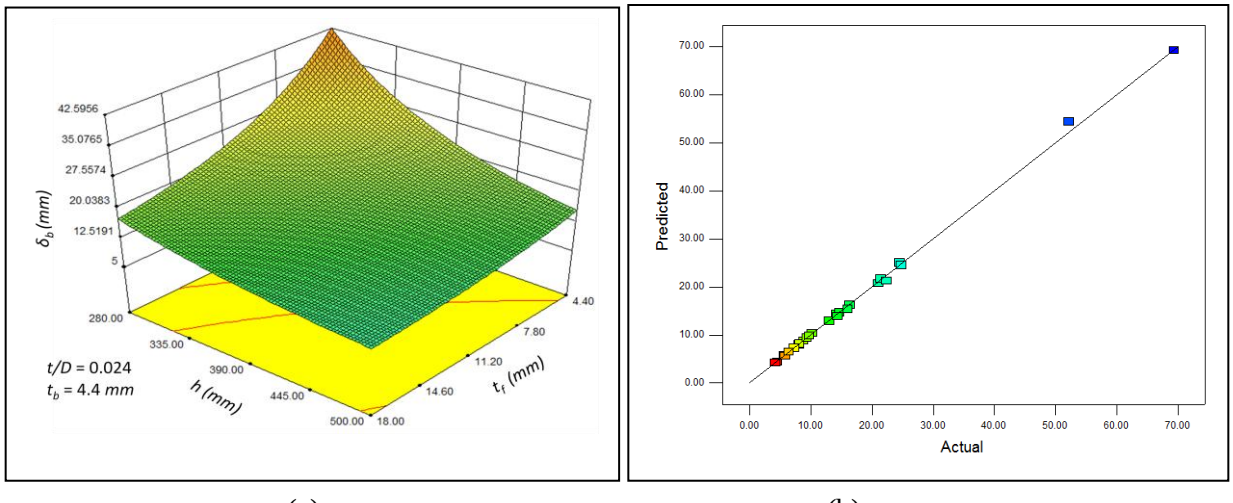

(a) (b)

Figure **5-5**: (a) Response surface and (b) Actual-predicted plot for δ_b minimization using sizing parameters

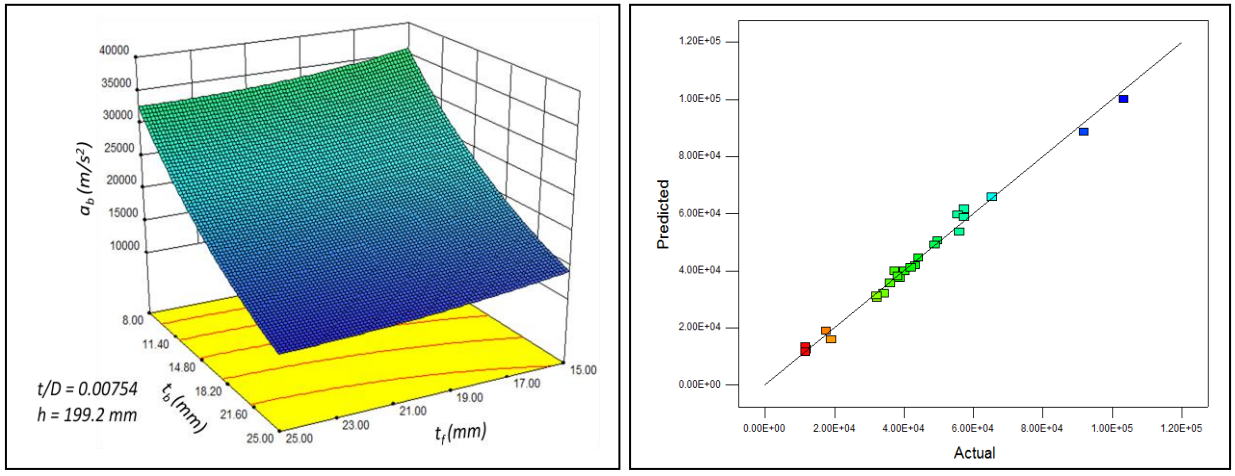

(a) (b)

Figure **5-6**: (a) Response surface and (b) Actual-predicted plot for a_b minimization using sizing parameters

5.2.2 Responses for size and shape optimization

In a similar fashion, the responses are mapped and the best response equations are selected. Since shapes are involved here, response equation for the mass is developed instead of building its complex analytical form. The response surface and actual-predicted plot for simultaneous size and shape optimization (k=6) are given in Figure 5-7. No size and shape optimization is carried out for minimizing a_b. The actual and predicted values are very close to each other.

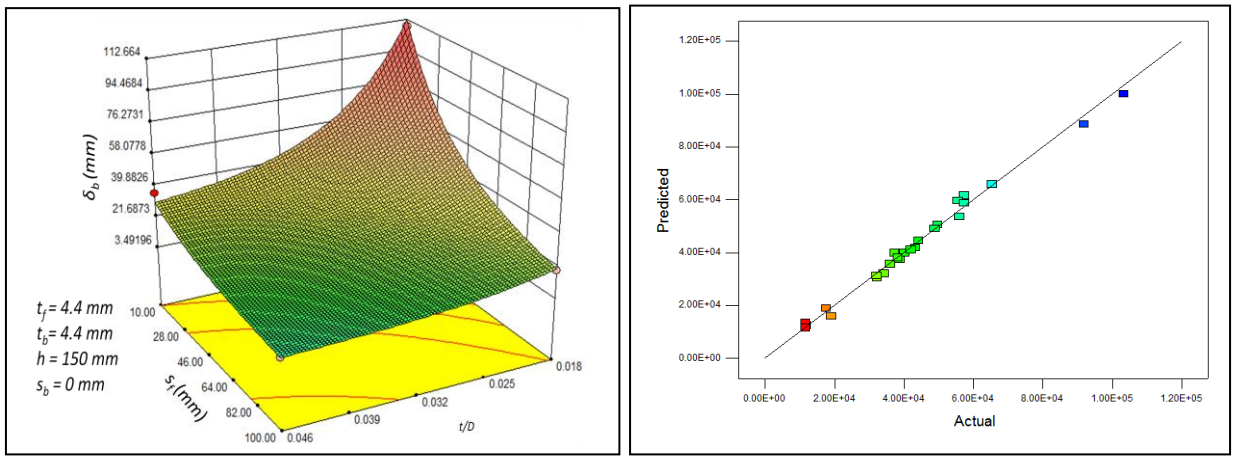

(a) (b)

Figure **5-7**: (a) Response surface and (b) Actual-predicted plot for δ_b minimization using sizing and shape parameters

Chapter 6

Optimization Results

6.1 Introduction

First, a simple parametric study is presented to investigate the optimum configuration of core parameters only to minimize the face plate deflections. Then thorough optimization results are presented at different mass limits of the sandwich for minimizing δ_b.and a_b. Detailed results are presented for 150 *kg* mass limit of the sandwich. The optimization study is carried out for a fixed amount of charge, viz. 8 *kg* TNT. The effective blast load on the structure varies with the shape of the front face as well as the magnitude of the concave deformation of the front face plate (Figure 6-1). Considering blast in air, a convex bulge reduces the effective blast load by deflecting the blast wave outward, while a concave shape increases the impulse imparted to the structure resulting in increased effective blast load. Further, a concave deformation in a flat panel also increases the effective blast load. This effective blast load is discussed in terms of the magnitude of the saturated Z-momentum of the whole structure, which equals the saturated Z-impulse imparted to it. The δ_b, a_b, ε_{pmax} and total *Z*-impulse values given in this Chapter refer to the LS-DYNA output.

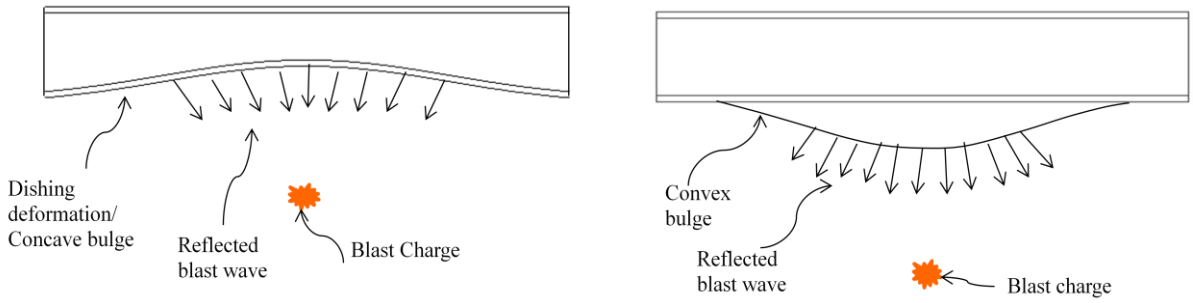

(a) (b)

Figure **6-1**: Reflection of blast wave from (a) concave deformation or bulge and (b) convex bulge at front face plate

6.2 Parametric study for minimum face plate displacement for comparing the result with published results

While diverse models have been used in the literature, a parametric study is presented here which shows that the LS-DYNA based model developed herein generates a trend that is similar to a published (analytical) model in [10]. The effect of core density on face plate deflections is studied for constant panel mass. To compare the results to the publication, nondimensional quantities are introduced, viz. mass per unit area $M/(\rho_f l)$, core thickness $\left(h/l\right)$ and relative core density ρ_c/ρ_f, where l is the half side length of the square panel. For both the cases, $M/(\rho_f l) = 0.0334$ is fixed. When the core density is varied, $\left(h/l\right) = 0.134$ is taken and when core depth is varied, ρ_c/ρ_f = 0.03 is taken. In both the cases, the value of *M =81.11 kg, l* = 0.6096 *m*, $\rho_f = 2680\ kg/m^3$ and blast load = 2.5 *kg* of TNT remains same, and ρ_c and *h* are varied. As a function of core density, the face plate deflections first decrease and then increase (Figure 6-2). Thus, there is an optimum core density which produces minimum face plate deflections. It can be noted that a weaker core undergoes large compression and hence produces large face plate deflections. When the core density increased (beyond relative density = 0.16), the face plate thickness becomes so small to keep panel mass constant, that again face plate deflections start to increase. With increase in core height, the nature of the plot is similar to the previous plot, but not that prominent. Front face deflection is minimum at $\left(h/l\right) = 0.17$ and backface plate deflection is minimum$\left(h/l\right) = 0.62$. This agreement adds confidence to carry out optimization within a more general framework, where several design variables are considered simultaneously.

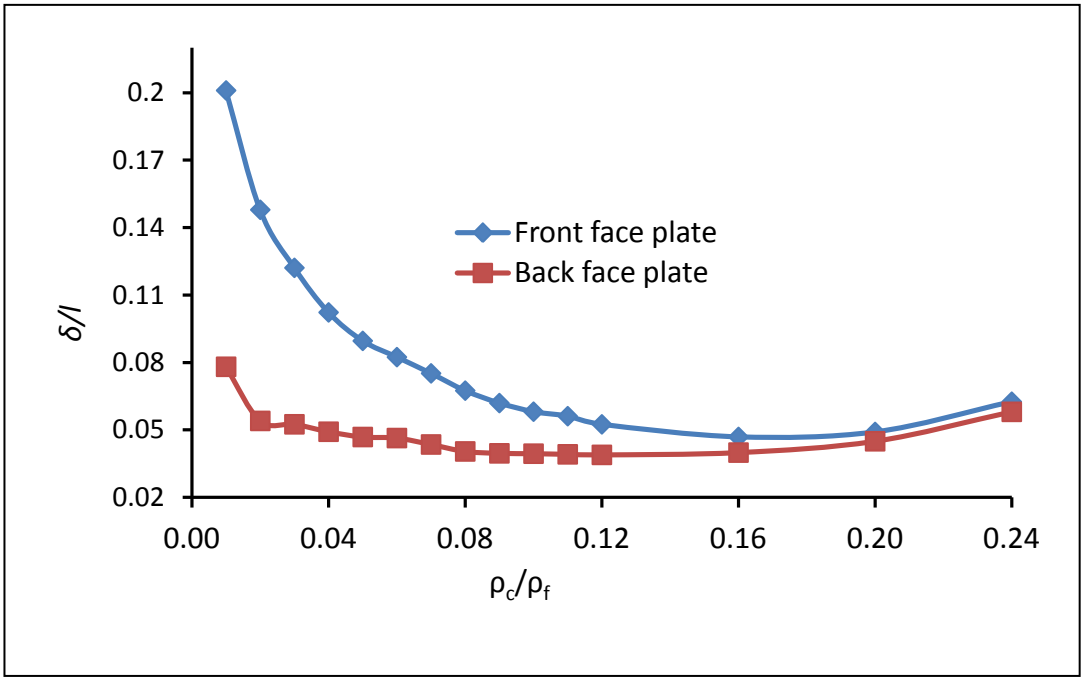

Figure **6-2**: Deflection of face plates with variation of core density

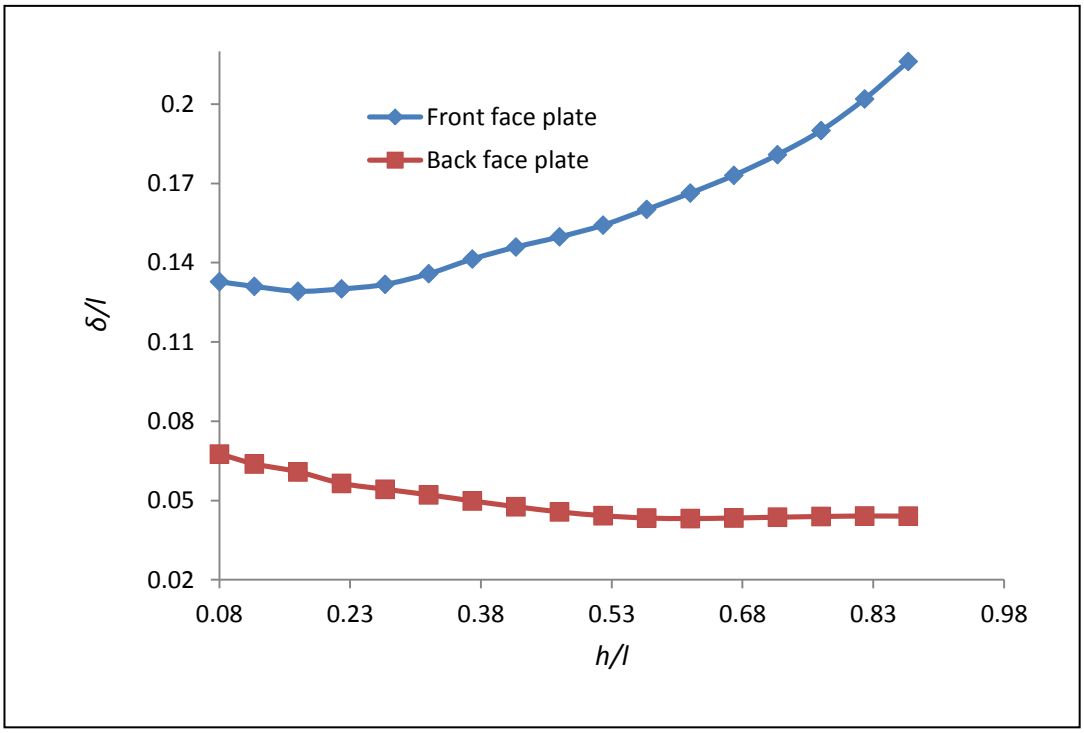

Figure **6-3**: Deflection of face plates with variation of core height

6.3 Optimization results for minimum displacement, δ_b

6.3.1 Optimization results for different mass limits of sandwich and monolithic plate

Table 6-1(a) shows the limits used and Table 6-1(b) summarizes the optimization results for different mass limits of the size (t_b, t_f, h, t/D) optimized sandwich panel. Table 6-2(a) shows the limits used and Table 6-2(b) summarizes the optimization results for different mass limits of the size+shape (t_b, t_f, h, t/D, s_b, s_f) optimized sandwich panel. Mass fraction of the front face plate increases with sandwich mass in terms of t_f in size optimization and s_f in simultaneous size and shape optimization. The bulge height s_f also provides overall stiffness to the sandwich. Thicker (stiffer) front face plate is good to transfer the blast load to a larger area of core and also reduces concave deformation which eventually decreases the impulse received by sandwich. Both the effects reduce backface displacement. The optimizer always keeps the backface plate thickness at its lower limit. Higher *t/D* (means higher core density) reduces the concave deformation and lowers δ_b. Larger core depth increases the overall stiffness of the sandwich and lowers δ_b. In size optimization, with sandwich mass, h first increases and then decreases and the core gets stiffer (due to increase of *t/D*). In size and shape optimization, with sandwich mass, h remains at lower limit and *t/D* increases. Maximum plastic is always at the center of front face plate for size optimization, while it is at backface plate for size + shape optimization. Mass is always active in both cases.

Table **6-1(a)**: Design limits for {t_b, t_f, h, t/D}-optimization, min. δ_b

Design limits	Lower limit	Upper limit
Front face plate thickness (*mm*), t_f	4.4	18
Core depth (*mm*), h	280	500
Foil thickness/cell size, *t/D*	0.018	0.046
Backface plate thickness (*mm*), t_b	4.4	10

Table **6-1(b)**: Optimization results for {t_b, t_f, h, t/D}-optimization with varying mass limits, min. δ_b (units: *mm*)

Sandwich Mass (*kg*)	Optimized parameters					ε_{pmax}
	t_f	h	t_b	(t/D)	δ_b (Obj)	
130	8.07	300.6	4.4	0.0252	24.3	0.0384
140	7.90	359.9	4.4	0.0238	19.96	0.0373
150	7.55	401.6	4.4	0.0240	16.92	0.033
160	8.4	390.2	4.4	0.0263	14.65	0.023
170	9.12	388	4.4	0.0282	12.43	0.017

Table **6-2(a)**: Design limits for {t_b, t_f, h, t/D, s_b, s_f}-optimization, min. δ_b

Design limits	Lower limit	Upper limit
Front face plate thickness (*mm*), t_f	4.4	10
Core depth (*mm*), h	150	500
Foil thickness/cell size, t/D	0.018	0.046
Backface plate thickness (*mm*), t_b	4.4	10
Front face plate bulge (*mm*), s_f	10	100
Backface plate bulge (*mm*), s_b	0	100

Table **6-2(b)**: Optimization results for {t_b, t_f, h, t/D, s_b, s_f}-optimization with varying mass limits, min. δ_b (units: *mm*)

Sandwich Mass (*kg*)	Optimized parameters							ε_{pmax}
	t_f	h	t_b	(t/D)	s_f	s_b	δ_b (Obj)	
130	4.4	150	4.4	0.0364	42.41	0	20.76	0.031
140	4.4	150	4.4	0.0371	52.69	0	17.04	0.020
150	4.4	150	4.4	0.0377	62.96	0	14.4	0.014
160	4.4	150	4.4	0.0384	73.24	0	12.25	0.012
170	4.4	150	4.4	0.039	83.52	0	10.73	0.001

Table 6-3(a) shows the limits used and Table 6-3(b) summarizes the optimization results for different mass limits of the shape $\{t_p, s_b, s_f\}$ optimized monolithic plate. Mass and front bulge height is always active ($s_f = 100\ mm$), back bulge height increases with mass while base plate thickness (t_p) decreases. Like front face bulge, backface bulge adds stiffness to the plate at its center.

Table **6-3(a)**: Design limits for $\{t_p, s_b, s_f\}$-optimization, min. δ_b

Design limits	Lower limit	Upper limit
Plate thickness (*mm*), t_p	4.4	38
Front bulge (*mm*), s_f	0	100
Back bulge (*mm*), s_b	0	100

Table **6-3(b)**: Optimization results for $\{t_p, s_b, s_f\}$-optimization with varying mass limits, min. δ_b (units: *mm*)

Plate Mass (*kg*)	Optimized parameters				ε_{pmax}
	t_p	s_f	s_b	δ_b (Obj)	
130	7.39	100	16.74	15.24	0.032
140	6.78	100	31.16	13.23	0.033
150	6.32	100	44.87	11.52	0.027
160	6	100	57.98	10.11	0.02
170	5.78	100	70.58	8.89	0.018

6.3.2 Comparison of results for 150 *kg* sandwich and monolithic plate

Now, focusing on the 150 *kg* mass limit, Figure 6-4 shows the performance of the optimized sandwich panel and how it compares with an all-aluminum monolithic plate. A non-optimized uniformly thick aluminum panel is also included in the comparison for reference purposes. The corresponding blackface deflection-time responses are shown in Figure 6-5(a), plastic strains in Figure 6-5(b) and *Z*–momentum in Figure 6-5(c). Compared to the uniformly thick aluminum panel, the sandwich panel shows significant reduction (by 66.4%). Shape optimization of the sandwich adds

to this improvement (by 14.9%). However, a shape-optimized all-aluminum panel scored a victory as compared to the sandwich (11.5 *mm* to 14.4 *mm* deflection). A physical explanation for this is given subsequently. In the sandwich, the mass fraction in the front face plate, core and the backface plate are 0.20, 0. 68 and 0.12, respectively, for the $\{t_b, t_f, h, t/D\}$-optimized panel and 0.48, 0.40 and 0.12, respectively, for the $\{t_b, t_f, h, t/D, s_b, s_f\}$, optimized panel.

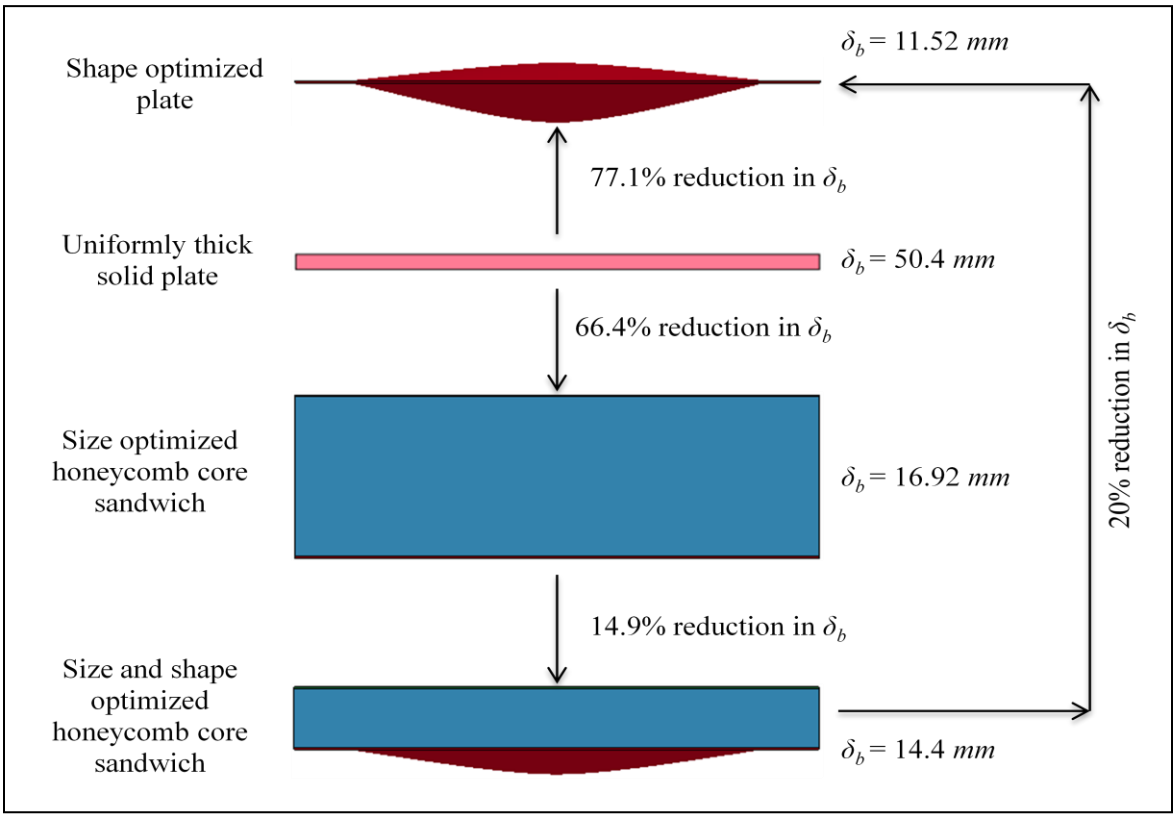

Figure **6-4**: Optimized sandwich panel and shape optimized monolithic plate of 150 *kg* mass for minimizing δ_b (stiffener not shown)

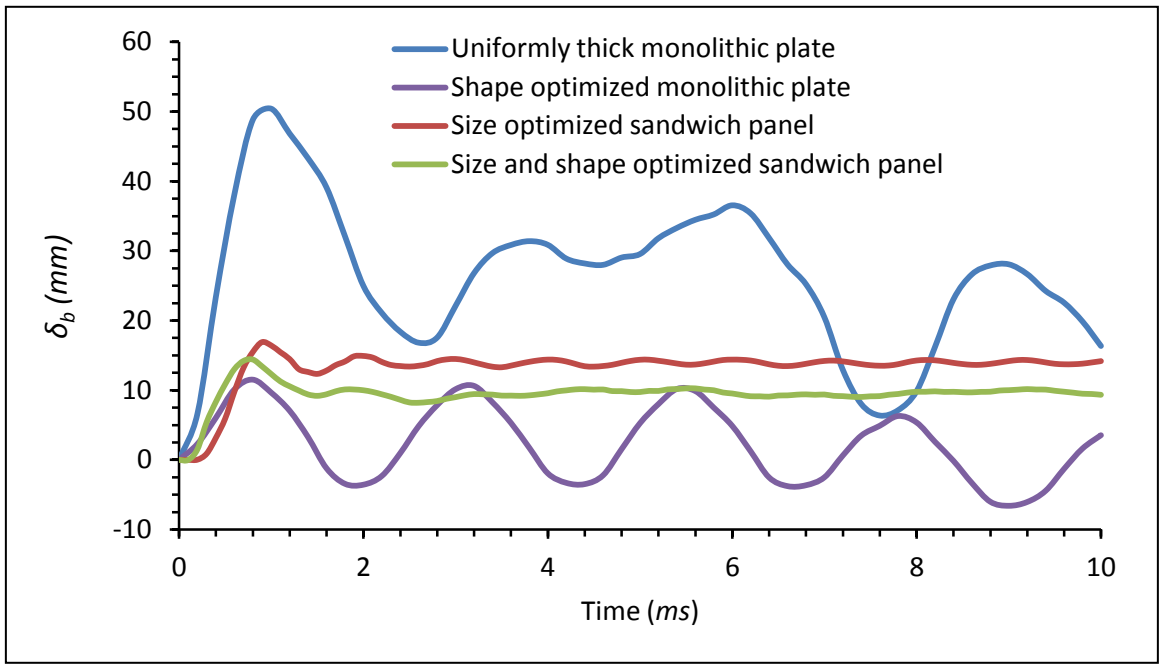
Uniformly thick monolithic plate
Shape optimized monolithic plate
Size optimized sandwich panel
Size and shape optimized sandwich panel
δ_b (mm)
60
50
40
30
20
10
0
-10
0
2
4
6
8
10
Time (ms)

(a)

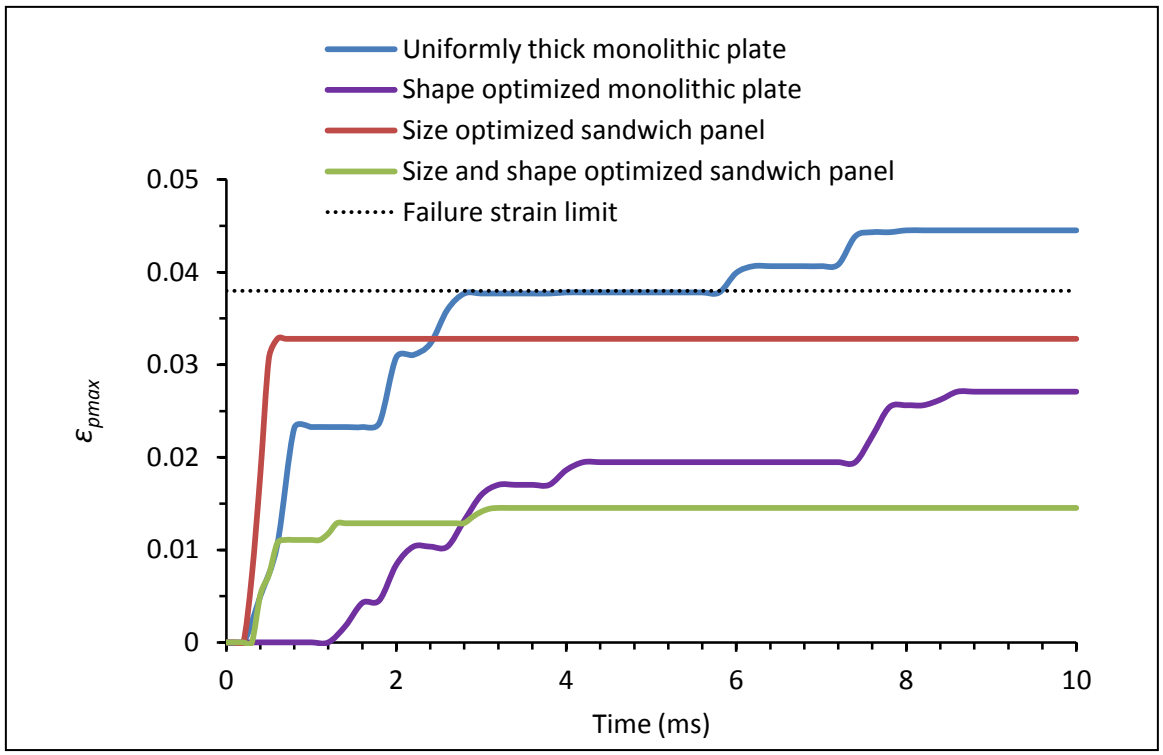
Uniformly thick monolithic plate
Shape optimized monolithic plate
Size optimized sandwich panel
Size and shape optimized sandwich panel
Failure strain limit
ε_{pmax}
0.05
0.04
0.03
0.02
0.01
0
0
2
4
6
8
10
Time (ms)

(b)

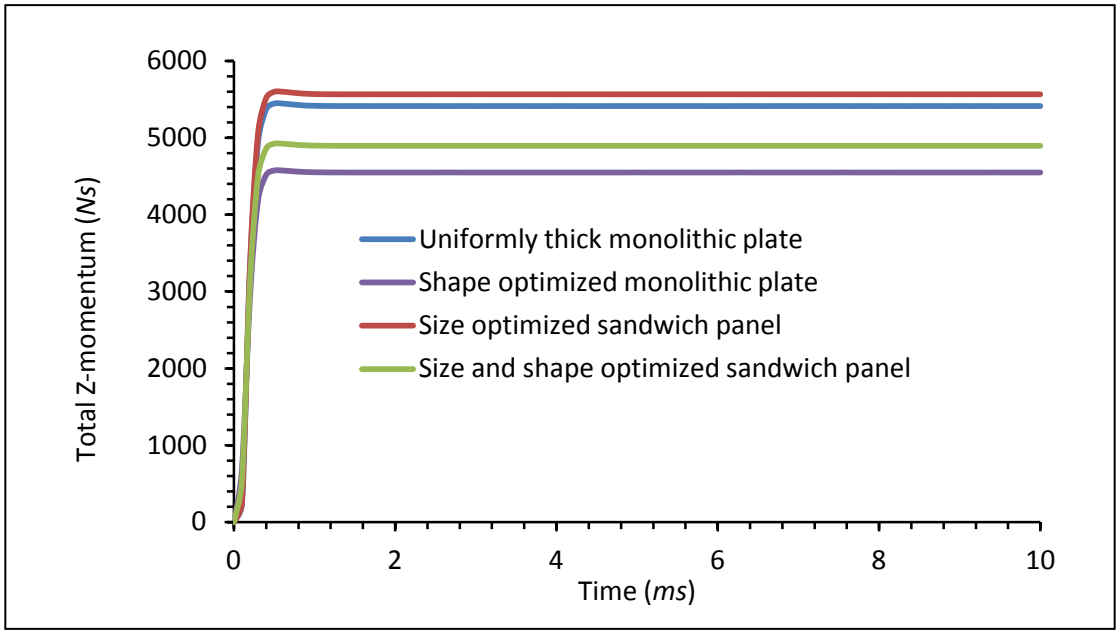

(c)

Figure **6-5**: Comparison for minimum δ_b of 150 *kg* mass limit: (a) δ_b, (b) ε_{pmax} and (c) total *Z*-momentum.

The deflection of monolithic flat plate and shape optimized plate is more oscillating (Figure 6-5(a)) than that of a sandwich. In a sandwich, the plastic deformation in core dampens the deflection. Maximum plastic strain (Figure 6-5(b)) in the monolithic flat plate has exceeded the failure limit whereas in case of size + shape optimized panel, it is well below the failure limit. Thus, further improvement can be made in case of size + shape optimized panel by expanding the design limits. Higher front bulge height (s_f =100 *mm*) for the shape optimized monolithic plate results in less *Z*-momentum (Figure 6-5 (c)) than that of size + shape optimized sandwich panel. Higher concave deformation of the front face plate of size optimized sandwich panel, results in higher Z-momentum than that of the monolithic plate.

6.3.3 Mechanism causing the improvement in backface deflection

In the {t_b, t_f, h, t/D}-optimized panel, the optimizer has chosen a larger core depth which increases the overall stiffness of the sandwich and lowers δ_b. The t_b is always at lower limit (4.4 *mm*) as it is sufficient to keep ε_{pmax} below the strain limit (0.038). The t_f is decided based on three things, viz. to keep ε_{pmax} below the strain limit, to provide sufficient stiffness for the front face plate to transfer the blast pressure load to a larger area of the core, and to reduce local concave deformation of the front face plate which will increase the impulse.

Compared to the {t_b, t_f, h, t/D}-optimized panel above, the {t_b, t_f, h, t/D, s_b, s_f}-optimized panel has further reduced the deflection by 14.9%. This may be attributed to the following mechanisms. A lesser core depth has been produced but with a bulge in the front face plate. The core is denser. The bulge deflects the blast wave and reduces the impulse imparted to the structure, and it also increases the moment of inertia of the sandwich at its center where blast load is maximum. The bulge also makes the front face plate stiffer, which helps to transfer the blast load to a large area of the core thereby reducing local deformation at the center.

In the all-aluminum monolithic plate, more mass is available to go in terms of bulge (Table 6-2(b) and 6-3(b)), whereas in the sandwich, mass is distributed between face plates and core. Higher the bulge height towards the blast, greater is the reduction in impulse and hence greater the reduction in backface deflection. This aspect and higher rigidity makes the monolithic plate slightly better than the sandwich panel as shown in Figure 6-5(a).

6.4 Optimization results for minimum acceleration, a_b

6.4.1 Optimization results for different mass limits of sandwich and monolithic plate

Table 6-4 summarizes the {t_b, t_f, h, t/D}-optimized results for different mass of the sandwich. With increase in mass, a_b decreases. It shows that both h and t_b increases with sandwich mass, but t_f does not vary much. For the reasons explained before, optimizer produces thicker front face plate [7]. The core density (proportional to *t/D)* always remains at the lower bound. The ε_{pmax} is always at the center of face plate and very close to the limiting value of 0.038 for all the mass limits. It can be observed that with increase in sandwich mass, the optimizer adds mass more to the backface plate than to the core; a_b not only depends upon the force transmitted to the backface plate but also on the backface plate mass [7, 11].

Table **6-4(a)**: Design limits for {t_b, t_f, h, t/D}-optimization, min. a_b

Design limits	Lower limit	Upper limit
Front face plate thickness (*mm*), t_f	15	25
Core depth (*mm*), h	120	400
Foil thickness/cell size, *t/D*	0.00754	0.025
Backface plate thickness (*mm*), t_b	8	25

Table **6-4(b)**: Optimization results for {t_b, t_f, h, t/D}-optimization with varying mass limits, min. a_b (units: *mm*, m/s^2)

Sandwich Mass (*kg*)	Optimized parameters					ε_{pmax}
	t_f	h	t_b	(t/D)	a_b (Obj)	
130	17.94	194.93	10.77	0.00754	2.77×10^4	0.0355
140	17.79	196.84	13.4	0.00754	2.22×10^4	0.0360
150	17.63	199.22	16.02	0.00754	1.84×10^4	0.0371
160	17.45	202.16	18.64	0.00754	1.57×10^4	0.0388
170	17.45	205.2	21.1	0.00754	1.37×10^4	0.0388

Table **6-5**: Optimization results for $\{t_p, s_b, s_f\}$-optimization with varying mass limits, min. a_b (units: *mm*, m/s^2)

Plate Mass (kg)	a_b
130	10.22×10^4
140	9.5×10^4
150	8.88×10^4
160	8.33×10^4
170	7.85×10^4

Table 6-5 summarizes the acceleration results for different mass limits of the shape $\{t_p, s_b, s_f\}$ optimized monolithic plate. Optimized parameters are same for both minimizing δ_b and a_b. Since the front bulge height remians same (s_f =100 *mm*) for all the mass limits, the impulse imparted (Z-momentum) to plate also remians almost same. Also, there is no mechanism available to absorb the blast energy in a monolithic plate, so with increase in mass, a_b decreases in the same ratio as mass increase.

6.4.2 Comparison of results for 150 *kg* sandwich and monolithic plate

Focusing on the 150 *kg* mass limit, Figure 6-6 shows the performance of the optimized sandwich panel and how it compares with an all-aluminum monolithic plate. The corresponding acceleration-time responses are shown in Fig. 14(a). $\{t_b, t_f, h, t/D\}$-optimized sandwich panel results in 84% reduction in a_b compared to a uniformly thick monolithic plate of equal mass. The location of the ε_{pmax} is at the center of the front face plate.

Now, comparing the optimized sandwich to an optimized all-aluminum monolithic panel, the sandwich scores a clear victory (compare 1.84×10^4 to 8.88×10^4 m/s^2). Recall that the victor was reversed for δ_b minimization. The monolithic plate has no mechanism for energy absorption. The mass fraction in the front face plate, core and the backface plate are 0.47, 0.11 and 0.42 respectively.

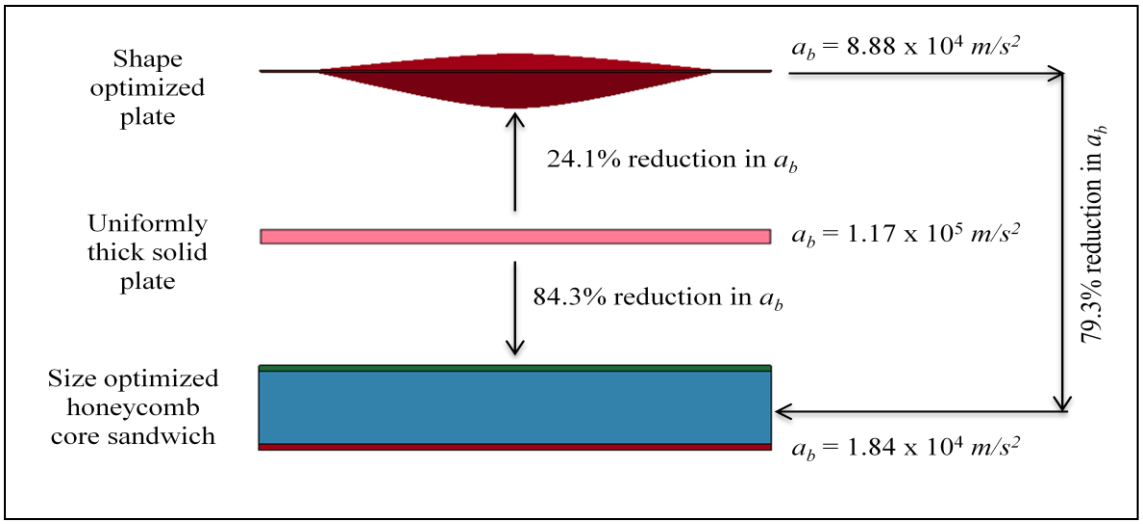

Figure **6-6**: Optimized sandwich panel and shape optimized monolithic plate of 150 *kg* mass for minimizing a_b (stiffener not shown)

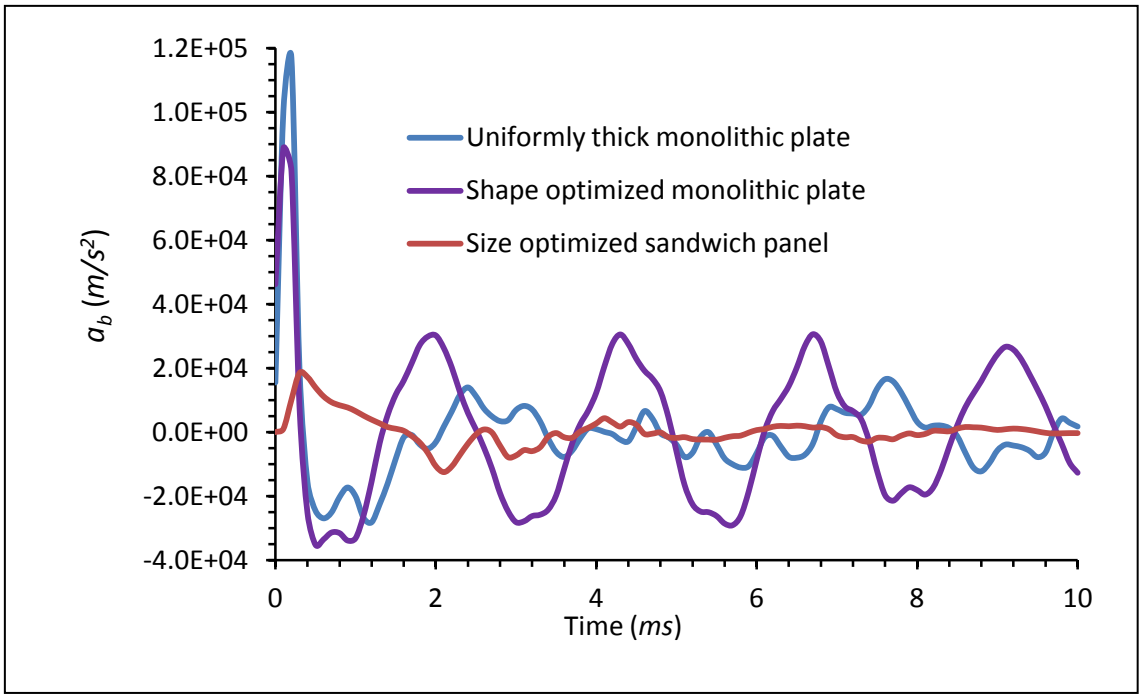

(a)

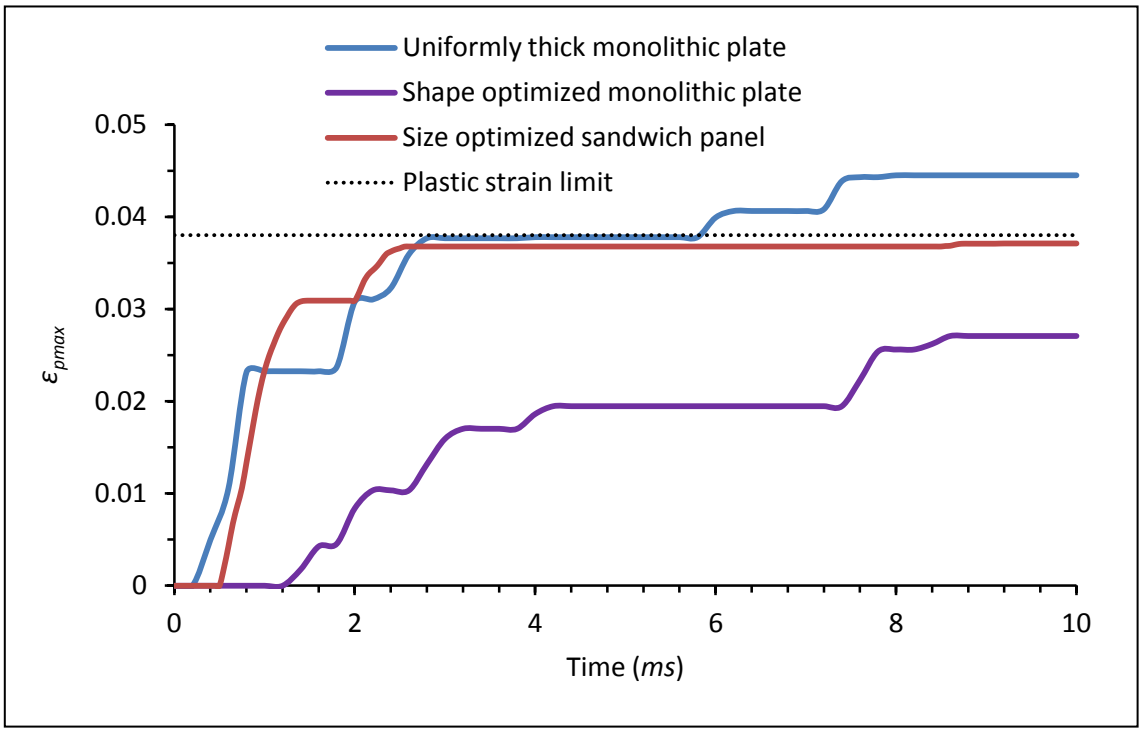

(b)

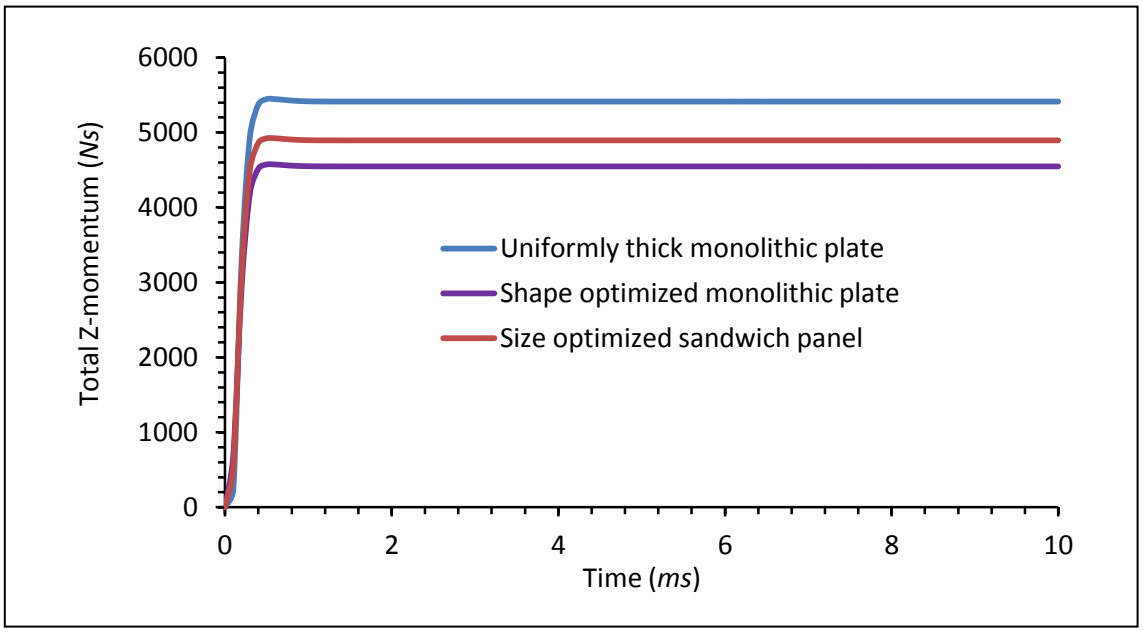

(c)

Figure **6-7**: Comparison for minimum a_b of 150 *kg* mass limit: (a) a_b, (b) ε_{pmax} and (c) total *Z*-momentum

6.4.3 Mechanism causing the improvement in backface acceleration

A paper by Avalle et al [21] explains the relation between energy absorption and transmitted force. We note that a_b is a direct measure of the transmitted force, and that core density ρ and t/D are linearly related. In Figure 6-8, the area under the three curves $\int \sigma \, d\varepsilon$ are the same. The area represents energy per unit volume, and σ_b denotes the corresponding stress value, which is here the compressive stress in the core elements in contact with the backface plate. For low density core ρ_1, the deformation is high and densification range is entered causing high stress; for high density core ρ_3, the energy is absorbed with low deformation and high stress. The medium density foam ρ_2 is optimum as σ_b is lowest. In fact, an efficiency index has been defined in [23] as

$$\eta = \frac{\int \sigma d\varepsilon}{\sigma_b} \tag{6.1}$$

Higher efficiency implies that the core absorbs a given amount of energy with lesser transmitted force. A look at the results show that optimization has exploited this physics: t/D and core depth have been adjusted so that even though the maximum strain in front face elements have gone to the densification region (strain > 0.744), the strain in the backface elements are well within the crushing zone avoiding complete densification (Figure 6-9). The t/D has been pushed to its lower bound. Further, a comparison of η between the optimized results for a_b vs. δ_b minimization (Table 6-6) clearly shows that the optimizer has done its task: when the objective is a_b, a more efficient core is designed. Of course, optimization also adjusts the mass distribution between face plates and core, subject to constraints on sandwich mass, plastic strain in plates and lower bounds on t/D.

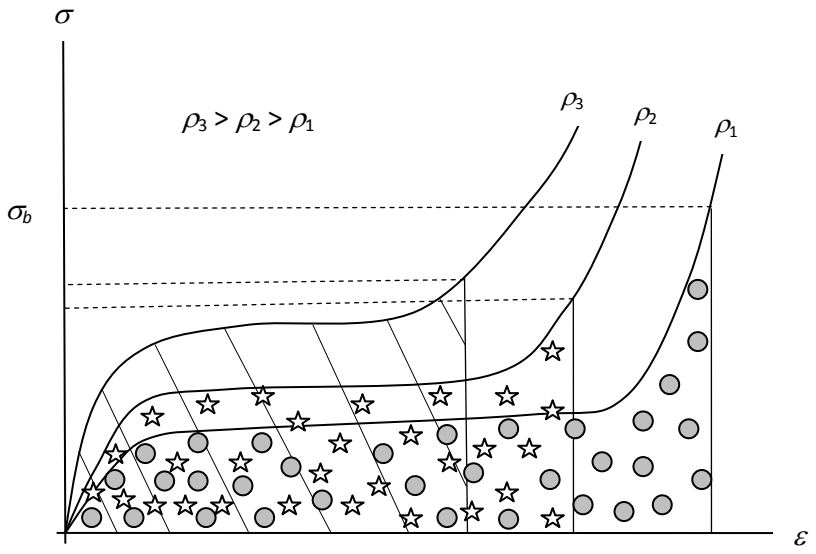

Figure **6-8**. Stress (at the backface) for different density foams corresponding to same energy absorption

Table **6-6**: Comparison of honeycomb core energy absorption efficiency

Case	*t*/*D*	$\int \sigma d\varepsilon$ (*Pa*)	σ_b (average) (*Pa*)	η
acceleration_ min ($a_b^* = 1.84 \times 10^4\ m/s^2$)	0.00754	702377.6	1.58×10^6	44.5 %
deflection_min ($a_b^* = 7.25 \times 10^4\ m/s^2$)	0.024	569514.2	5.59×10^6	10.2 %

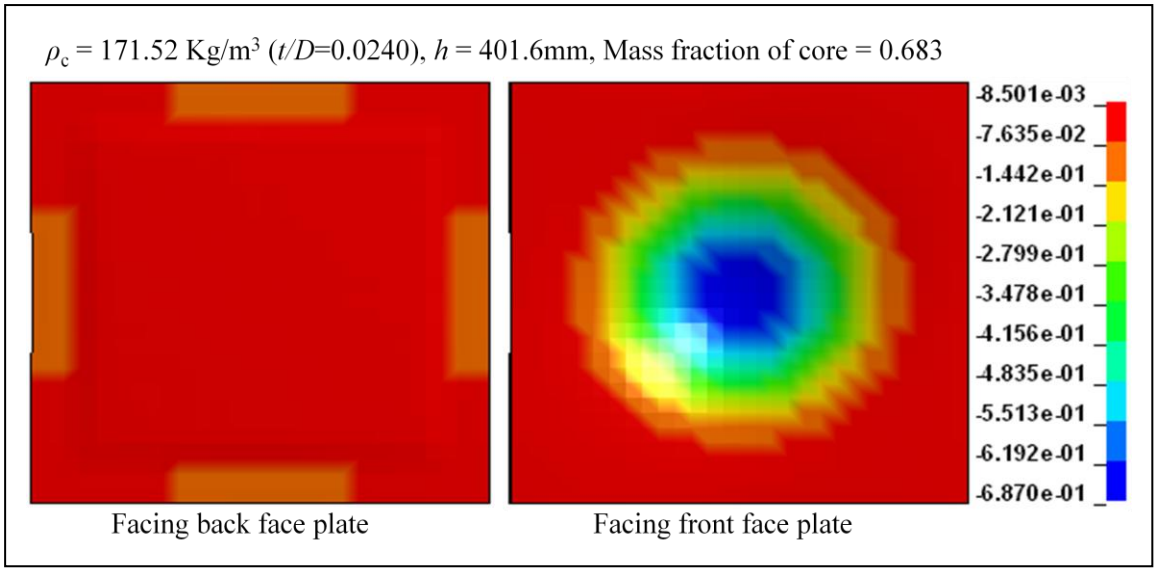

(a)

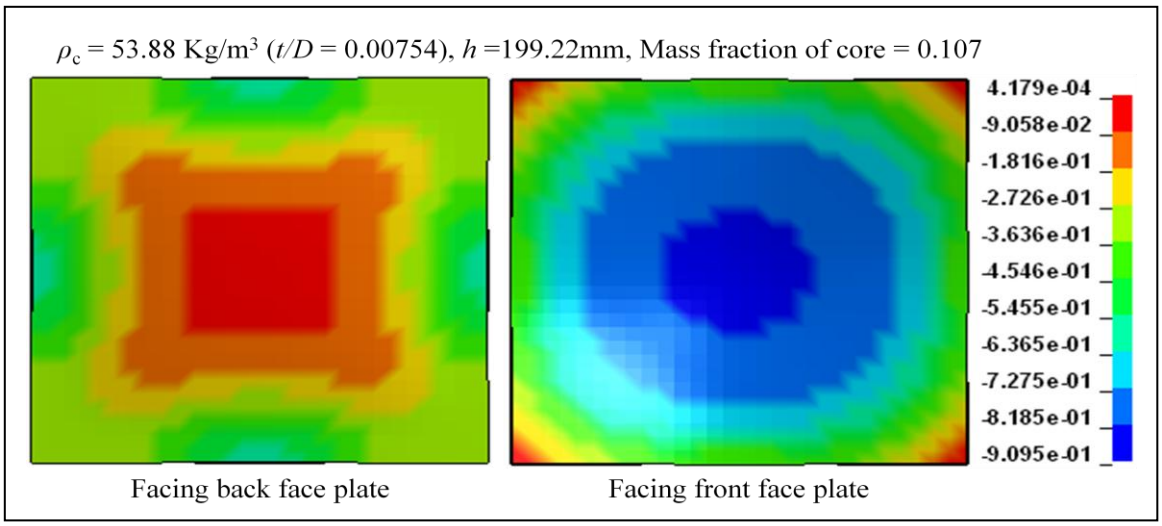

(b)

Figure **6-9**: Distribution of the *z*-strain (engineering strain) in the *x*-*y* plane of core at the layer facing the front face, and at the layer facing the back face, respectively, for (a) δ_b -minimization, and (b) a_b-minimization

6.5 Analysis of energy absorption in 150 *kg* size optimized sandwich

Table 6-7 shows the energy absorption in the 150 *kg* size optimized sandwich panel for the two objectives. Total energy (TE) for minimization of δ_b (lesser t_f) is higher than that of a_b (higher t_f). Lesser is the front face plate thickness, higher is the energy received by the core (Equation 2.2)[24]. The core internal energy (*CIE*) is calculated on the basis of area under the stress strain curve by taking the *z*-strain reported by LS-DYNA. This matched well with the *CIE* reported by LS-DYNA. So it can be concluded that *CIE* is mainly due to *z*-strain and the effect of lateral strain is small. The fraction *CIE*/*TE* is 0.82 and 0.62 for minimizing δ_b and a_b, respectively. The former is higher because of higher mass fraction of core (0.683) in case of minimizing δ_b, compared to 0.107 in the case of minimizing a_b [27]. However, the energy absorbed per unit mass of core is 1.3 x 10^4 *J/kg* for size optimized panel for minimizing a_b compared to a smaller 0.332x10^4 J/*kg* for minimizing δ_b. Higher energy per unit mass indicates that larger portion of the core has crushed to a higher strain to absorb the energy. Figure 6-9 shows that core in case of a_b minimization has been crushed to a large extent than that of δ_b minimization.

Table **6-7**: Energy absorption in the sandwich

150 *kg* Size optimized sandwich	P_z (*Ns*)	*TE* (*J*)	*TIE* (*J*)	*CIE (J)*	*CIE* in crushing from stress-strain curve (*J*)	*CIE/TE*	*CIE per unit mass of core* (*J/kg* of core)
δ_b	5564.67	4.14 x10^5	3.76x10^5	3.40 x10^5	3.38 x 10^5	0.82	3.32x10^3
a_b	5504.6	3.00 x10^5	2.77x10^5	2.08 x 10^5	1.86 x 10^5	0.62	13.0 x 10^3

As the blast impulse is delivered to front face plate of the sandwich, the front face plate attains the KE while the core and backface plate remains stationary [10]. This statement is more valid for very soft core. Figure 6-10 (a) shows that most of the initial blast energy is delivered to front face plate in the form of KE. However in Figure 6-11, the initial KE is well shared by both front face plate and core.

This can be explained by the fact that the core in the later case is much stiffer and denser than the former. This KE is subsequently transferred to the sandwich and major part of it converted to IE.

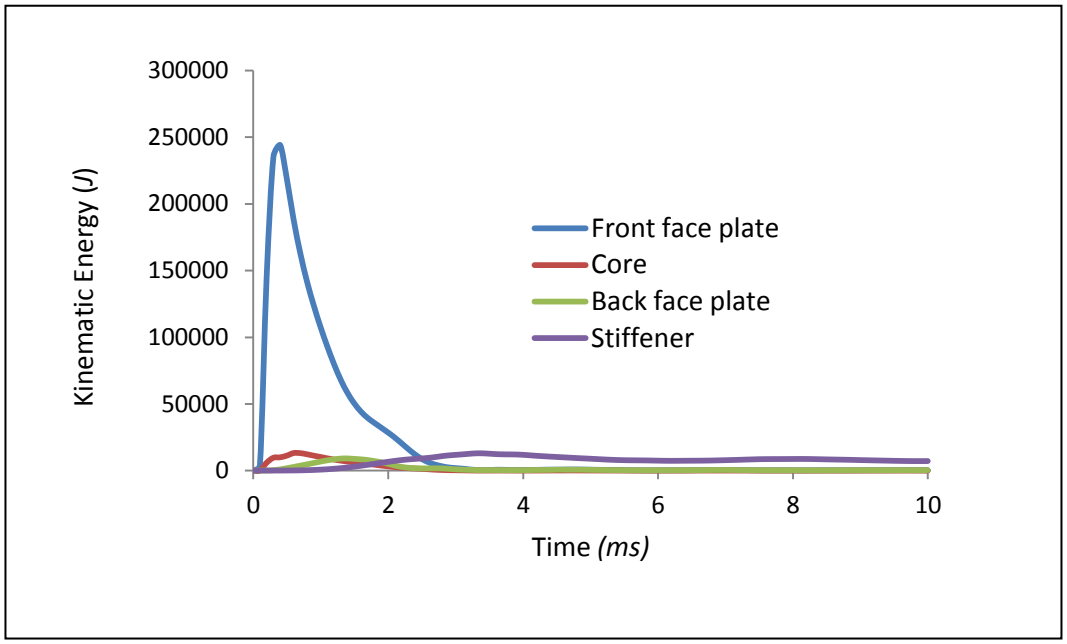

(a)

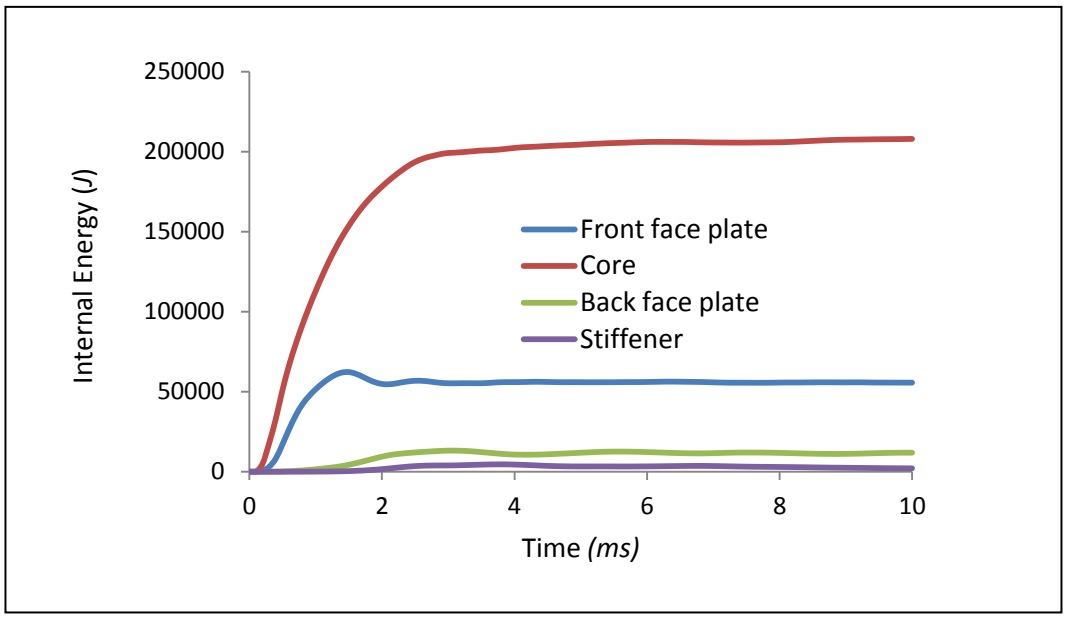

(b)

Figure **6-10**: Energy gained by different layers of sandwich of 150 *kg* size optimized sandwich for minimizing a_b, (a) KE and (b) IE

IE of the front face plate as shown Figure 6-10 (b) is higher than that of shown in Figure 6-11(b) due to higher thickness.

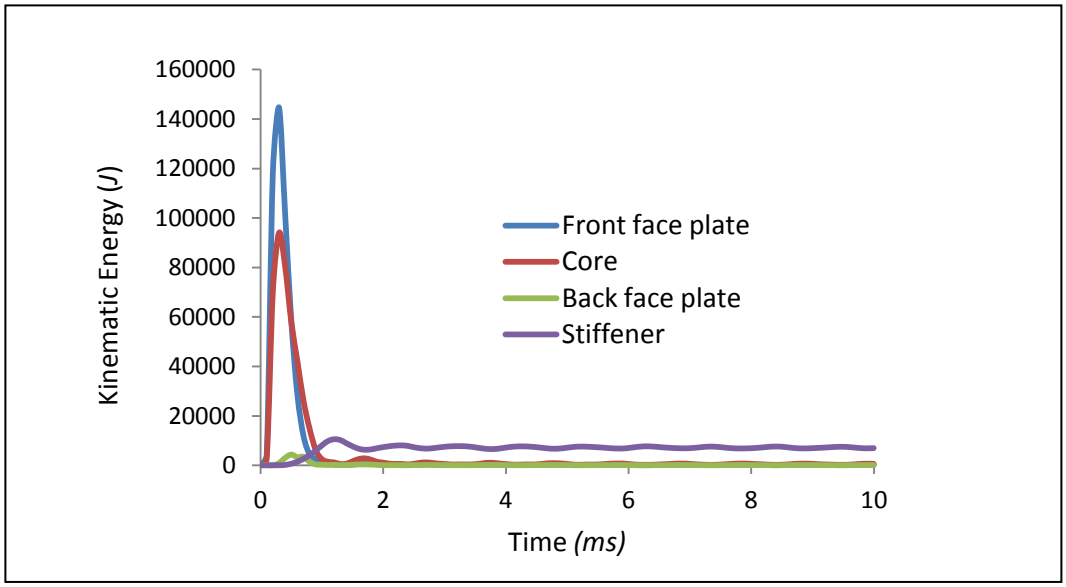

(a)

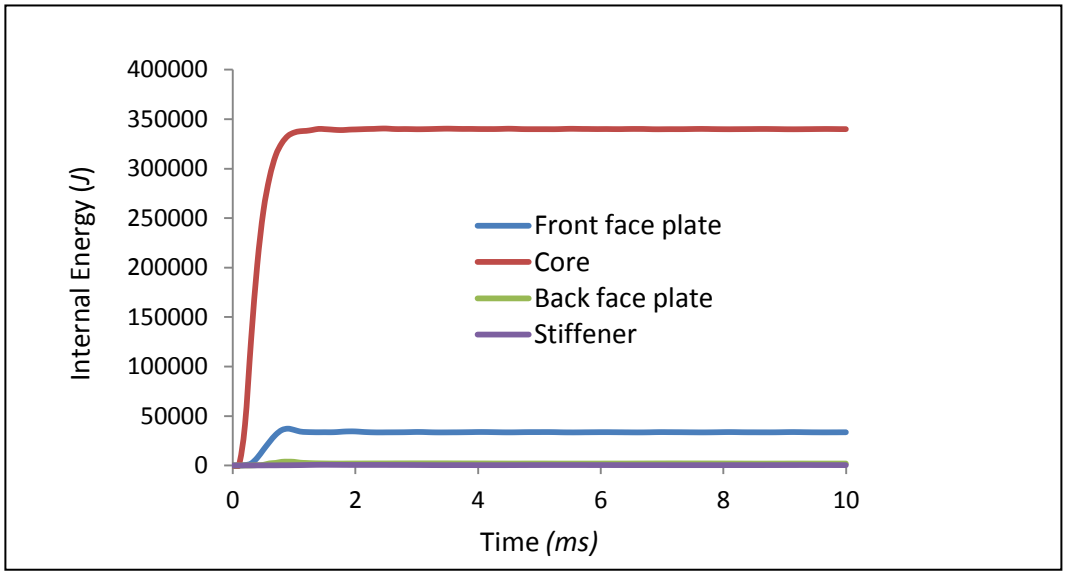

(b)

Figure **6-11**: Energy gained by different layers of sandwich of 150 *kg* size optimized sandwich for minimizing δ_b, (a) KE and (b) IE

6.6 Sensitivity analysis

Sensitivity of the optimized results with respect to stiffener mass and blast location, respectively, is presented below.

6.6.1 Sensitivity analysis with respect to stiffener mass

The effect of mass of stiffener on δ_b is shown in Table 6-11 by varying its mass by ±15% and ±30%. With increase in stiffener mass, δ_b increases but by a very small amount. ε_{pmax} remains same.

Table **6-8**: Siffener mass sensitivity for 150 *kg* size optimized sandwich for δ_b minimum

Stiffener mass (kg)	δ_b (mm)	ε_{pmax}
1295	16.42	0.0328
1572.5	16.70	0.0328
1850	16.92	0.0328
2127.5	17.06	0.0328
2405	17.18	0.0328

6.6.2 Sensitivity analysis with respect to blast location

For all three 150 *kg* optimized sandwich configurations discussed in section 6.3 and 6.4, blast locations are varied by 0.15 *m*, 0.3 *m* and 0.45 *m* along the x-axis and results are analyzed. Due to off-center blast, the panel translates as well as rotates. Here δ_b refers to the maximum deflection of the backface plate relative to stiffener and measured along the normal direction to the plane of stiffener.

With increase in off-center location of the charge, peak blast pressure gets closer to the edge of the panel and front face plate deflection increases for all the cases, whereas δ_b first increases and then decreases (due to the presence of stiffener towards the edge of panel) in case of size optimized panel

and increases in case of size and shape optimized panel. In case of size and shape optimized panel, since the blast hit the side of the bulge, the effective blast load becomes high and δ_b continues to increase. Same trend is also found for maximum plastic strain and can be explained similarly. Impulse (or change in momentum) delivered to the sandwich decreases with increase in off-center location of the charge, however the rate of decrease in case of size and shape optimized panel is less because of relatively higher effective blast load due to the bulge. Variation of a_b, ε_{pmax} and momentum for size optimized panel for min a_b is similar to the case for size optimized panel for min δ_b.

Chapter 7

Miscellaneous Studies

7.1 Strain rate effect on the 150 *kg* optimized sandwich panels

Strain rate effects are introduced to the homogenized honeycomb core by defining *MAT_MODIFIED _CRUSHABLE_FOAM material model. This model allows to define the load curve of honeycomb at different strain rate (Figure 3-24). Strain rate effects on load curve are discussed in section 3.4.2. Strain rate effects in the face plates are defined using Cowper-Symonds constitutive model (C =6500 s^{-1} p =4) as explained in Equation 3.8. Strain rate in the core of 150 *kg* optimized panel for the element having maximum strain is shown in Figure 7-1. Softer is the core, higher is the strain rate, so higher strain rate effect.

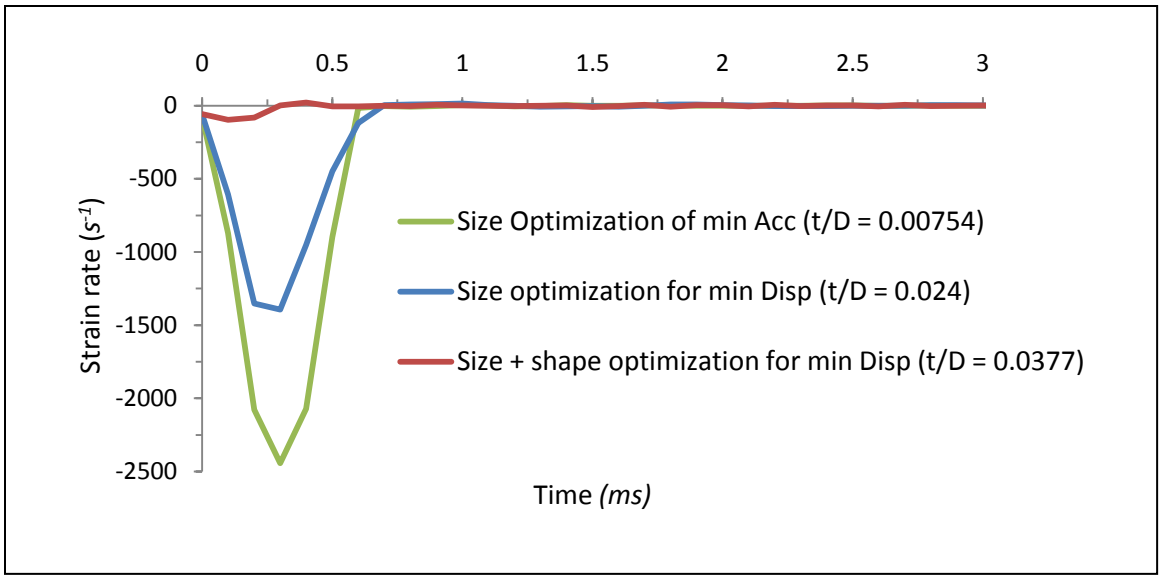

Figure **7-1**: Strain rate in the core of 150 *kg* optimized panel for the element having maximum strain

Table **7-1**: Strain rate effect on the performance of 150 *kg* optimized sandwich and monolithic plate

Case	Without strain rate effect	With strain rate effect	% change
a_b, sandwich-acceleration_ min (m/s^2)	1.84×10^4	2.53×10^4	37.5 ↑
δ_b, sandwich-deflection_ min *(mm)* Size Opt	16.92	13.18	22.1 ↓
δ_b, sandwich-deflection_ min *(mm)* Size + shape Opt	14.4	12.58	12.66 ↓
δ_b, monolithic plate- deflection_ min *(mm)* Shape Opt	11.52	11.5	~ 0
a_b, monolithic plate- acceleration_ min (m/s^2) Shape Opt	8.88×10^4	8.88×10^4	0

Due to strain rate effect, core becomes stiffer, so a_b increases due to higher force transmission and δ_b decreases. Since strain rate is maximum (2442 s^{-1}) in the core for size optimized panel for minimizing a_b, there is 37.5% increase in a_b. In size optimized panel for minimizing δ_b, maximum strain rate is 1393 s^{-1} and it decreases the δ_b by 22.1%. In size + shape optimized panel for minimizing δ_b, maximum strain rate is 97 s^{-1} and it decreases the δ_b by 12.66%. Strain rate effect on the performance of monolithic plate is negligible.

7.2 Preliminary study on delamination in sandwich

Delamination between core and face plates is a dominating failure mechanism found in the sandwich. Due to large difference in modulus between face plates and the core, during bending a high shear stress is generated at the interface which can peel the face plates off the honeycomb core. Load bearing capacity of the sandwich depends upon the bonding strength between core and face plates. Any delamination failure could lead to catastrophic failure of the structure.

Bonding strength depends upon the type and amount of adhesive used. Since the area of contact between honeycomb core and face plate is very small, more is the smearing area for the adhesive more is bonding strength [35]. For metallic panels, welding can be used for higher bonding strength.

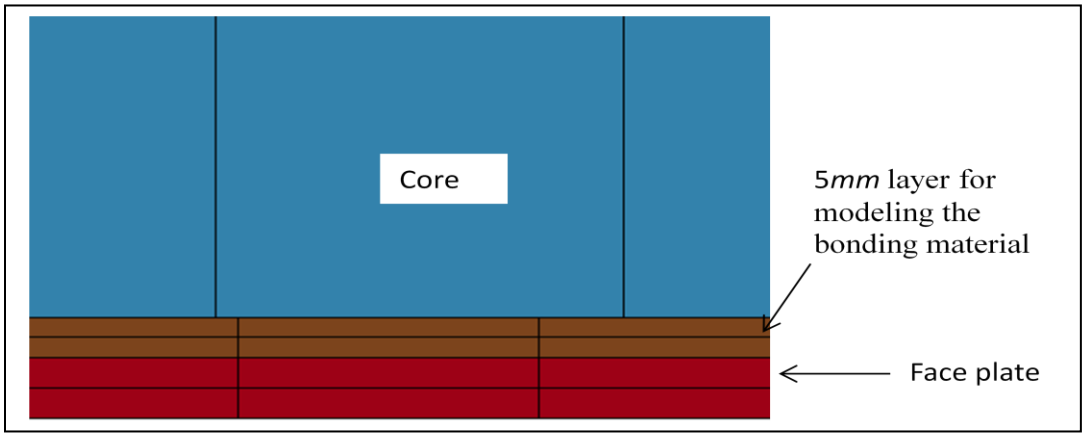

Figure **7-2**: Model for delamination study

Here, a very simplified model is used to simulate the delamination (Figure 7-2) in 150 *kg* size optimized sandwich panel for minimizing δ_b. The core is subdivided such that 5 *mm* thick layer is present at both interfaces. The bonded material is modeled by *MAT_PLASTIC_KINEMATIC material model and activating its material erosion capability. *TIED_SURFACE_TO_SURFACE contact is defined between bonding layer and face plate, and core. The property of the bonding material is decided assuming that (1) core and face plates are welded together and (2) welding strength is same as the base material (i.e Aluminum). For t/D = 0.024, the cross-sectional area of foil per unit cell area is 0.064 (= (8/3)*(t/D)). Since bonding surface is discontinuous and the bonding material is modeled as a homogenized plate, Young's modulus, yield stress and tangent modulus are scaled down by a factor of 0.064. Table 7-2 shows the properties used for the bonding material. When the plastic strain in the elements of bonding material exceeds 0.038, those elements are removed from simulation.

Table 7-**2**: Material properties of the bonding material for 150 *kg* size sandwich for δ_b minimum

Material	Density (kg/m^3)	Young's Modulus *(GPa)*	Yield Stress *(MPa)*	Tangent Modulus *(MPa)*	Poison's Ratio
Bonding material	171.52	4.61	19.2	3.2	0.34

Figure 7-3 shows that delamination occurred at the center of interface between front face plate and core. There is a complete delamination at the interface between backface plate and core. Delamination is near the center of front face plate is very common as observed in experiments [9, 24], however such a catastrophic failure at the backface plate interface is not observed in experiments. The high inertia force of the stiffener starts delaminating from the edges of backface plate (since higher plastic strain occurs near the edges), then completely tear down the bond. This could have been avoided by using suitable fixture which can hold the sandwich together.

Delamination increased both front and back plate deflection. Backface deflection increased from 16.92 to 48.98 *mm*. Such a large amount of increase in δ_b is due to complete delamination at the backface plate. After 1 *ms* delamination occurs at the backface plate and deflection increases by large amount due to sudden decrease in bending stiffness. Maximum plastic strain in front face plate and backface plate increased from 0.0328 and 0.0066 to 0.0376 and 0.0149 respectively. There is an increase in backface plate acceleration from 7.25×10^4 to 7.36×10^4 m/s^2.

When delamination at backface plate is artificially (by removing the element erosion option) restricted, then δ_b only increased from 16.92 to 16.95 *mm*.

So it is concluded that partial delamination in frontface plate would not affect the backface plate deflection much, however delamination at backface plate would increase its deflection by a large amount. Acceleration is not significantly affected due to delamination as it depends upon the force transmitted by core and core is still there to do so.

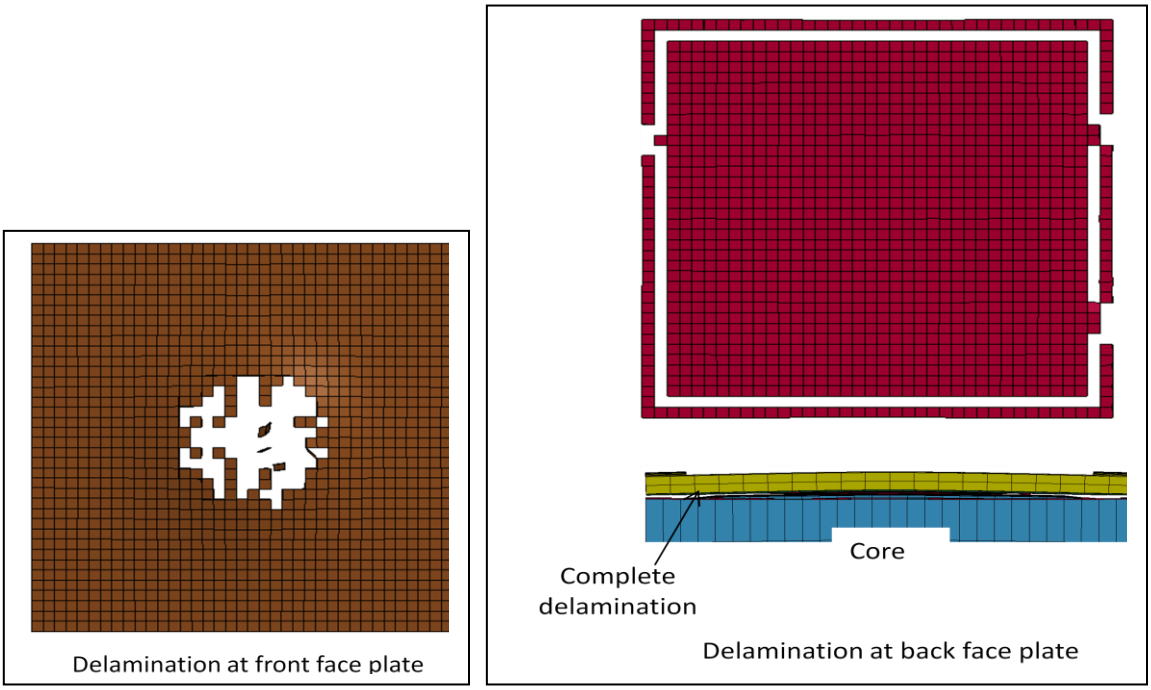

Figure **7-3**: Delaminations in sandwich

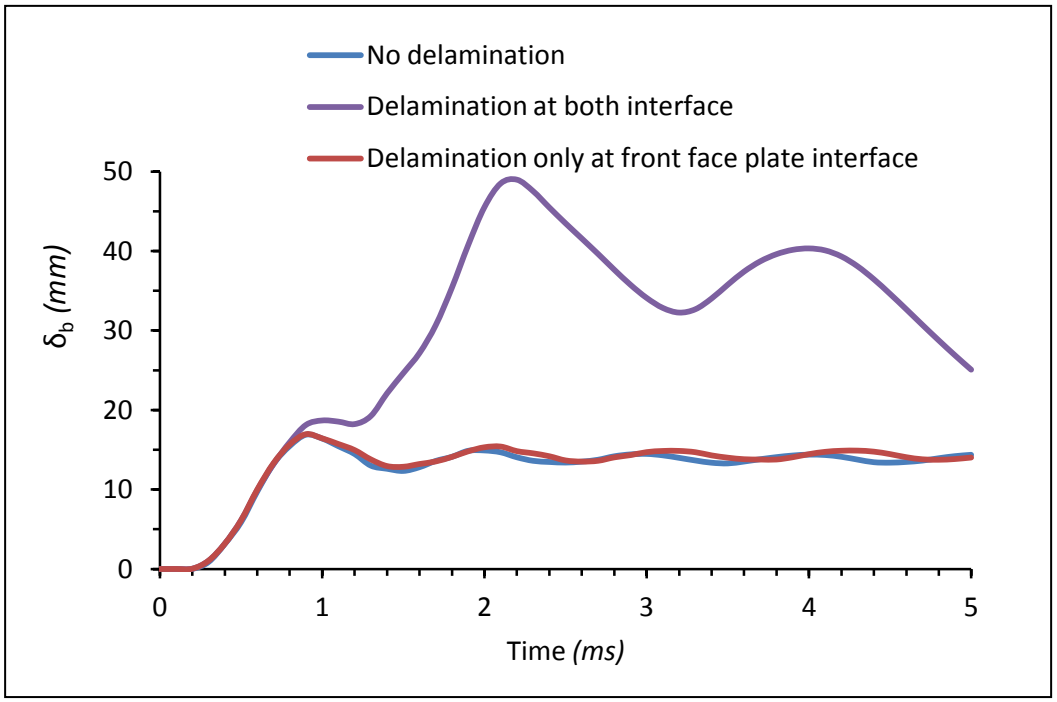

Figure **7-4**: Comparison of δ_b at different delamination case

7.3 Effect of off-center hammer load

Effect of off-center hammer load on the load curve is presented here. Figure 7-5 shows the model (D = 9.52 *mm*, t = 0.0724 *mm*) and off-center locations used for this study. Eight different off-center positions (1-8) are used. In each case, the hammer is moved so that its CG is coincident to these positions. A large square block hammer is taken such that for each position it can cover the unit cell. For all practical purpose, the position '0' is regarded as the CG of the unit cell, though it's correct CG will lie somewhere between number '0' and '1'. To simulate the effect of off-center hammer load, displacement load is not applied to all the nodes of the top face of hammer, rather to nine nodes at the center of top face. Figure 7-6 shows the load curve for center and three extreme off-center positions. No significant changes to the load curve is observed, however there is a minor fall in peak strength with off-center load.

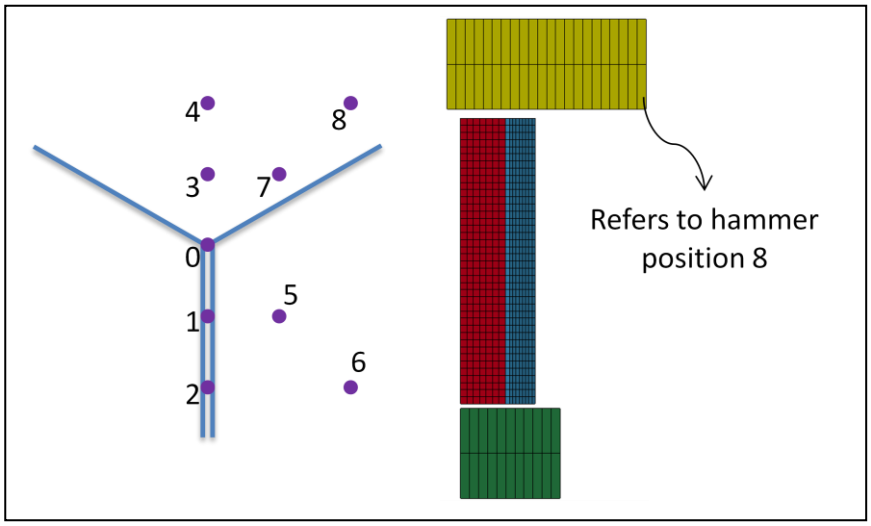

Figure **7-5**: Model details for off-center hammer travel to crush the honeycomb

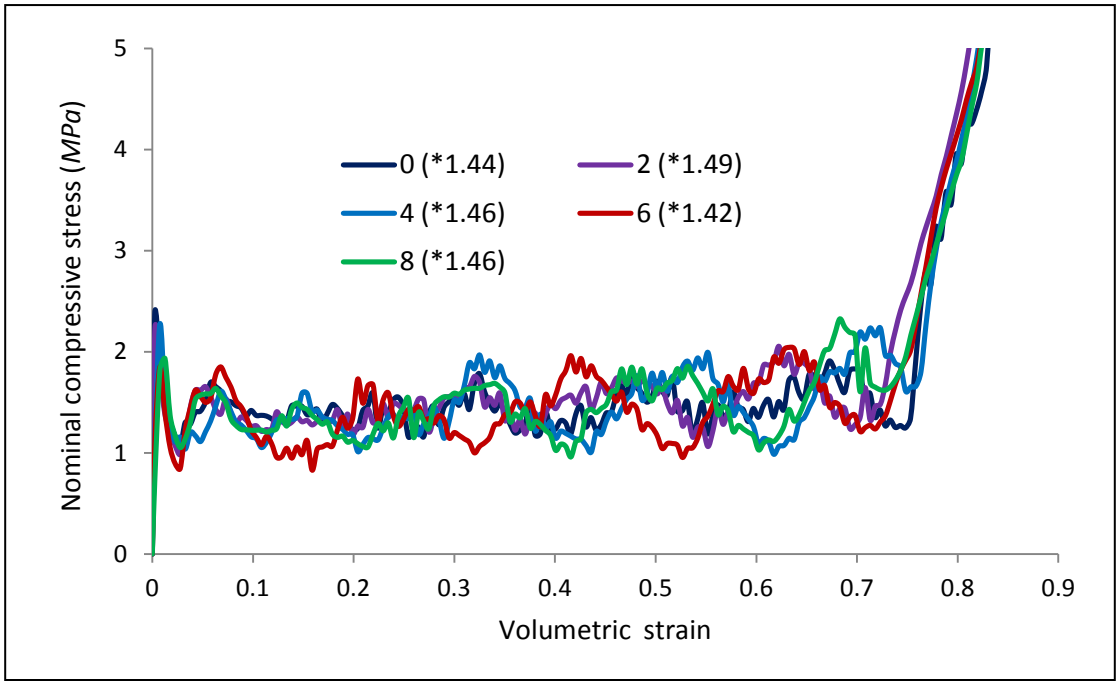

Figure **7-6**: Effect of off-center crushing on load curve (* refers to average crush strength)

7.4 Effect of hammer travel at an angle to transverse direction

The effect of hammer travel at an angle to the transverse direction of the honeycomb on the load curve is presented here. As shown in Figure 7-7, honeycomb is crushed from double foil layer side ($\theta = -10^0, -20^0$ and -30^0) and also from the opposite to double foil layer side ($\theta = 10^0, 20^0$ and 30^0). Hammer travels along a direction perpendicular to its face. Nominal volumetric strain is equal to volume crushed (pyramidal volume) by hammer by volume of unit cell.

As the angle of hammer increases peak stress and densification-start strain decreases (Figure 7-8). When the hammer touches the unit cell, it does not crush the entire cross-section of the unit cell, but start crushing from edges and that is why peak stress decreases with the angle of hammer travel. Towards the end of crushing, one side of unit cell densified sooner than it's opposite side. Since the strain is calculated based on entire unit cell triangular volume, densification-start strain decreases with the angle of hammer travel. When θ is positive, peak strain value increases due to the fact that

initially there will be strain without any stress. The way volumetric strain is calculated, before the hammer touches the foil there will be volumetric compression as shown in Figure 7-7. No significant changes to crush stress observed.

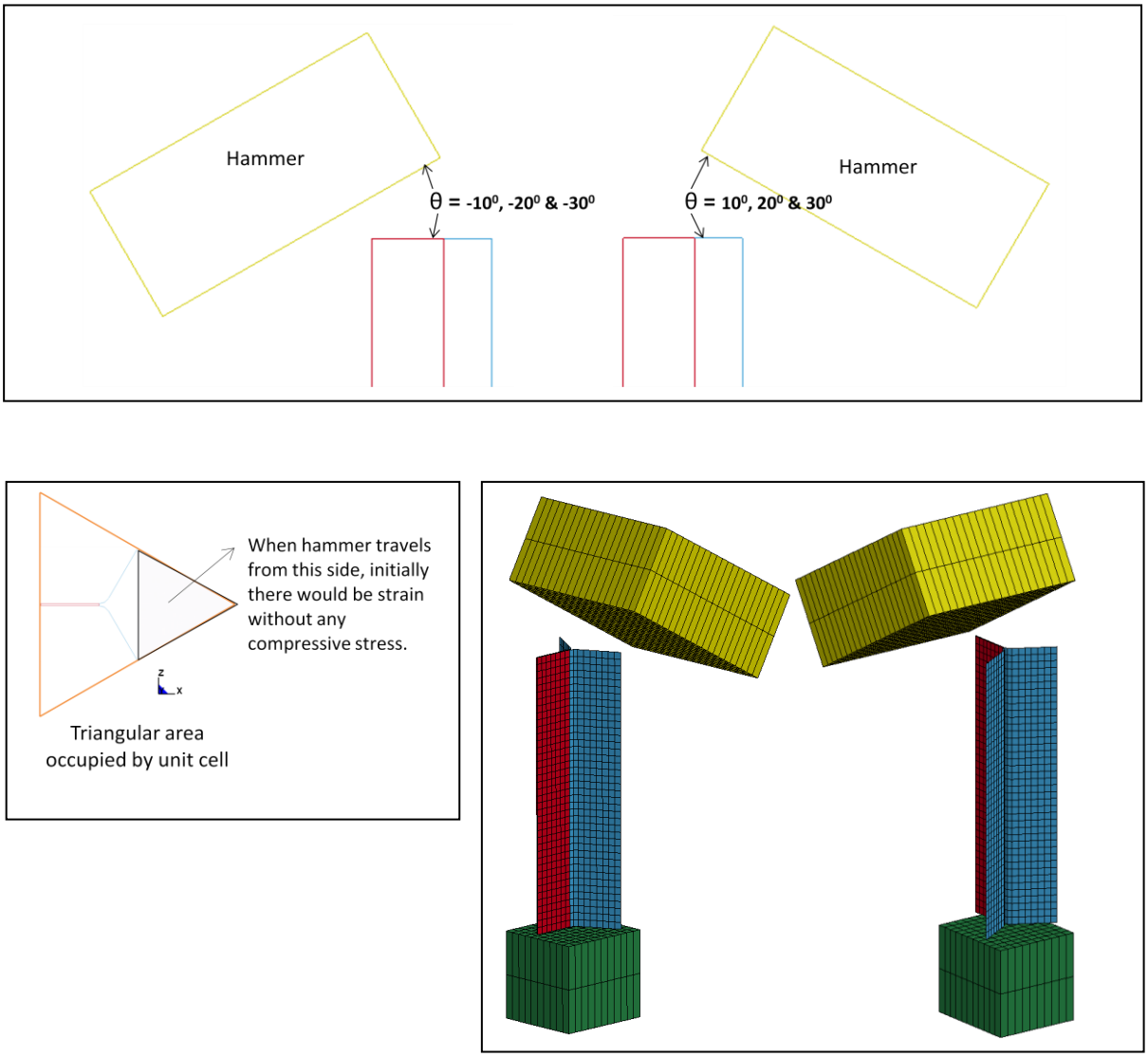

Figure **7-7**: Model details for crushing the core when hammer travel at an angle to transverse direction (D = 9.52 *mm*, t = 0.0724 *mm*)

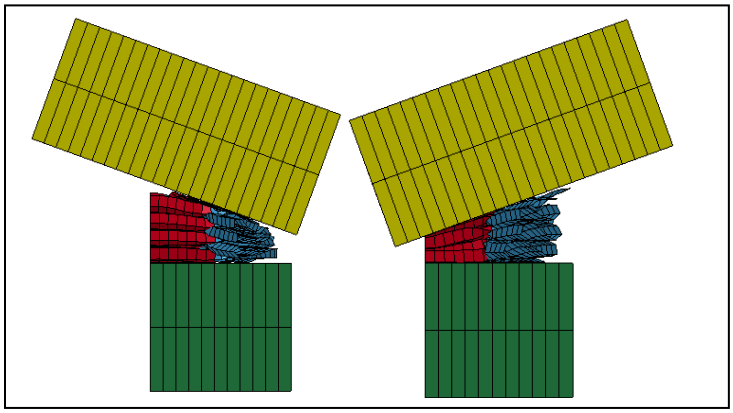

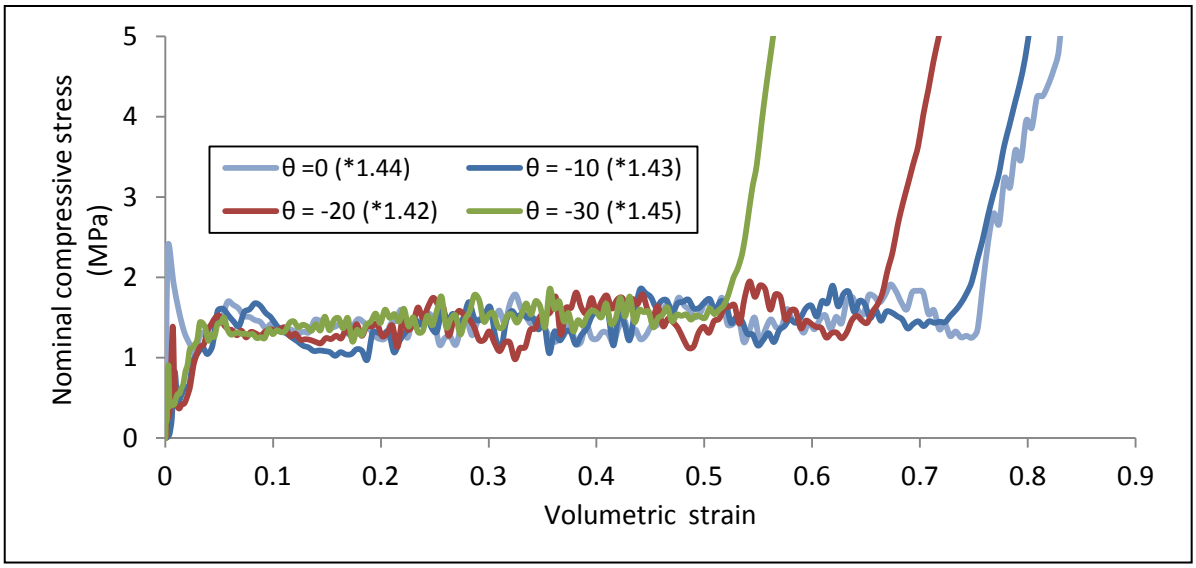

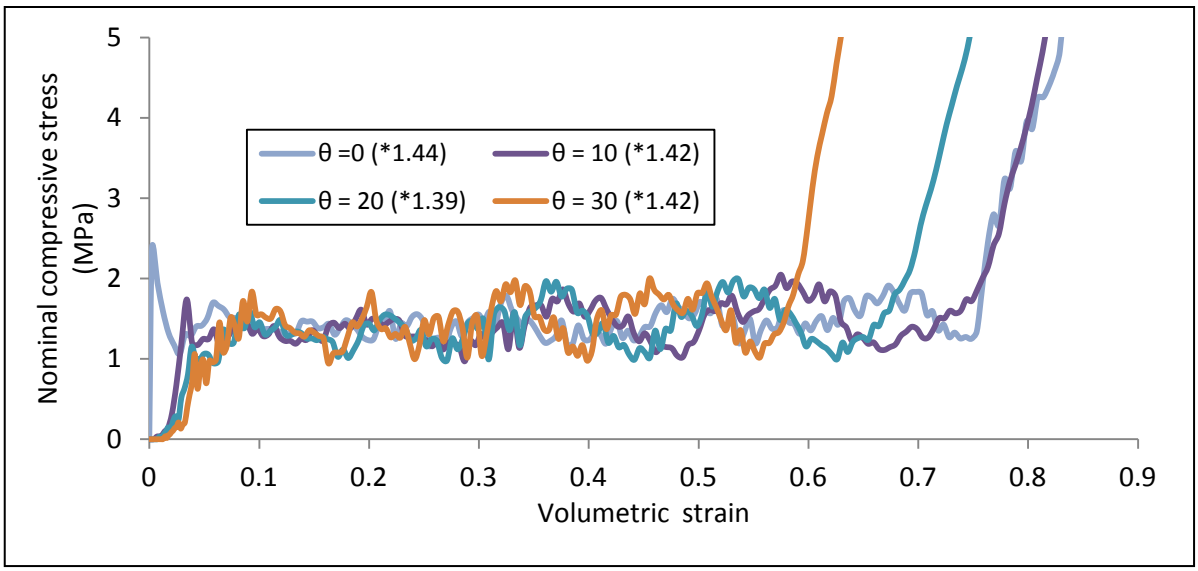

Figure **7-8**: Effect of crushing at an angle on load curve (* refers to average crush strength)

Chapter 8

Conclusions and Future work

8.1 Summary

A process for optimizing sandwich panels to mitigate blast loading is presented. While honeycomb core has been used in the study, the process is also applicable to other types of cellular core. Two independent design objectives, backface deflection of the plate and backface acceleration, are minimized subject to mass and plastic strain constraints. The optimization is carried out using DOE response surface methodology. LS-DYNA is used for finite element simulations. Virtual testing is used to develop a homogenized model for the stress-strain curve of the honeycomb core, and this model has been validated by comparison to existing results as well as to detailed FE model results.

The mechanism of lowering the backface deflection is by increasing front face plate thickness which effectively distributes the blast load to a larger area of the core and avoids increase in impulse stemming from local concave deformation of the front face plate. Further, core depth is increased which increases panel stiffness. In the sandwich, the mass fraction in the front face plate, core and the backface plate are 0.20, 0. 68 and 0.12, respectively, for the $\{t_b, t_f, h, t/D\}$-optimized panel. Interestingly, for the same mass, the shape-optimized monolithic panel is more effective than the optimized honeycomb core sandwich panel (11.5 *mm* vs. 14.4 *mm*). In the all-aluminum monolithic plate, more mass is available to go in terms of bulge, whereas in the sandwich, mass is distributed between face plates and core. Higher the bulge height towards the blast, greater is the reduction in impulse and hence greater the reduction in backface deflection. This aspect and higher rigidity makes the monolithic plate slightly better than the sandwich panel.

Considering acceleration minimization, results produce a stiffer front face plate, which helps to distribute the crushing load to a wider region of the core, and a soft core by reducing t/D to its

minimum value. The mechanism of lowering the backface acceleration is by absorbing energy with low transmitted stress. In this case, honeycomb core sandwich panel proves to be significantly more effective than an optimized monolithic panel (1.84e4 m/s^2 vs. 8.88e4 m/s^2). With increase in sandwich mass, the optimizer adds mass more to the backface plate rather than the core; acceleration not only depends upon the force transmitted to the backface plate but also on the backface plate mass. In the sandwich, the mass fraction in the front face plate, core and the backface plate are 0.47, 0.11 and 0.42 respectively.

In displacement minimization, the core is 68% of the total mass and absorbs 62% of the total energy, whereas in case of acceleration, the core is only 11% of the total mass and absorbs 82% of the total energy.

As noted earlier, Yen, Skaggs and Cheeseman [5] had carried out an experimental and computational study, and concluded that significant reduction in maximum stress amplitude propagating within the core can be achieved by suitable selection of honeycomb material with proper crush strength. This observation has been borne out by the results here, as optimization with LS-DYNA achieves a proper balance, accounting for different interacting physics. A general and efficient design process has been presented. The effect of strain rate on the homogenization model for the core has been studied.

The mechanisms causing improvement in deflection / acceleration as identified in Chapter 6 are expected to hold true regardless of the dimensions of the plate or of the magnitude of the blast load. In particular, the distribution of mass within the sandwich for the two objective functions, as given here for specific data, are expected to be in the same range for other data as well.

8.2 Contributions of the research

The present study contributes to the homogenization of cellular structure and optimization of sandwich panel for blast load mitigation in the following ways.

- Several design variables of the sandwich panels are considered simultaneously for optimization which enables capturing interacting physics. Most of the published results are based upon parametric studies and a methodology for detailed design, giving specific mass distribution in the sandwich, has not been published.
- Virtual testing based approach presented in this research to homogenize the nonlinear stress-strain curve of the honeycomb core can be applied to any type of cellular core, and this approach can also incorporate strain rate effect.
- One-on-one comparison between a sandwich and a monolithic panel has been presented in the same framework.
- Optimization results have been physically interpreted. The roles played by the front and backface plates and the core have been clearly understood for the two objectives. Optimized mass and energy absorption within the sandwich has been presented.

8.3 Future work

Some of the recommended future work are described as follows.

- Though the mechanism of lowering the backface acceleration is through energy absorption with low transmitted stress by core, a little additional improvement is still possible by simultaneous size and shape optimization of the sandwich panel.
- It will be beneficial to develop optimized mass distribution in the sandwich parametrically, in terms of panel size, charge amount and standoff distance.

- A detailed study of delamination between the core and the face plates and its effect on the performance of the sandwich should be considered in this study.
- It is observed that due to strain rate effect, core becomes stiffer which results in increase in backface plate acceleration and decrease in backface plate deflection. It would be appropriate to include this effect in the optimization process.
- A topological optimization of the core resulting in new graded honeycomb core (or foam) concepts may prove beneficial.

Bibliography

1. Argod, V., Nayak, S.K., Singh, A.K., Belegundu, A.D., *Shape optimization of solid isotropic plates to mitigate the effects of air blast loading*,
2. Argod, V., Belegundu, A.D., Aziz, A., Agrawala, V., Jain, R., and Rajan, S.D., *MPI-enabled Shape Optimization of Panels Subjected to Air Blast Loading,* Intl J of Simulation of multidisciplinary Design Optimization (2008)
3. Xue, Z. and Hutchinson, J.W., *A Comparative study of impulse-resistant metal sandwich plates*, International Journal of Impact Engineering, 30, 1283–1305 (2004)
4. Fleck, N.A. and Deshpande, V.S., *The Resistance of Clamped Sandwich Beams to Shock Loading*, vol. 71, J. of Applied Mechanics, Transactions of the ASME, 386-401, (2004)
5. Yen, C.F., Skaggs, R., Cheeseman, B.A., *Modeling of shock mitigation sandwich structures for blast protection*. The 3rd First International Conference on structural stability and dynamics, Kissimmee, Florida, June 19-22 (2005)
6. Hanssen, A.G., Enstock, L., and Langseth, M., *Close-range blast loading of aluminium foam panels. International journal of Impact Engineering* 27, 593-618 (2002)
7. Main, J.A. and Gazonas, G.A, *Uniaxial crushing of sandwich plates under air blast: Influence of mass distribution*, International Journal of Solids and Structures. 45, 2297–2321 (2008)
8. Chi, Y., Langdon, G.S., and Nurick, G.N., *The influence of core height and face plate thickness on the response of honeycomb sandwich panels subjected to blast loading.* Materials and Design 31, 1887-1899 (2010)
9. Zhu, Feng., Zhao, Longmao., Lu, Guoxing., and Wang, Zhihua., *Deformation and failure of blast-loaded metallic sandwich panels-Experimental investigations.* International journal of Impact Engineering 35, 937-951 (2008)

10. Zhu, Feng., Wang, Zhihua., Lu, Guoxing., and Zhao, Longmao., *Analytical investigation and optimal design of sandwich panels subjected to shock loading.* Materials and Design 30, 91-100 (2009)
11. Karagiozova, D., Nurick, G.N., and Langdon, G.S., *Behaviour of sandwich panels subject to intense air blasts-Parts 2: Numerical simulation.* Composite Structures 91, 442-450 (2009)
12. Yamashita, M., and Gotoh, M., *Impact behavior of honeycomb structures with various cell specifications- numerical simulation and experiment.* International journal of Impact Engineering 32, 618-630 (2005)
13. Wierzbicki, Tomasz., *Crushing analysis of metal honeycombs.* International journal of impact engineering 1, 157-174 (1983)
14. Zhang, J., and Ashby, M. F., *Buckling of honeycombs under in-plane biaxial stress.* International journal of mechanical sciences 34, 491-509 (1992)
15. Wu, Enboa., and Jiang, Wu-Shung., *Axial crushing of metallic honeycomb.* International journal of impact engineering 19, 439-456 (1997)
16. Hexcel Corp., *Hexweb honeycomb attributes and properties.* (1999).
17. Stuhmiller, James. H., *Blast injury translating research into operational medicine.* United states army medical research and material command, Maryland.
18. Bulmash, G.and Kingery, C.N *Computational Determination of blast wave pressure-time histories*, Computers in Engineering., Proceedings of the International Computers in Engineering Conference, Volume 2 p 343-347 (1986)
19. Sriram, R., Vaidya, U.K. and Kim, J., *Blast Impact response of aluminum foam sandwich composites*. Journal of Material Science 41,4023-4039 (2006)
20. LS-DYNA Keyword Manual version 971
21. Timoshenko, S. P. and Woinowsky-Krieger, S. *Theory of plates and shells*, Engineering Societies Monographs, New York: McGraw-Hill, 2nd edition (1959)

22. Myers, R., and Montgomery, D., (2009). *Response surface methodology- process and product optimization using designed experiments*, John Wiley & Sons, Inc.
23. Avalle, M., Belingardi, G., Montanini, R., *Characterization of polymeric structural foams under compressive impact loading by means of energy-absorption diagram*", Intl. J. of Impact Engineering, 25, 455-472, 2001.
24. Zhu, Feng., Zhao, Longmao., Lu, Guoxing., and Wang, Zhihua., *Structural response and energy absorption of sandwich panels with an aluminium foam core under blast loading*. Advances in Structural Engineering 11, 525-536 (2008)
25. Singh, A. K., M.S. Thesis, Department of mechanical and Nuclear Engineering, The Pennsylvania State University, University Park, PA 16802 (Dec. 2011)
26. Belegundu, A.D., and Rajan, S.D., *A Shape Optimization Approach Based on Natural Design Variables and Shape Functions*. J. Computer Methods in Applied Mechanics and Engineering, 66, 87-106 (1988)
27. Paulius, G., Daiva, Z., Vitalis, L. and Marian, O., *Experimental and numerical study of impact energy absorption of safety important honeycomb core sandwich structure*. Journal of Materials Science 16, 2 (2010)
28. Hexcel Corp., *Hexweb honeycomb sandwich design technology*. (2000).
29. Altenhof, W., and Ames, W., *Strain rate effects for aluminum and magnesium alloys in finite element simulations of steering wheel armature impact tests.* Fatigue Fract Engng Struct 25, 1149-1156 (2002)
30. Su, X. Y., Yu, T. X., and Reid, S. R., *Inertia-sensitive impact energy-absorbing structure, Part-II effect of strain rate. International Journal of Impact Engineering 16*, 673-689 (1995)
31. Nayak, S.K., *Optimization Of Honeycomb Core Sandwich Panel To Mitigate The Effects Of Air Blast Loading*, M.S. Thesis, The Pennsylvania State University, 8-22 (August 2010)

32. Belegundu, A. D., Rajan, S. D., Wuppalapati, S., Nandakwang, P., Gianforcaro, R., and Ville, J. St., *Structural topology optimization based on virtual testing with general constraints*. 47th AIAA/ASME/ASCE/AHS/ASC Structures, Structural dynamics, and Materials Confere, Rhode Island (2006)
33. Lee, C. S., Chung, S. W., Shin, H., and Kim, S. J., *Virtual material characterization of 3D orthogonal woven composite materials by large scale computing*. Journal of Composite Materials, 39:10, 851-863 (2005)
34. BendsØe, M. P., and Kikuchi, N., *Generating optimal topologies in structural design using a homogenization method*. Computer Methods in Applied Mechanics and Engineering, 71, 197-224 (1988)
35. Jen, Y-M., Ko, C-W., and Lin, H-B., *Effect of the amount of adhesive on the bending fatigue strength of adhesively bonded aluminum honeycomb sandwich beams*. International Journal of Fatigue, 31, 455-462 (2009)

VITA

Sumanta Kumar Nayak

Sumanta Kumar Nayak was born in Jagatsinghpur, Orissa, India to Kshetramani and Surendra Kumar Nayak. He received his Bachelor's degree in Mechanical Engineering from National Institute of Technology, Rourkela. He completed One Year Orientation Course in Nuclear Science & Engineering at Bhabha Atomic Research Centre, Mumbai, India. Then he worked as a Scientific Officer at Variable Energy Cyclotron Centre at Kolkata, India. He came to Pennsylvania State University in Spring 2007 for study and finished his Master's degree in 2010. In the mean time, he joined Brookhaven National Laboratory to work for the development of Accelerators. He is happily married to Dr. Damayanti Naik since December 2006 and father of a son.